DEVELOPMENT OF A JOHNSON NOISE THERMOMETER FOR NUCLEAR POWER USE

Subtask 2.2 of

INTERNATIONAL NUCLEAR ENERGY RESEARCH INITIATIVE

Between
United States of America and Republic of Korea

Project 2002-020-K

Development of Enhanced Reactor Operation Strategy through Improved Sensing and Control at Nuclear Power Plants

Roger A. Kisner, Charles L. Britton Jr., Usha Jagadish, David E. Holcomb, and Miljko Bobrek—Oak Ridge National Laboratory
Michael J. Roberts—University of Tennessee
In Koo Hwang & Byung Soo Moon—Korean Atomic Energy Research Institute
Don W. Miller & Joseph W. Talnagi—The Ohio State University

Final Project Report

March 2005

This Page Intentionally Left Blank

Table of Contents

1. Executive Summary 1
2. Introduction 3
3. Background 5
   3.1. Johnson Noise 5
   3.2. Integrating Traditional Resistance Thermometry with Johnson Noise Methodology 9
      3.2.1. Temperature Measurement Using Resistance Thermometry 9
      3.2.2. RTD Failure Mechanisms 10
      3.2.3. RTD Calibration Errors and Drift 11
      3.2.4. RTD Readout Methods 12
      3.2.5. Combining the RTD and JNT 15
4. System Implementation 20
   4.1. I-NERI JNT Implementation 20
      4.1.1. Dual Mode System 20
   4.2. Instrument Head Overview 24
      4.2.1. Purpose/Description 24
      4.2.2. Connections 25
      4.2.3. System Performance 25
      4.2.4. Size 26
      4.2.5. Materials 26
      4.2.6. Temperature and other Environment 26
      4.2.7. Mounting 27
   4.3. Receiver Description 27
   4.4. DSP Subsystem 27
      4.4.1. Data Acquisition 27
      4.4.2. Windowing 27
   4.5. Discrete Fourier Transform 28
   4.6. Cross Power Spectral Density 28
      4.6.1. Short-term Average 29
      4.6.2. Magnitude of CPSD 30
      4.6.3. Bandwidth Cut-Off 30
      4.6.4. Gain Correction and EMI cancellation 30
   4.7. Temperature Calculation and Display 34
      4.7.1. Conversion of CPDS to JNT Value 34
      4.7.2. Update the Resistance-to-Temperature conversion table 34
      4.7.3. Temperature Display from the R-T Table 36
5. Equipment Development 36
6. Implementation of Digital Signal Processing 42
   6.1. Field Programmable Gate Array Implementation 42
   6.2. Digital Signal Processing Chip Implementation 42
7. Software Design for JNT Systems 43
8. System Implementation 49
   8.1. RTD Placement 49
   8.2. System Layout 50

9. System Results 52
9.1. Performance 52
9.2. Technical Barriers and Issues 53
9.2.1. Discrepancy between Swept and Noise Spectrums 53
9.2.2. Effect of Electromagnetic Noise 54
9.2.3. Environmental 55
9.2.4. Time Response 55
10. Conclusions and Recommendations 55
11. Appendix A — Principles of Temperature Measurement Using Johnson Noise Thermometry 57
11.1. Correlated Voltage JNT 57
11.2. Tuned Circuit JNT 58
11.3. Digital Signal Processing 60
11.4. Statistical Uncertainty Analysis 61
11.4.1. Analysis of Measurement Uncertainty Using Noiseless Amplifiers 63
11.4.2. Analysis of Measurement Uncertainty Using Real Amplifiers with Noise 64
12. Appendix B — RTD to Front-End Electronics Cable Calculations 68
13. Appendix C — User's Guide to ORNL Johnson Noise Thermometry System 71
14. Appendix D — Schematic Diagrams 76
15. Appendix E — ORNL JNT Parts List 80

Table of Figures

FIGURE 1. LAYOUT OF THE JOHNSON NOISE TEMPERATURE MEASUREMENT SYSTEM SHOWING MAJOR SUBSYSTEMS. 5
FIGURE 2. PSD OF EACH AMPLIFIER CHANNEL CONTAINING BOTH CORRELATED AND UNCORRELATED NOISE AND THE CPSD FUNCTION FROM BOTH AMPLIFIERS CONTAINING ONLY CORRELATED NOISE. 7
FIGURE 3. CPSD WITH NARROWBAND EMI SPIKES. 8
FIGURE 4. JOHNSON NOISE THERMOMETRY BASED ON DIRECT MEASUREMENT OF A RESISTANCE ELEMENT NOISE. 8
FIGURE 5. JOHNSON NOISE THERMOMETRY BASED ON RESONANT NOISE MEASUREMENT. 9
FIGURE 6. CONFIGURATION OF A FOUR-WIRE RTD. 13
FIGURE 7. LINEAR FIT TO AN RTD CURVE. 14
FIGURE 8. BASIC FUNCTIONS REQUIRED TO AUTOMATICALLY CALIBRATE RTD FROM JOHNSON NOISE MEASUREMENT. 16
FIGURE 9. NOISE SIGNAL VERSUS RTD RESISTANCE (293 K TEMPERATURE). 18
FIGURE 10. CORNER FREQUENCY (BANDWIDTH) OF SIMPLE RC VERSUS RTD RESISTANCE. 18
FIGURE 11. CABLE BANDWIDTH AS A FUNCTION OF LENGTH. 19
FIGURE 12. JOHNSON NOISE THERMOMETRY MEASUREMENT PROCESS BLOCK DIAGRAM. 21
FIGURE 13. PRINCIPAL COMPONENTS AND CONCEPTUAL CONFIGURATION OF THE DUAL MODE RESISTANCE AND JOHNSON NOISE THERMOMETER INCORPORATING THE CROSS-CORRELATION TECHNIQUE, DIGITAL SIGNAL PROCESSING, AND CHANNEL GAIN CALIBRATION 22
FIGURE 14. SYSTEM BLOCK DIAGRAM 23
FIGURE 15. BLOCK DIAGRAM OF THE RECEIVER SECTION 24
FIGURE 16. DETECTOR HEAD ENCLOSURE WITH ATTACHED RTD PROBE 25
FIGURE 17. HANNING WINDOW FUNCTION 28
FIGURE 18. ENERGY LEAKAGE ENHANCEMENT OF HANNING WINDOW RESPONSE 28
FIGURE 19. CPSD FLATTENING 32
FIGURE 20. CPSD DE-FLATTENING. 34
FIGURE 21. R-T CONVERSION TABLE FORMAT. 35
FIGURE 22. PRINCIPLE OF R-T CONVERSION TABLE MODIFICATION. 35
FIGURE 23. INTERPOLATION OF TEMPERATURE VALUE. 36
FIGURE 24. DC RESISTANCE MEASUREMENT AND NOISE CHANNEL CALIBRATION CIRCUIT BOARD. 37
FIGURE 25. DUAL CHANNEL, LOW NOISE PREAMPLIFIER CIRCUIT BOARD. 38
FIGURE 26. CAL BOARD (PREAMPLIFIERS MOUNTED ON REVERSE SIDE) MOUNTED IN ENCLOSURE. (NOTE METAL SHIELD BETWEEN BOARDS.) 39
FIGURE 27. PREAMPLIFIER CIRCUIT BOARD (CAL BOARD ON REVERSE SIDE) MOUNTED IN ENCLOSURE. 39
FIGURE 28. HEAD BOX SHOWING PREAMPLIFIER CIRCUIT BOARD. 40
FIGURE 29. RECEIVER CIRCUIT BOARD. 40
FIGURE 30. RECEIVER ENCLOSURE (TOP) AND POWER SUPPLY BOX (BOTTOM). 41
FIGURE 31. JNT HEAD ENCLOSURE (ELECTRICAL CONNECTION SIDE). 41
FIGURE 32. BLOCK DIAGRAM OF SIGNAL PROCESSING FOR JOHNSON NOISE THERMOMETRY 42
FIGURE 33. MAJOR COMPONENTS OF DSP MODULE 43
FIGURE 34. ENCLOSURE OF JNT DSP SYSTEM 43
FIGURE 35. ONE BLOCK OF TYPICAL NOISE-VOLTAGE DATA FROM THE TWO NOISE-VOLTAGE CHANNELS. 44
FIGURE 36. SIGNALS FROM FIGURE 35 TIME-EXPANDED TO ILLUSTRATE THEIR PARTIAL CORRELATION. 45
FIGURE 37. ONE-BLOCK ESTIMATES OF THE CPSD BETWEEN THE TWO NOISE-VOLTAGE SIGNALS AND THE PSD OF THE SENSOR VOLTAGE 46
FIGURE 38. AVERAGED CPSD BETWEEN THE TWO NOISE VOLTAGE SIGNALS AND ESTIMATED PSD OF SENSOR NOISE VOLTAGE (200-BLOCK AVERAGES). 47
FIGURE 39. REACTOR COOLANT PIPING TEMPERATURE MEASUREMENT MADE IN THREE LOCATIONS AROUND PIPE. 50
FIGURE 40. POSSIBLE SYSTEM CONFIGURATION AT A NUCLEAR POWER FACILITY 51
FIGURE 41. TRACKING OF THE DC RESISTANCE MEASUREMENT SUBSYSTEM. 52
FIGURE 42. LINEAR RESPONSE AS PREDICTED BY THEORY IS MEASURED IN PRACTICAL CIRCUIT. 53

FIGURE 43. DIFFERENCES IN SPECTRAL RESPONSE BETWEEN PILOT-TONE AND JOHNSON NOISE IN THE SAME CHANNEL. 54
FIGURE 44. FOUR-WIRE RTD CONFIGURATION ON WHICH MODEL IS BASED....68
FIGURE 45. SIMPLE RC MODEL SHOWING USE OF BISECTION THEOREM 69
FIGURE 46. ESTIMATED CABLE LOSSES DUE TO SEPARATION DISTANCE....70
FIGURE 47. ORNL JOHNSON NOISE THERMOMETRY AC CALIBRATION AND DC READOUT CIRCUIT BOARD 77
FIGURE 48. ORNL JOHNSON NOISE THERMOMETRY PREAMP CIRCUIT BOARD....78
FIGURE 49. JOHNSON NOISE THERMOMETRY DIFFERENTIAL RECEIVER CIRCUIT BOARD 79

Table of Tables

TABLE 1. CALLENDAR-VAN DUSEN COEFFICIENTS FOR COMMON RTD RESISTANCE TEMPERATURE COEFFICIENTS. 14
TABLE 2. COMPARISON OF STANDARD RTD AND JOHNSON NOISE METHODS. 15
TABLE 3. THERMAL (JOHNSON) NOISE VOLTAGES AT ROOM TEMPERATURE. 17

Table of Acronyms

ADC----------Analog to Digital Converter
CPSD----------Cross Power Spectral Density
DFT ----------Discrete Fourier Transform
DSP ----------Digital Signal Processing
EMI ----------Electromagnetic Interference
EPRI----------Electric Power Research Institute
FFT----------Fast Fourier Transform
FPGA ----------Field Programmable Gate Array
JFET----------Junction Field Effect Transistor
JNT----------Johnson Noise Thermometry
KAERI----------Korean Atomic Energy Research Institute
ORNL----------Oak Ridge National Laboratory
OSU----------The Ohio State University
PRT ----------Platinum Resistance Thermometer
PSD ----------Power Spectral Density
PWR----------Pressurized Water Reactor
RTD----------Resistance Temperature Detector

This Page Intentionally Left Blank

DEVELOPMENT OF A JOHNSON NOISE THERMOMETER FOR NUCLEAR POWER USE

Abstract

Although Johnson noise has been employed as a thermometry method for several decades, it is only recently that advances in digital and analog electronics have made it a technologically reasonable alternative for widespread deployment. Johnson noise is a fundamental physical phenomenon that arises mostly from the random thermal motions of electrons in all materials. Its fundamental nature allows construction of temperature measurement systems that do not require exogenous periodic recalibration. Oak Ridge National Laboratory (ORNL) in partnership with the Korean Atomic Energy Research Institute (KAERI) and The Ohio State University (OSU) has developed a temperature measurement system that combines the absolute accuracy of Johnson noise thermometry (JNT), with high accuracy resistance temperature measurement. System design, construction, and the theory of operation are discussed in this report.

1. Executive Summary

Oak Ridge National Laboratory (ORNL) in partnership with Korean Atomic Energy Research Institute (KAERI) and The Ohio State University (OSU) developed a temperature measurement system that combines Johnson noise thermometry (JNT) and a traditional resistance-based temperature measurement system. The Johnson noise-based temperature measurement relies on fundamental physics and provides the calibration for the resistance thermometry. The resistance temperature measurement is a standard four-wire system using an industrial grade platinum resistance thermometer (PRT).

Temperature measurement uncertainty requires that nuclear power plant operating temperatures (thermal efficiency) be reduced by an amount sufficient such that the plant does not operate beyond its design rating. Further, in high temperature reactor designs, resistance thermometers change calibration more rapidly than available calibration opportunities making their use impractical. Calibration activities are time consuming, costly, and increase radiation exposure to technicians. The current project demonstrates the feasibility of measuring coolant temperatures with a continuous low level of measurement uncertainty without field calibration. This improves plant thermal efficiency while saving significant time and effort as well as eliminating potential errors introduced by the act of calibration.

ORNL had the responsibility of developing the overall system design, the analog electronics hardware, and managing the combined efforts. OSU was responsible for environmental testing and calibrating the JNT hardware. KAERI's role was to develop the digital signal processing algorithms and hardware. This report documents development of the hardware and signal processing portion of the JNT system. The theory of operation and the underlying theory of Johnson noise are covered in detail.

Johnson noise arises from the random thermal motions of electrons in a material. This motion causes a random open-circuit voltage with zero mean across any resistance. The Nyquist equation describes the voltage produced by the vibration of the electrons within a

resistor at a given temperature providing a mathematical relationship between temperature, resistance, and voltage generated. For frequencies below a few gigahertz, the equation shown following gives the relationship between the absolute temperature of a resistor (T), its resistance (R), the frequency band of measurement Δf, and the measured mean-square noise voltage:

$$\overline{V^2} = 4k_B TR\Delta f \,, \tag{1}$$

where k_B represents Boltzmann's constant (1.38×10^{-23} Joules/Kelvin).

The project's approach to temperature measurement combines resistance measurement using industrial type PRTs and noise measurement methods to achieve a precise, prompt temperature measurement without the need for external recalibration. The JNT implementation described in this report combines several features to minimize overall measurement uncertainty.

1. Standard, high-precision, four-wire resistance thermometry using a rugged industrial grade PRT
2. Quasi-continuous sampling of the Johnson noise of the thermometer resistance
3. Two parallel first stage amplifier channels—used to reduce the amplifier contribution to the measured noise by only accepting the correlated noise from the two amplifier channels
4. Digital signal processing algorithms to recognize the fundamental frequency shape of Johnson noise and reject narrow band noise spikes
5. Continuous end-to-end channel gain correction—achieved by injecting a tone signal onto the Johnson noise that passes through the measurement electronics and cabling

The temperature measurement system developed for this project is intended to demonstrate system architecture implementable at a nuclear power plant. A principal reason why Johnson noise temperature measurement has not heretofore been widely implemented in high value industrial temperature measurement situations is the fact that Johnson noise is a small signal phenomena distributed over a wide frequency band. This means that intervening cables between the sensing resistance and the signal measurement electronics distort the Johnson noise signal and that first stage amplification of the Johnson noise signal needs to be made within several meters of the sensing resistance. Nuclear power plants do not provide the benign, well-regulated environments required for precision, high-gain electronics near the core or primary coolant loop. The measurement hardware developed for this project is, therefore, split into a field and a control room portion that can be separated by up to 300 m. The field portion of the hardware only uses technologies that can be implemented in a ruggedized, radiation hardened form. This project, however, was not large enough to allow implementation of a radiation hardened field electronics set.

The field portion of the hardware system fabricated for this project consists of a detector head enclosure containing: the first stage Johnson noise amplifiers, a calibration tone

generator, signal drive electronics, and a dc power supply. The control room portion of the hardware consists of a receiver box and a digital-signal-processing (DSP) unit with its associated signal processing algorithms.

The detector enclosure contains two circuit boards. The first circuit board includes two preamplifier channels for the Johnson noise coming from the resistance temperature detector (RTD) and differential driving of coaxial cables connecting to the control room portion of the system; the second circuit board contains circuitry for the RTD resistance measurement and a noise-channel calibration signal generator. The detector head enclosure is connected to the receiver by six coaxial cables. The receiver contains circuitry to receive the differential inputs, perform filtering, and convert to voltages suitable to deliver to a multichannel analog-to-digital converter (ADC).

While the digital signal processing system was under development at KAERI, ORNL developed a computer based DSP system to read-out the Johnson noise temperature and test the functionality of the developed analog hardware. Project staff also developed a more advanced software package that implements the full set of digital signal processing algorithms in a viewable and modifiable computer based form. The two principal advantages of implementing the DSP in a dedicated hardware format are the increased speed of signal processing possible with a dedicated, custom hardware (the computer based system samples only ~15% of the available signals) and the increased system reliability of not employing a computer with its associated operating system, user interface, disk drives, etc.

While initial hardware and software have been completed, significant technical hurdles must be overcome before JNT can be implemented in nuclear power plant safety or control. The current implementation exhibits a small residual measurement anomaly, which although compensated for needs to be understood and corrected. The present implementation of JNT is designed to demonstrate quasi-continuous thermometer re-calibration. However, this implementation lacks several features required for practical nuclear power plant application. The front-end electronics in the current device are not radiation hardened. While care was exercised in the system design to select technologies that can be radiation hardened, this has yet to be done. Further, in most industrial environments it would be advantageous to be able to locate the front-end electronics remotely from the transducer. In the current system, the electronics are limited to being at most one meter from the resistive element. Finally, the current electronics are optimized to correct for rapid transducer drift that is not realistic for normal operation. The design needs to be modified to, instead, correct for slow transducer drifts, which are more difficult to simulate in the laboratory.

2. Introduction

The purpose of this project is to demonstrate the electronics technologies required for a Johnson-noise-based thermometry system for measuring reactor coolant-leg temperature. However, no radiation hardening has been performed. The demonstration, although not necessarily optimal, shows the feasibility of Johnson noise technology implementation. The theory and fundamental design elements for a practical Johnson noise thermometry

(JNT) measurement system have been developing over the last 50 years[1,2,3] but the technology to successfully implement JNT in industrial environments has only become practical within the past decade. The key enabling technology development has been inexpensive, high-speed, DSP. The reason the modern DSP is required for industrial JNT implementation is that Johnson noise is a wideband, very small signal phenomenon. As such, it is vulnerable to contamination by unrelated noise sources. Johnson noise, however, unlike contaminating noise sources is distributed evenly across the frequency spectrum. DSP is employed to recognize the frequency distribution of the measured noise and remove the contaminations.

The underlying rationale for the Johnson noise thermometry project is that all available versions of temperature measurement technology drift under the harsh environment of a nuclear power plant. Knowledge of the plant thermodynamic state is a primary performance and a safety requirement for current reactors as well as all of the proposed future reactors. While the device being developed and demonstrated in this project is specifically intended to provide a first-principle measurement of temperature within the primary coolant loop of PWRs, Johnson noise is a general technology equally applicable to direct in-core temperature measurement. The technology developed under the current program can be applied to the reactors of the GenIV and nuclear hydrogen initiatives.

Variation in materials or changes in material characteristics over time do not affect the fundamental physics of how Johnson noise is produced. Because of the fundamental nature of JNT, calibration is not needed. The NRC mandates periodic calibration of primary coolant-temperature measurement instruments. Without an assured measurement uncertainty, safety margins would be required to be increased leading to reduced plant thermal efficiency. In high temperature reactor designs, sensors change calibration rapidly making their use impractical. Calibration activities are time consuming, costly, and increase radiation exposure to technicians. The results of work on JNT development under subtask 2.2 demonstrate the feasibility of JNT to measure coolant temperatures with the added bonus of eliminating the need for periodic external calibration. This saves significant time and effort as well as eliminating potential errors introduced by the act of calibration.

The developed temperature measurement system consists of two major subsystems: (1) instrument head and (2) receiver and signal processing. The instrument head portion contains analog amplifier components. The system functions have been segmented to restrict the components in and functionality of the instrument head to only those components and functions that can be implemented in a rugged, radiation tolerant form. The receiver and signal processing subsystem, which contains both analog and digital electronic components, can be located remotely from the head in an environmentally conditioned instrument cabinet. Interconnection between the two subsystems is made by

---

[1] Brixy, H. G., "Temperature Measurement in Nuclear Reactors by Noise Thermometry," Nuclear Instruments and Methods, 97(1) 75-80 (November 1971).

[2] Garrison, J. B. and Lawson, A. W., "An Absolute Noise Thermometer for High Temperatures and High Pressures," Review of Scientific Instruments, 20, 785-94 (1949)

[3] David E. Holcomb, Roger A. Kisner, and Michael J. Roberts, Johnson Noise Thermometry For Space Reactor Temperature Measurement, Space Technology and Applications International Forum—STAIF 2004, AIP Conference 699, 567- 573, Albuquerque, NM (February 2004)

a bundle of shielded cables that can extend their separation to 300 meters. The major subsystems are shown below:

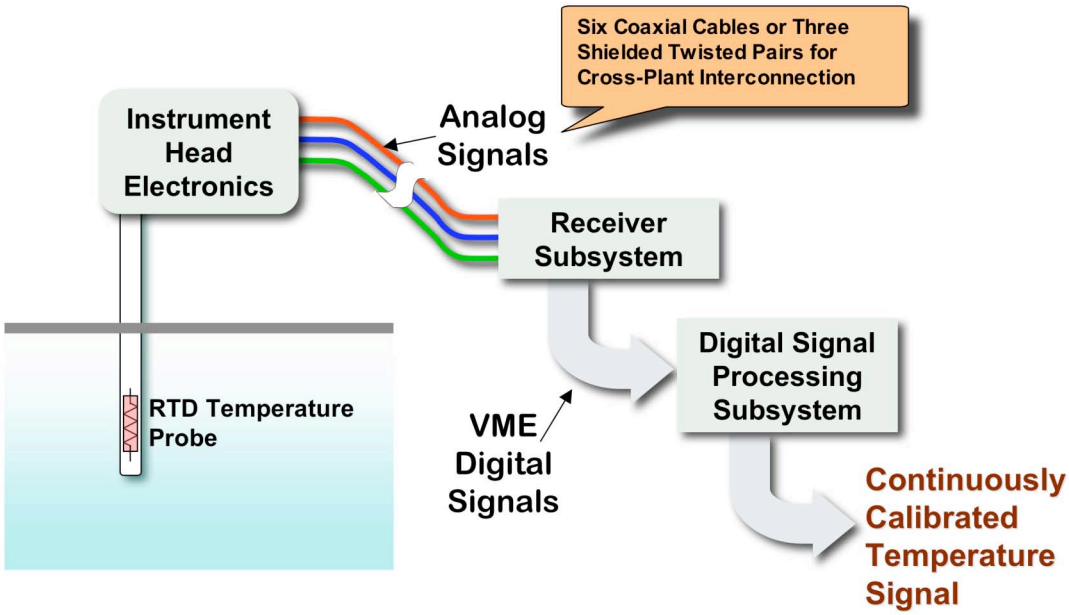

Figure 1. Layout of the Johnson noise temperature measurement system showing major subsystems.

3. Background

3.1. Johnson Noise

Johnson noise arises mostly from the random thermal motions of electrons in any materials. This motion causes an open-circuit voltage across any resistance, which is random with zero mean. The Nyquist equation describes the voltage produced by the vibration of the electrons within a resistor at a given temperature providing a mathematical relationship between temperature, resistance, and voltage generated. For frequencies below a few gigahertz, the power spectral density (PSD) of the noise voltage across the resistor is four times the product of Boltzmann's constant, the absolute temperature in Kelvin, and the resistance in ohms. Refer to Appendix A for detailed mathematical development.

To make a temperature measurement using Johnson noise in the current measurement implementation, the frequency response of the measurement system must be known as well as the sensor resistance. Temperature is then computed by dividing the power spectral density of the noise voltage by $4k_BR$. Because of the statistical nature of the voltage measurement, there is uncertainty in the solution, which is progressively decreased by increasing the integration time of the measurement.

A direct measurement of the Johnson noise for temperature measurement presents several challenges. First, the amplifier gain needs to be both known and stable. Second, the amplifier passband and filtering effects of connection cabling must be known to within the required measurement accuracy. Finally, the resistance of the sensor must be

independently and accurately measured. To avoid these difficulties, early Johnson noise thermometers performed a ratio of two noise voltage measurements, one with a resistor at the measurement temperature and the other at a known temperature, switched onto a single amplifier channel. However, changing the connection of the sensor to the high-gain measurement circuit introduced noise and decreased reliability[4].

The approach that ORNL staff took to minimize these difficulties in previous designs was to follow the work of Pepper and Brown[5] in which a resistive sensor is connected in series with an inductor and a capacitor forming a tuned circuit. In this approach, the ideal mean squared noise voltage is given by

$$\overline{V^2} = \int S_v(f)df = 4k_B TR\frac{\pi}{2}\frac{f_0}{Q} = \frac{k_B T}{C}, \tag{2}$$

where S_v is the spectral density, f_0 is the resonant frequency, Q is the resonance quality factor, and C is the capacitance of the capacitor. The major advantage of this measurement technique is that for lossless inductors and capacitors (if the measurement bandwidth is greater than the tuned circuit bandpass), the measured voltage output is independent of the sensor resistance and the inductance. No measurement of the sensor resistance is needed. Another advantage of the technique is that for a properly tuned circuit, most of the signal power lies in a relatively small band near the resonant frequency. This allows the amplifier bandwidth to be relatively small and reduces its noise contribution to the measurement uncertainty.

A practical limitation with tuned-circuit approach, however, is loss in the inductors. Real inductors have winding resistances (typically frequency dependent) and magnetic core losses that dissipate energy. In practice, this limits the overall accuracy obtainable with a tuned-circuit implementation of Johnson noise thermometry. Refer to Appendix A for development of tuned circuit JNT method.

Another implementation restriction for Johnson noise thermometry is the capacitive effect of the cable connecting the sensing resistor to the first stage amplifiers. If the cable has significant capacitance, it will block the high frequency portion of the sensor noise before it reaches the measurement system. This filtering of the upper frequencies reduces the bandwidth of the Johnson noise signal. Under the high temperature and radiation environment of a nuclear power plant, the cable capacitance will change over time. One way of compensating for the cable effect is to periodically measure its input impedance and calculate its transfer function. However, the best technique remains to locate the first-stage amplifier near the sensor.

Two additional signal-processing concepts were investigated by ORNL for NASA applications (further work was done under Electric Power Research Institute (EPRI) sponsorship). In the first of these, the temperature measurement resistor is connected in

---

[4] Garrison, J. B. and Lawson, A. W., "An Absolute Noise Thermometer for High Temperatures and High Pressures," Review of Scientific Instruments, 20, 785-94 (1949).

[5] Pepper, M. G. and Brown, J. B., "Absolute High-Temperature Johnson Noise Thermometry," J. Phys. E: Sci. Instrum., 12, 31-34(January 1979).

parallel to two separate high input impedance amplifiers. The output of these amplifiers is partially correlated since each consists of the sum of a correlated noise voltage and uncorrelated amplifier noise voltage. If two Johnson noise amplifier signals, connected to the same resistance, are combined and time averaged, the correlated part of the noise will persist, but the uncorrelated amplifier noise will approach zero. Figure 2 illustrates the concept of cross-correlation; the measured voltage from one amplifier channel is Fourier transformed and multiplied by the other to form a cross power spectral density (CPSD), effectively eliminating the noise contribution from the amplifier electronics.

Johnson noise has a flat (white) spectral energy distribution. The shapes of the power spectral density functions are a result of the combined effects of filtering out both the low and high frequencies from the noise and the frequency dependent gain of the amplifier circuit. The low frequency filtering is applied to eliminate the non-thermal noise generated by mechanical vibrations. These microphonic and triboelectric signals are limited to less than a few tens of kilohertz. The upper frequency filtering is applied both to avoid aliasing higher frequencies into the measurement band as well as to minimize the impact of sensor-to-amplifier cable-capacitance induced restriction of high frequency transmission.

The CPSD function has units of volts squared per hertz and expresses the voltage-squared content per unit frequency of the measured voltage signal. Figure 2 illustrates the relations between the PSDs of the individual channel voltages and the CPSD between them.

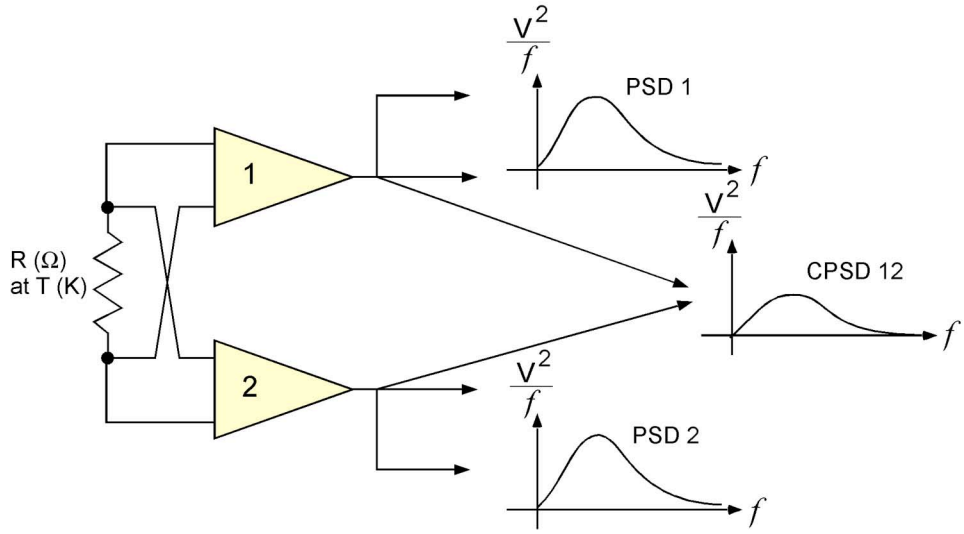

Figure 2. PSD of each amplifier channel containing both correlated and uncorrelated noise and the CPSD Function from both amplifiers containing only correlated noise.

Electromagnetic interference spikes and microphonics are two of the biggest problems for a practical implementation of JNT. In many situations, these effects can completely dominate the noise measurement. This puts a premium on well-implemented grounding, shielding, and filtering. A complementary technique to reduce these effects is to use both knowledge of the spectral energy content of Johnson noise and digital signal processing to recognize and eliminate interferences. Typically, narrowband electromagnetic

interference (EMI) appears as spikes in the long-term average CPSD that can be recognized and removed with only a small reduction in measurement bandwidth as illustrated in Figure 3.

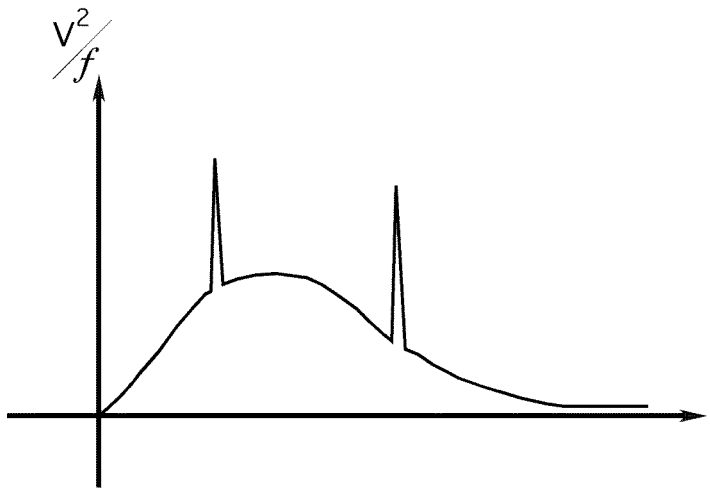

Figure 3. CPSD with Narrowband EMI Spikes.

Two distinct implementations of JNT measurement are possible: (1) the direct measurement of wideband, white spectral noise from a resistance utilizing Equation (1) as illustrated in Figure 4, and (2) measurement of the noise in a resonant circuit utilizing Equation (2) as illustrated in Figure 5.[6] The direct noise measurement technique can be combined with a standard RTD measurement to form a fast response, continuously calibrated measurement system. This combination is discussed in the next section. The resonant implementation can be made to measure temperatures without contact to the measured surface by turning the inductor into an antenna.

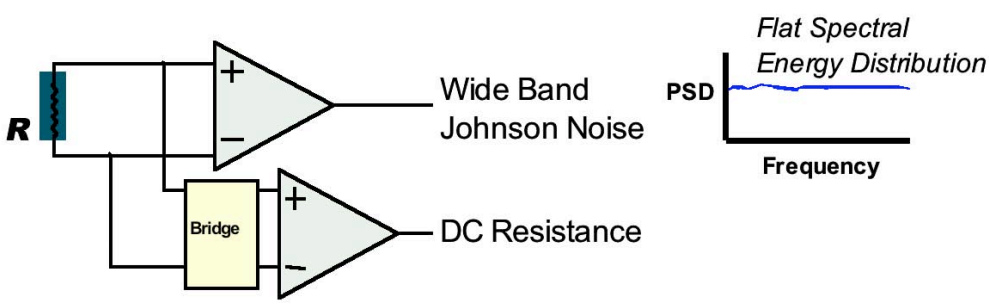

Figure 4. Johnson noise thermometry based on direct measurement of a resistance element noise.

[6] R. A. Kisner, C.L. Britton, U. Jagadish, J.B. Wilgen, M. Roberts, T.V. Blalock, D. E. Holcomb, M. Bobrek, M.N. Ericson, "Johnson Noise Thermometry for Harsh Environments," Proceedings of the 2004 IEEE Aerospace Conference, March 6-14, 2004, Big Sky, MT.

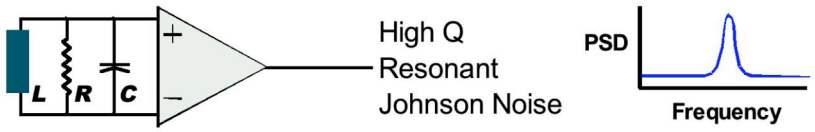

Figure 5. Johnson noise thermometry based on resonant noise measurement.

3.2. Integrating Traditional Resistance Thermometry with Johnson Noise Methodology

One of the drawbacks of previous JNT measurement systems has been the degradation of noise signals from shielded signal cables. To overcome this problem, our approach has been to place the sensitive preamplifiers close to the thermal noise source (i.e., the RTD element). Once amplified and conditioned, the noise signals can pass over longer cable lengths with minimum degradation. However, cables and amplifiers can change operating parameters over time; most importantly, the changes in frequency-dependent attenuation of the cable must be compensated for in the long term. We accomplish this compensation by sweeping a sinusoidal signal across the full channel spectrum. The calibration sweep signal originates in the instrument head. The signal is received and analyzed by the digital signal processing system, which determines the channel gain and spectral response independent from the Johnson noise signal. The sweep calibration permits continuous end-to-end calibration of channel gain.

Other noise, besides the thermally-generated noise, of the RTD is introduced into the signal flow. For example, noise introduced by the high-gain, high-frequency preamplifiers adds to the Johnson noise from the RTD and contaminates the calculation of equivalent temperature of the RTD noise. To reduce this, we amplify the RTD noise signal using two identical preamplifiers and send their noise signals to the receiver and DSP subsystems over two independent channels. Within the DSP subsystem, cross-correlation methods remove uncorrelated signals. This step greatly decreases the uncertainty of the measured temperature.

Temperature values derived from Johnson noise are relatively slow in responding owing to the statistical processes from which the value is calculated. To achieve a faster response, the RTD's actual resistance value is measured and a transfer function applied to calculate the actual temperature. This process is the traditional method for reading an RTD's temperature. Continuing to use this technique allows the new measurement system to respond rapidly to temperature change. The transfer function of the RTD, however, drifts over time requiring periodic recalibration. The non-drifting Johnson noise temperature is used to periodically recalibrate the RTD resistance to temperature transfer function.

3.2.1. Temperature Measurement Using Resistance Thermometry

The same year that Seebeck made his discovery about thermoelectricity from which the thermocouple evolved, Sir Humphrey Davy announced that the resistivity of metals demonstrated temperature dependence. Sir William Siemens, some fifty years later, suggested the use of platinum as the element in a resistance thermometer device. Very

pure, well annealed platinum is still used to form the resistive element in most high-accuracy resistance thermometers. In fact, the standard platinum resistance temperature detector is currently used as a transfer standard for temperature up to the silver melting point (961.78 °C). A commonly used RTD structure using platinum was proposed by C.H. Meyers in 1932.[7] He wound helical platinum on a crossed mica web and mounted the assembly inside a tube. This construction minimized strain on the wire while maximizing total resistance. Although this construction produces a very stable element, the thermal contact between the platinum and the measured spot is poor, which results in a slow thermal response time.

As an alternative to Meyers' construction, the birdcage element was proposed by Evans and Burns.[8] The element remains largely unsupported, allowing it to expand or contract freely with temperature variation. However, the construction was still not suitably rugged enough for industrial use. Other construction methods have been developed that result in a more rugged construction. An example is thin wire bifilarly wound on a ceramic bobbin. This style of construction was employed in previous ORNL designs.[9] Careful design must be applied to match the thermal expansion properties of bobbin and wire to minimize mechanical stress, as a principal mechanism of RTD drift is strain-induced resistance change, which permanently changes the resistance of the wire.

Other construction techniques have been applied to the resistance element besides wire winding. In the newest construction technique, a platinum or platinum-glass slurry film is deposited onto a small flat ceramic substrate, etched with a laser-trimming system, and sealed. The film RTD offers substantial reduction in assembly time and has the further advantage of increased resistance for a given size. Due to the manufacturing technology, the device size itself is small, which means it can respond quickly to step changes in temperature. However, film-type RTD's are less stable than their wire-wound counterparts are, but are more popular because of their decided advantages in size, cost, and ruggedness.

3.2.2. RTD Failure Mechanisms

The local temperature alters the electrical resistance value of the sensor element of an RTD. The temperature is then determined by measuring the sensor element's resistance value. Uncertainty in the measurement comes from every component along the signal path; however, the single greatest source of measurement error comes from the RTD itself. Temperature calculation depends on precisely knowing the RTD's temperature-to-resistance transfer function over the full range of measurement. The transfer function, however, drifts due to several different environmental effects. Simple exposure to elevated temperature leads to corrosion and diffusion of contaminants into the sensing element of the RTD. Similar processes impact the insulative wire supports. In addition,

---

[7] C.H. Meyers: Coiled Filament Resistance Thermometers, NBS Journal of Research, Vol. 9, 1932.

[8] J.P. Evans and G.W. Burns: A Study of Stability of High Temperature Platinum Resistance Thermometers, in Temperature - Its Measurement and Control on Science and Industry, Reinhold, New York, 1962.

[9] R. M. Carroll and R. L. Shepard, The Method of Construction of a Dual Johnson-Noise-Power and Resistance Thermometer for 1375K (1100°C) Service in a Vacuum Environment," ORNL/TM-12696, September 1994.

vibration leads to fatigue and creep. Built-in stresses from initial fabrication annealed throughout the RTD's operating life producing a progressive resistance shift. All of these influences lead to measurement drift. Three dominant failure mechanisms are discussed below:

1. Contamination and corrosion at high temperature have historically been a major problem starting at about 300 °C and especially above 660 °C. Contamination arises primarily from the connection welds and sheath material. At higher temperatures, this problem becomes more serious. Higher temperatures allow increased mobility of ions and hence more rapid diffusion of contaminant atoms. Contamination of the resistance material and electrical connections changes the resistance, which is interpreted as a real temperature change. To a large part, employing a platinum sheath, welding under a high purity inert atmosphere, and using very high purity insulators can alleviate this contamination.

2. Thermomechanical stability remains a principal challenge for high temperature RTDs. Normally, for secondary standard PRTs and industrial RTDs, manufacturers tend to use materials such as ceramic or cement to support the platinum coils. If the coefficient of thermal expansion (CTE) of the bobbin or support material does not precisely match that of the resistance wire over the full range of temperature measurement, the RTD will become progressively more mechanically strained over time and have a large thermal hysteresis. It is this mismatch in thermal expansion that ultimately limits the upper working temperature of an RTD.

3. Vibration, thermal cycling, and severe mechanical stress at the limits of the devices working temperature eventually lead to breakage (i.e., open circuit) of the RTD wire. Catastrophic failure often occurs at temperatures much below the softening or melting points of the materials. It is ironic that methods to reduce vibration of the resistance element contribute to the contamination diffusion problem.

In addition to the three RTD principal failure mechanism for nuclear reactor environments, ionizing radiation especially neutrons can produce temporary or permanent calibration shifts.

3.2.3. RTD Calibration Errors and Drift

The initial accuracy of an RTD is established by combining the uncertainties involved in its laboratory calibration. Uncertainties fall into three groups: (1) uncertainty arising from calibration equipment; (2) inherent RTD errors such as hysteresis, repeatability, and self-heating; and (3) interpolation and curve-fitting errors. Examining the inherent

uncertainties more closely reveals that the inherent RTD errors are a dominant source of uncertainty in the long term.

An industrial platinum RTD's drift after calibration (initial accuracy of 0.001 to 0.005 °C) is in the range of 0.005 to 0.01 °C per year for temperatures up to 300 °C.[10] Thermal hysteresis is caused by differences in thermal expansion coefficients between the platinum element and the structure in contact with the element. A range of 0.01 to 0.3 °C was found for hysteresis error for RTDs between 20 °C and 300 °C. The aging of RTDs in tests performed by Hashemian and Petersen[10] did not result in a monotonic drift from which a reliable drift rate could be obtained. No data are available on calibration drift characteristics for many year periods.

Most RTD users replace their RTDs after 18 months because of the possibility of catastrophic failure. Better sheath materials can solve the failure issue for many industrial applications. However, the drift of calibration is the result of many effects (corrosion, strain, creep, diffusion, nuclear transmutation) and while not usually catastrophic must be compensated for.

High quality, metal-sheathed precision RTD thermometers have recently been developed for both laboratory and industrial applications with temperature ranges to 1,100 °C. The issue of contamination was addressed using proprietary materials and assembly. Data from drift studies on these proprietary technologies show drifts of about 25 mK over a 350 hour test.[11] No long-term survival information is yet available about the new, proprietary technology, RTDs.

It is clear that RTDs must be periodically calibrated to maintain low uncertainty of temperature measurement. Calibration by human intervention is routinely employed in industrial systems. For nuclear power plant systems, human intervention is restricted to limited periods when the reactor containment is inhabitable, usually during a refueling outage.

3.2.4. RTD Readout Methods

The four-wire resistance measurement method for determining an RTD's resistance is preferred to minimize systematic uncertainty introduced by lead-wire resistance. The typical four-wire circuit configuration is shown in Figure 6. A constant current is passed through the RTD wire, film, or ceramic material through the outer path. The inner two wires become the voltage measurement, which yields the resistance by Ohm's law. A high-input-impedance device must make the voltage measurement since the resistance of the measurement device is placed in parallel with the RTD's resistance value — another source of systematic uncertainty.

---

[10] H. M. Hashemian and K. M. Petersen, "Achievable Accuracy and Stability of Industrial RTDs," from Seventh International Symposium on Temperature, Vol.6, Part 1, April 28 – May 1, 1992, Toronto, Canada, pp 427-432.

[11] X. Chaoying, "Development of Metal Sheathed Secondary Standard and Precision RTD Thermometers at Temperatures up to 960 °C and 1,100 °C," in *Temperature: Its Measurement and Control in Science and Industry*, D. C. Ripple (ed.), Vol. 7, 2003, pp 375-380.

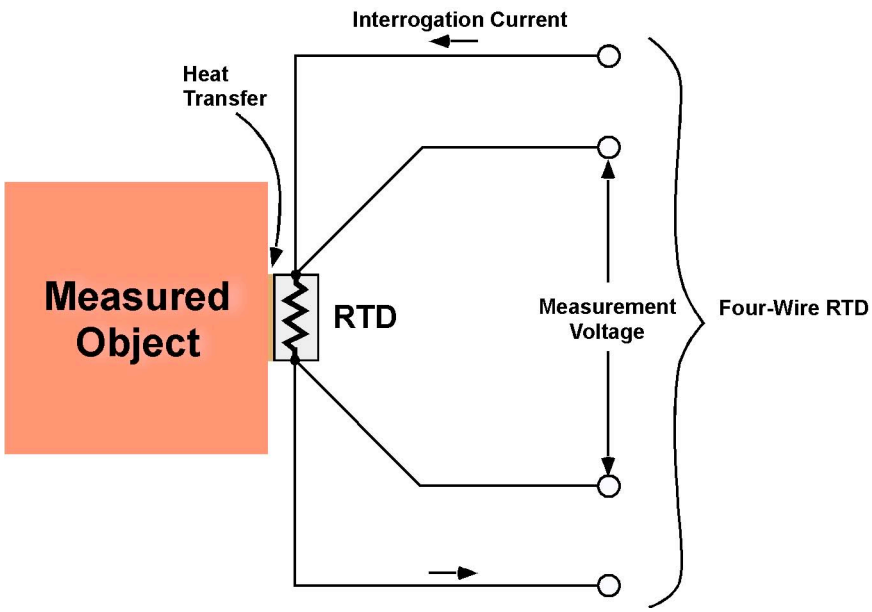

Figure 6. Configuration of a four-wire RTD.

Once a voltage measurement is made, corresponding to the resistance, temperature can be calculated. Unfortunately, the resistance-to-temperature transfer function not only varies over time because of corrosion and thermo-mechanically induced stress but it is also non-linear, i.e., a first-order multiplying factor is not sufficient to cover a wide temperature range with low error values. Therefore, two options are possible for converting the resistance value to the corresponding temperature: look-up table or equation. The equation method is easier to implement for fine temperature resolution and flexibility. The traditional, low-fidelity, method employs the Callendar-Van Dusen equation [Equation(3)] and coefficients. Table 1 displays the starting point coefficients for a third-order Callendar-Van Dusen equation. Note that while the Callendar-Van Dusen is not an especially accurate transfer function,[12] the new temperature measurement system only uses its second order extrapolation until sufficient time elapses for the stochastic Johnson noise temperature measurement to arrive at a sufficiently accurate measurement of the current temperature.

$$RTD = R_0\left[1 + AT + BT^2 + C\left(T - 100\right)^3\right], \tag{3}$$

where: RTD = RTD resistance at temperature T [°C],
R_0 = RTD resistance at 0 °C, and
A, B, and C are Callendar-Van Dusen coefficients (Table 1).

[12] http://www.its-90.com/its-90p3.html

Table 1. Callendar-Van Dusen coefficients for common RTD resistance temperature coefficients.

Standard	RTD Temperature Coefficient (α)	A	B	C*
DIN 43760	0.003850	3.9080×10^{-3}	-5.8019×10^{-7}	-4.2735×10^{-12}
American	0.003911	3.9692×10^{-3}	-5.8495×10^{-7}	-4.2325×10^{-12}
ITS-90/IEC751	0.0038505	3.9083×10^{-3}	5.775×10^{-7}	-4.183×10^{-12}

* Used for temperatures less than 0°C only. For temperatures higher than 0°C, C=0

A typical linearity fit is shown in Figure 7. The need for higher-order curve fitting is apparent.

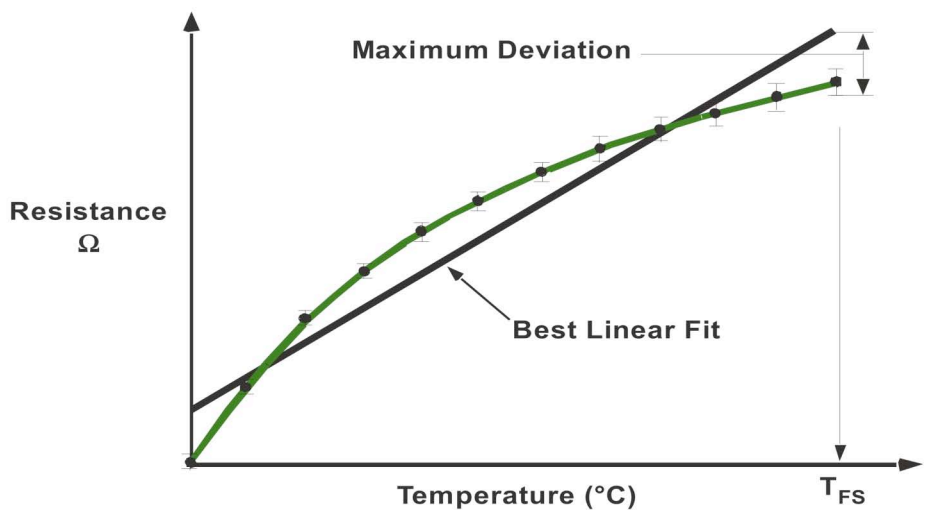

Figure 7. Linear fit to an RTD curve.

For temperatures greater than 0°C, "C" is 0, and the equation becomes:

$$RTD = R_0\left[1 + AT + BT^2\right]. \tag{4}$$

If a current I_{RTD} is passed through the RTD, and the voltage V_{RTD} measured, this equation can be solved for T [see Equation (5)], which becomes the transfer function for conversion of measured resistance to temperature value.

$$T = \frac{2\left(V_{RTD} - I_{RTD}R_0\right)}{I_{RTD}R_0\left[A^2 + \sqrt{A^2 + 4B\left(V_{RTD} - I_{RTD}R_0\right)/I_{RTD}R_O}\right]}. \tag{5}$$

RTDs provide accuracy and repeatability that are among the best of all temperature sensors, over a wide temperature range. Four-wire measurement techniques provide the highest accuracy because variation in lead wire resistance is compensated. However, time, temperature, mechanical stress, and neutron capture alter the transfer function

requiring a recalibration of the thermometer. The measurement system concept is to allow the temperature as measured by the JNT method periodically to correct the coefficients.

3.2.5. Combining the RTD and JNT

JNT is best understood as a continuous, first-principles recalibration methodology for a conventional resistance-based temperature measurement technique. The traditional method of directly measuring temperature from an RTD has unavoidable, unacceptable drift as described in previous sections. The JNT measurement is applied in parallel to the RTD lead wires along with the resistance measurement circuit without altering the traditional resistance measurement circuit. Note an issue to be addressed in the practical design is that the resistance measurement circuit must not introduce any significant noise into the frequency band used by the Johnson noise system.

One of the features of being a first-principles measurement is that Johnson noise does not require periodic calibration. Thus, the combined temperature measurement approach achieves the speed and accuracy of traditional resistance thermometry while adding the feature of automatic calibration. The benefits and detriments of un-calibrated resistance temperature measurement and the Johnson noise augmentation methods are compared in Table 2.

Table 2. Comparison of standard RTD and Johnson noise methods.

Measurement Method	Advantage	Disadvantage
Simple Resistance	• Fast Response • Less Complex Circuit Required	• RTD Transfer Function Drifts • Need to Calibrate
Johnson Noise	• Fundamental Temperature Measurement • Needs No Calibration	• Noise Signal Must Be Processed and Integrated

Overall, the long-term measurement uncertainty at moderate to high temperatures is greatly reduced by supplementing the resistance temperature measurement with Johnson noise-based re-calibration.

A block diagram illustrating the combined measurement process is shown in Figure 8. In the diagram, the RTD, which is exposed to process temperature, exhibits both a resistance value and Johnson noise. These two signals are separable and thus can be processed independently. The RTD's resistance measurement becomes input to the transfer function module, which uses a second order polynomial, similar to the Callendar-Van Dusen equation, to calculate temperature. Conceptually, the RTD's noise signal is processed according to the Nyquist equation to arrive at a non-drifting, low-uncertainty temperature value. The RTD's resistance temperature value is compared with the Johnson noise temperature and a correction is made to the transfer function. This correction can be made quasi-continuously or on a periodic basis (e.g., daily) depending on the RTD's drift-rate and target uncertainty values. As shown in Figure 8, the output of

the RTD resistance measurement system with Johnson noise correction periodically applied provides a prompt temperature measurement with consistently high accuracy.

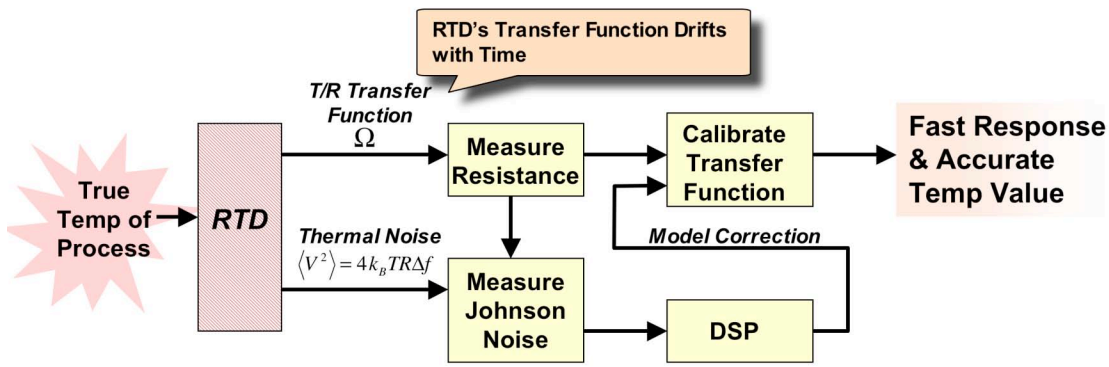

Figure 8. Basic functions required to automatically calibrate RTD from Johnson noise measurement.

3.2.5.1 RTD Resistance Selection for Johnson Noise Thermometry

High frequency filtering of the Johnson noise signals increases as the source resistance of the RTD increases; therefore, it is advantageous to keep the RTD resistance value low to preserve signal bandwidth. However, as resistance decreases so does the signal level because the Johnson noise signal-level is proportional to the real part of impedance (resistance). Further, the RTD's resistance should be somewhat above the noise equivalent resistance of the input preamplifiers to minimize contamination of the Johnson noise with unrelated amplifier noise. Note that a low-noise, wide-bandwidth preamplifier has a noise-equivalent resistance of about 25 ohms. All of these competing factors (maximize bandwidth, maximize signal level, and stay above the amplifier's noise floor) must be balanced to select an RTD's operating resistance value.

Maximizing Johnson noise bandwidth is important in achieving accurate temperature readings in a short time. The bandwidth directly affects the averaging time to achieve a desired uncertainty in the temperature measurement. The fractional standard deviation, which is the standard deviation divided by the expected value, is given by Equation (6) as

$$\frac{\sigma}{E} = \sqrt{\frac{1}{\Delta t \cdot \Delta f}}\ , \tag{6}$$

where σ/E is the fractional standard deviation, Δt is the measurement time, and Δf is the bandwidth. Therefore, to achieve 0.1 percent uncertainty with a bandwidth of 100 kHz requires at least 10 seconds of measurement time or averaging of samples. Refer to Appendix A for detailed statistical analysis.

The lower cut-off frequency of the Johnson noise measurement must be selected sufficiently high to exclude cable triboelectric and microphonic noise. These vibration-induced noises can overload the preamplifier input and contaminate the Johnson noise

signal. Experience has shown that many of these effects are do not exceed about 20 kHz. A lower bandpass frequency 50 kHz is sufficient to suppress these effects.

The Johnson noise signal is very low amplitude as indicated in Table 3, which relates typical resistances to impedances in electronics systems. Figure 9 graphically shows Johnson noise voltages for resistances up to 1000 ohms. The effect of RTD resistance on the corner frequency of a single pole filter (as formed by a simple RC network) is shown in Figure 10 with a family of three capacitance values: 100 pF, 10 nF, and 1 μF.

Table 3. Thermal (Johnson) noise voltages at room temperature.

Resistance (Ω)	Noise voltage spectral density (nV/√Hz)	Applications
1	0.127	Reference value and low temperature resistances
25	0.635	Lower noise limit of very good wideband amplifier
50	0.899	Instrumentation and RF
75	1.10	CATV
100	1.27	Commonly used Platinum RTD
150	1.56	Professional microphones
200	1.80	Platinum RTD
600	3.12	Professional audio, DSL, traditional telephone system
1000	4.02	Reference value
4700	8.72	Consumer electronics
10,000	12.7	Reference value
47,000	27.6	Consumer electronics
1 million	127.0	Reference value

Note: Resistance at room temperature [293 K (20°C)]

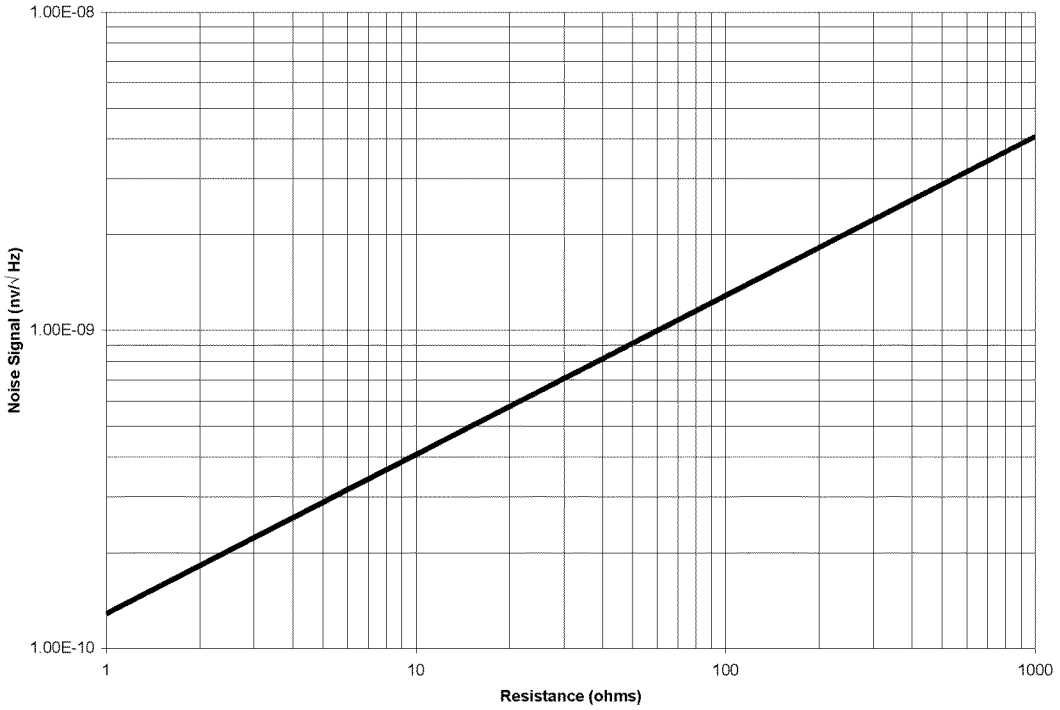

Figure 9. Noise signal versus RTD resistance (293 K temperature).

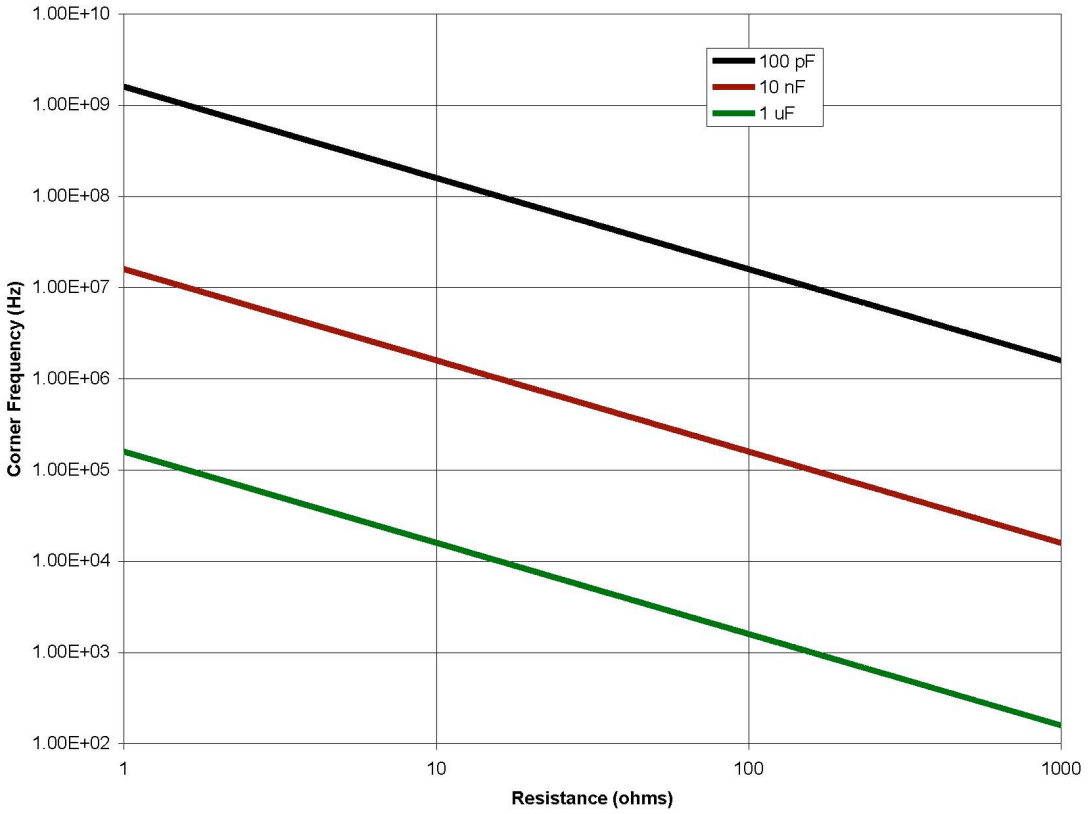

Figure 10. Corner frequency (bandwidth) of simple RC versus RTD resistance.

3.2.5.2 Cabling Considerations

The Johnson noise augmentation to RTD temperature measurement requires additional electronics. The electronics require high-gain amplifiers with junction field-effect transistor (JFET) input and digital signal processing algorithms. Johnson noise is a temperature proportioned small signal, whose frequency content is significant to the measurement. Long cables reduce the amplitude of high-frequency signals by filtering the upper frequencies, which reduces signal bandwidth. Ultimately, lower bandwidth increases the interval between Johnson noise corrections of the RTD transfer function.

Cable capacitance directly limits the allowable separation distance between RTD and input electronics. Typical coaxial cables exhibit a distributed capacitance of about 100 pF/m. As an example, the maximum available bandwidth versus cable length for a 100 Ω RTD that exhibits losses of less than 0.1 percent of the noise power is shown in Figure 11, given a 50 pF input capacitance of the JFET. For a five-meter separation between RTD and input electronics, a 100 kHz bandwidth is predicted given these assumptions. In fact, this calculation is conservative since an RTD housed in a mineral insulation sheath may actually have much less effective capacitance. For the recently fabricated ORNL system, the head box containing the JFET input preamplifier is located about one meter from the RTD. The bandwidth of that system, in actual experience, is close to one MHz; whereas a 350 kHz bandwidth is predicted from Figure 11. Refer to Appendix B for more details on cable effects modeling.

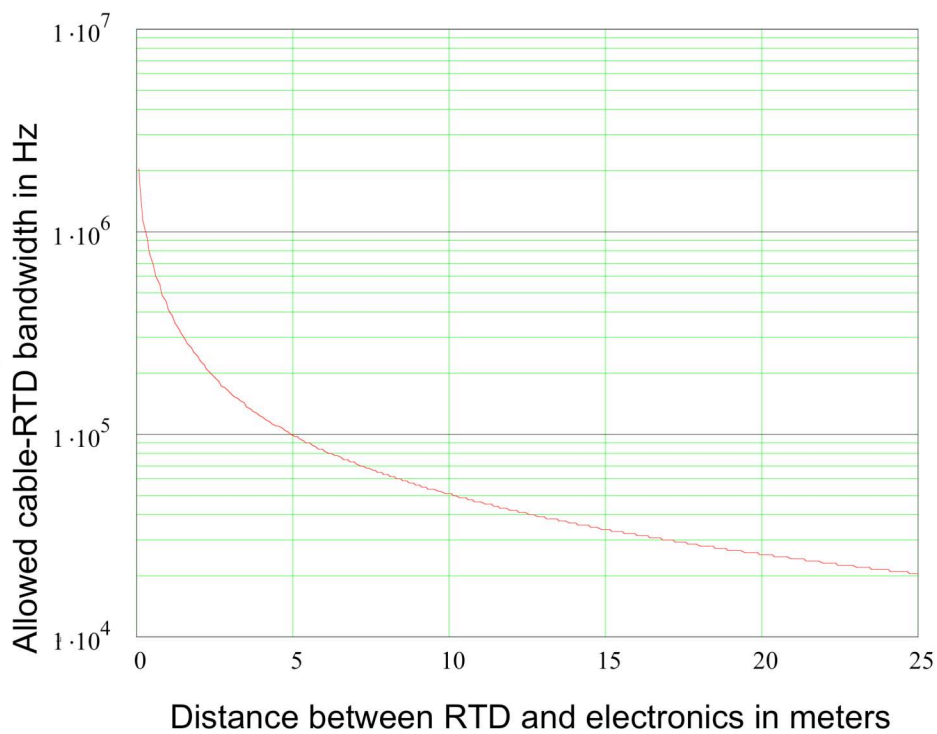

Figure 11. Cable bandwidth as a function of length.

4. System Implementation

The JNT development has progressed to the point of fabrication of two duplicate JNT instruments. This represents a significant technical achievement, as these units are by far the most advanced Johnson noise measurement systems ever built. Attempts to measure temperatures at nuclear power plants using Johnson noise thermometry have now been going on for more than 30 years and the use of Johnson noise for temperature measurement is now more than 50 years old. While several of the attempts to employ Johnson noise thermometry at nuclear plants have been significant accomplishments, JNT is not yet used at any nuclear plant and more generally, JNT measurement instrumentation is not currently commercially available. Simply put, Johnson noise thermometry while conceptually highly appealing has in-practice proven very difficult to implement in a sufficiently robust and cost-effective manner as to be viable. ORNL's fabrication and replication of a mechanically robust JNT instrument using standard electronics and instrumentation technology within the first two years of this project is a dramatic technical advance and appears likely to lead towards general application of this technology in nuclear reactor thermometry throughout GenIV plants. Further, KAERI has supported JNT deployment in a plant environment by transferring the high-speed digital signal processing of the ORNL units performed at the control room from a personal computer based system to a dedicated digital signal processing system employing technologies that could be licensed for nuclear plant control system use. Ohio State has created a testing environment for the ORNL Johnson noise thermometry instruments to allow demonstrating the performance and viability of the instruments under simulated nuclear power plant operational conditions.

4.1. I-NERI JNT Implementation

While the underlying concepts (under NASA sponsorship) and a laboratory prototype (under EPRI sponsorship) of both the cross correlation and digital signal processing had previously been developed by ORNL and the University of Tennessee, the high speed digital signal processing required remained prohibitively expensive in the early 1990s. Consequently, the cross-correlation amplifier electronics were never implemented in an integrated form, and the signal processing software was never finalized.

4.1.1. Dual Mode System

The current project is focused on implementing a dual-mode resistance and Johnson noise thermometer in a rugged, integrated, prototype form. The resistance measurement serves the dual purpose of providing the necessary impedance measurement for the Nyquist equation as well as providing a prompt temperature measurement. Since Johnson noise is a stochastic process, some time is required to perform a measurement. The temperature measurement in the dual mode thermometer is therefore made as a simple resistance measurement whose resistance-to-temperature conversion is quasi-continuously updated using Johnson noise.

The dual-measurement-mode process block diagram of Figure 8 is expanded in Figure 12 to show the additional function of end-to-end channel calibration. In the diagram, the RTD, which is exposed to process temperature, produces both a resistance value and

Johnson noise. These two signal types are separated in the instrument head and processed independently. The head system generates a dc resistance value and two Johnson noise outputs from two independent amplifier channels. These signals are buffered allowing them to pass over long distances (up to 300 meters). A receiver converts the three signals for delivery to a computer system. In the computer software, DSP is applied to derive the Johnson noise temperature and the transfer function is corrected with the noise temperature to generate a fast-responding temperature. The channel gain measurement is necessary to compensate for changes in amplifier gains and cabling attenuation. The outputs shown are a fast response RTD output, which is periodically calibrated by the slower Johnson noise temperature, and a slow output from the Johnson noise thermometry portion of the system. In reality, the only necessary output is the fast response temperature since it has been corrected to match the Johnson noise temperature.

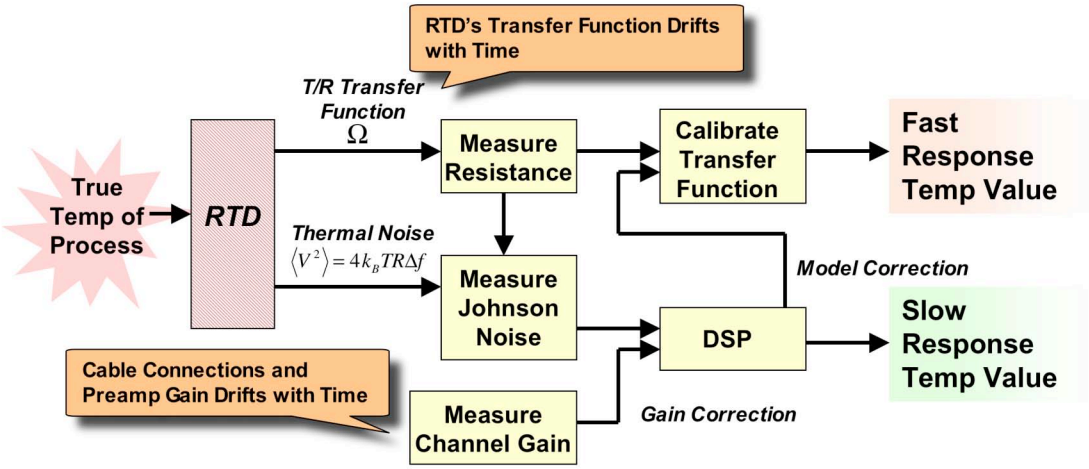

Figure 12. Johnson noise thermometry measurement process block diagram.

The DSP software derives the CPSD from the two noise channels, from which the CPSD is obtained. The CPSD is divided by the cross-power transfer function (CPTF) of the amplifiers to estimate the sensor noise voltage PSD. The resistance is independently measured and the temperature is estimated by dividing the sensor noise PSD by $4k_BR$.

A layout of the system hardware components is shown in Figure 13. High-gain, wide-band preamplifiers for the Johnson noise signals and a precision resistance bridge have been implemented in high-density, discrete component electronics. A continuous amplifier-gain-calibration scheme has also been implemented. The digital signal processing logic has been implemented in LabVIEW™ on a desktop computer and also has been implemented as a field programmable gate array (FPGA) and dedicated DSP chip format. The preamplifier head and resistance probe have been packaged in a shielded aluminum enclosure and a coaxial signal interconnection scheme has been implemented. Details of the design are provided in the Appendices.

End-to-end channel gain is measured by slowly frequency-modulating a sinusoidal signal of known and constant amplitude from lowest to highest channel bandpass frequencies.

The block entitled Channel Calibration Generator in Figure 13 capacitively couples the sweep signal in parallel with the Johnson noise signal, which all is amplified by successive gain and driver stages. The analog-to-digital converters (ADC) are located in the computer as a PCI card. Computer software calculates a transfer function for the noise channel and normalizes the system response to that transfer function.

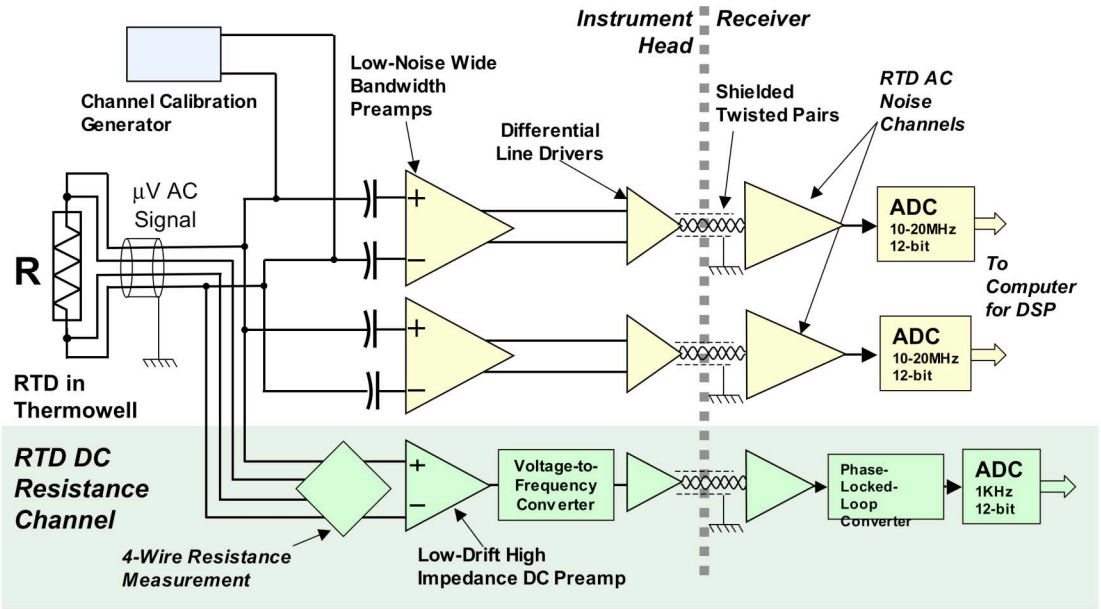

Figure 13. Principal Components and conceptual configuration of the dual mode resistance and Johnson noise thermometer incorporating the cross-correlation technique, digital signal processing, and channel gain calibration

Figure 14 presents a general block diagram of the connectivity of the receiver system. Each of the two noise channels connects from the preamp/cal head-end box via two sets of coaxial cables arranged in differential pairs. The preamplifier board contains two identical differential-input JFET preamplifiers/filters/gain sections each with a voltage gain of approximately 80 dB and a center frequency of approximately 650 kHz. Each of the two single-ended signal paths is converted to differential with a high-bandwidth differential amplifier capable of driving 300 m of coaxial cable. Each of these cables is terminated in 50 ohms at the receiver box with the shields tied together at the head-end box and isolated. The conductors are further isolated by using capacitive coupling instead of transformer coupling to minimize pickup. The calibration board contains a swept-frequency oscillator. The oscillator supplies the calibration signal over the noise bandwidth of the amplification chain by sweeping continuously from 50 kHz to 2.5 MHz over about a 2-second period. The oscillator is coupled directly into the front-end preamplifier. A 100 μA current is supplied to the input also and a separate differential amplifier measures the voltage drop across the RTD. This voltage is amplified and converted to a 20 kHz to 90 kHz differential pulse stream that is then sent to the receiver box, which converts it back into a voltage proportional to the value of the resistor. The voltage to frequency conversion is done to eliminate cable resistance effects and in-band

noise pickup problems. The head-end box has an associated power-supply box, which supplies all dc voltages necessary for operation. The preamplifier and calibration boards are mounted as a sandwiched pair separated by a sheet steel shield.

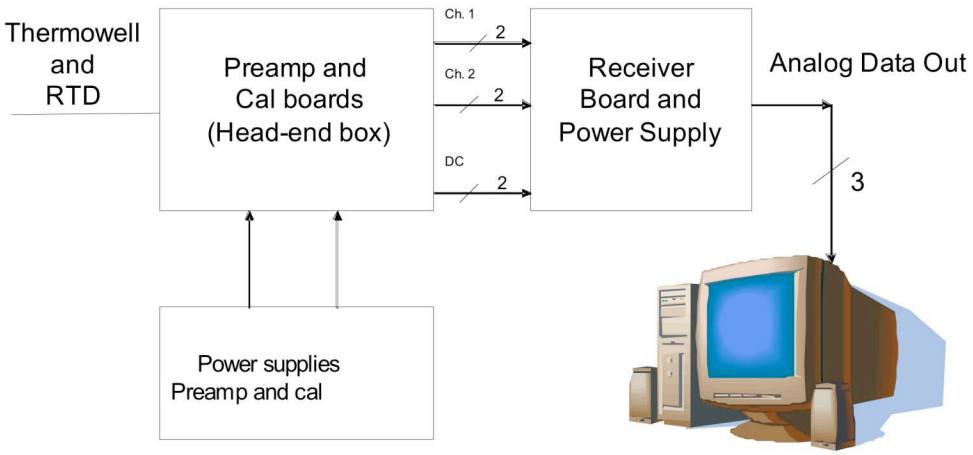

Figure 14. System block diagram

The receiver box of the JNT setup shown in Figure 15 consists of two Johnson noise measurement channels and one dc resistance measurement channel. Variable gain 250 MHz differential-to-single-ended amplifiers receive the signals for the three channels differentially. The Johnson noise channels consist of this amplifier followed by a 4-pole Sallen-Key High pass filter with a low-frequency cut-off of approximately 80 kHz. This is then followed by a 4-pole Sallen-Key low-pass filter with a high-frequency cut-off of approximately 2 MHz. The entire channel has a variable gain of 1 to 10. The dc resistance channel has a front-end differential receiver amplifier similar to the Johnson noise channel. The signal then passes through a 2-pole Sallen-Key high pass filter that has a low-frequency cutoff of approximately 15 kHz. The filtered signal is discriminated to get a rail-to-rail equivalent frequency signal, which is then passed into a phase-locked loop used as a frequency-to-voltage converter. The resulting output voltage is proportional to the dc equivalent of the resistance measured at the transmitter front-end. The single-ended signals out of these three channels are sent to a computer-based DSP using a 4-channel 20 M sample/second ADC board.

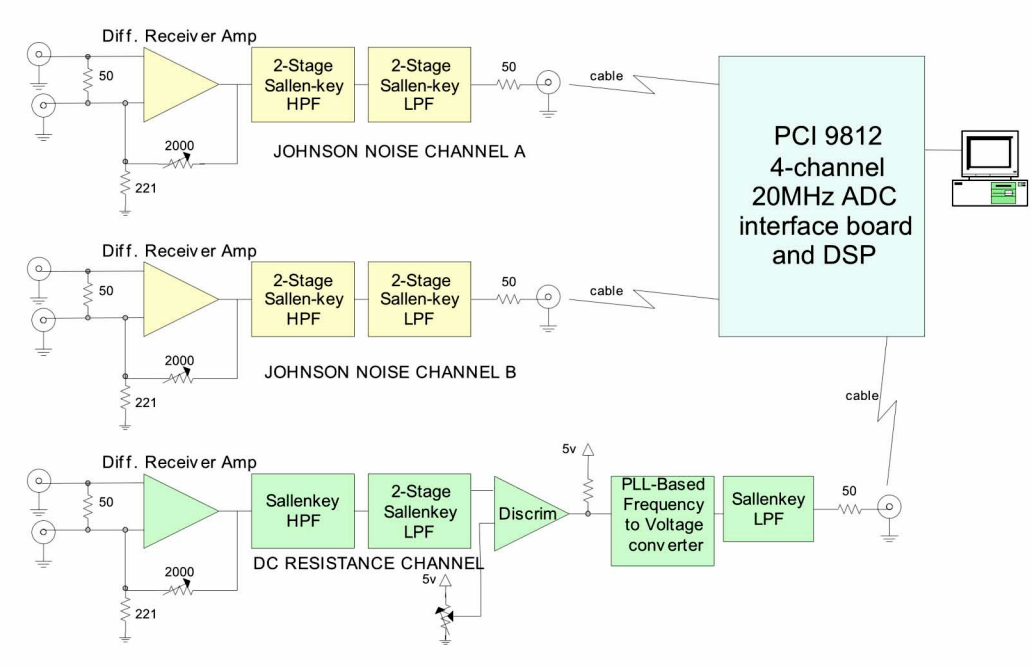

Figure 15. Block diagram of the receiver section

4.2. Instrument Head Overview

4.2.1. Purpose/Description

The JNT instrument head consists of a sealed RTD thermowell suitable for reactor coolant applications mated with a specially designed electronics head assembly. The head assembly contains two sets of measurement electronics. (1) A low frequency, low-drift amplifier subsystem measures the RTD's resistance value for rapid tracking (τ = 0.1 s) of temperature change and passes the signal by a current loop through coaxial cables to receiver electronics in a rack-mounted cabinet. The RTD resistance measurement subsystem employs either a current source or balanced bridge or combination of both to convert RTD resistance to a voltage/current signal. (2) A high frequency, low-noise amplifier subsystem amplifies the RTD's temperature-dependent Johnson noise for transmission over coaxial cables also to the receiver electronics. Two identical high-frequency preamplifiers and line drivers are employed, which allow cross-correlation methods to reduce internal preamplifier noise contribution. An in-band reference calibration variable frequency signal is injected into the front-end of the preamplifiers, which is used calculate channel gain and linearity—thus compensating for variations in amplifier gain, cable attenuation, and other factors that would contaminate the Johnson noise spectrum. A layout of the detector head is shown in Figure 16.

.

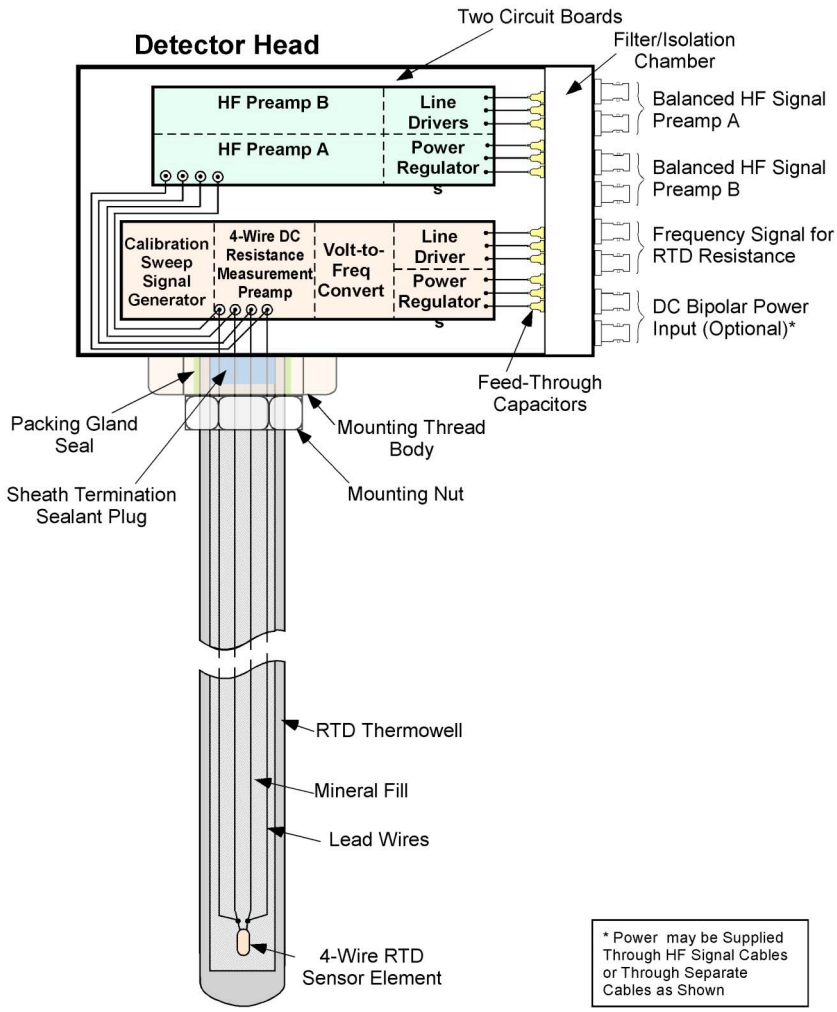

Figure 16. Detector head enclosure with attached RTD probe

4.2.2. Connections

Electrical connections between the instrument head and the receiver are made by coaxial cables using BNC connections. The design was to drive signals to a distance up to 300 meters. Balanced drive is used to reduce external noise pickup. Four 50-Ohm cables are used for the two high-frequency channels and one shielded twisted pair cable will be used for the RTD resistance signal, which will be a current drive. dc operating power may be sent down the high-frequency signal cables if it does not cause interference. The fabricated system used a separate shielded twisted pair for supply power.

4.2.3. System Performance

The following are target values for the system that were set at the start of the project.

4.2.3.1 RTD Element

Thin Film Platinum
100 Ohm @ 0°C
$\alpha = 0.00385\ \Omega/\Omega/°C$
Measurement Range: 25°C to 450°C

4.2.3.2 High Frequency Preamplifiers

Response: 20 kHz to 5 MHz
Gain: >1000 (to get noise signal up to about 1 VRMS on head-end to receiver cables)
Preamplifier Noise: <10 nV/√Hz
Input Impedance: >10MΩ

4.2.3.3 Line Drivers

Output Impedance: 50Ω
Drive distances may be up to 300 meters

4.2.3.4 Low Frequency Preamplifier and Resistance to Frequency Conversion

Measurement resolution: 0.1ºC over range of 25ºC to 450ºC
Noise: below resolution limit
Frequency Drive: 15 kHz to 150 kHz

4.2.4. Size

Head assembly is not important to fit a particular minimum or maximum profile. Recommend dimensions of 25 cm longest side.

Sheath diameter: 9.525 mm OD or equivalent

4.2.5. Materials

Case should provide good magnetic as well as electrostatic shielding. Recommend 400 series stainless steel (could also user 300 series with an inner liner of mu-metal). Thermowell must be compatible with piping. Note that enclosure used in the current implementation is aluminum.

4.2.6. Temperature and other Environment

Measurement will be made in water with a range from 25ºC to 450ºC. Environment surrounding the detector head will be from 25ºC to 40ºC with up to 95% RH. The equipment is not required to survive in a condensing atmosphere or submerged.

High vibration is expected. Internal components should have low mass and be well secured.

Instrument head electronics are not radiation hardened. Hence, shielding will be required for sustained operation within containment.

4.2.7. Mounting

A thermowell will be the reactor-system pressure boundary (2200 psi, 15MPa). RTD sheath inserts into thermowell. Head assembly will either be self-supporting or require separate supports. Detector heat must survive constant vibration.

4.3. Receiver Description

The receiver box has three differential input channels: two for receiving the noise signals from the ultra-high gain preamplifiers in the head box and one for receiving the dc temperature values (as a frequency-encoded signal). The receiver contains additional filtering and buffering to reduce non-signal noise contamination. The single-ended outputs from the receiver box are connected to a PCI9812 ADC board mounted in a computer with which the values are processed using software. The ADC board is equipped with four input channels with a sampling rate up to 20 MHz. The receiver box has a built-in 120 V_{AC} power supply.

4.4. DSP Subsystem

KAERI researchers developed a FPGA implementation of the digital signal processing system based on theoretical work done at ORNL. The following subsections describe their FPGA implementation.

4.4.1. Data Acquisition

The voltage signals of the two Johnson noise channels and the dc resistance channel are converted into 12-bit digital numbers by three ADC channels. The digital data are stored in the arrays for each channel. The sampling time of the data is the same as the sampling time of the A/D converter in the DSP subsystem. The number of samples for one block period is 1024 samples. Therefore, the array [block] size of each input array is the same as the number of samples for one block period. The signal of each channel is gathered in the same time scan of the A/D data acquisition scan. Channel A, Channel B, and dc resistance measurement channel are measured in one scan time.

4.4.2. Windowing

The Hanning windowing technique is used in the first part of the digital signal-processing algorithm. It drastically decreases the energy leakage caused by the frequency-resolution mismatch problem of a practical Discrete Fourier Transform (DFT). The windowing function shrinks the first and last data to zero and smoothly increases the magnitude as shown in Equation (7) and Figure 17. Figure 18 illustrates the change in the energy leakage when the Hanning windowing is used, compared to non-windowing (or rectangular windowing) method, where a sinusoidal signal of frequency 255.5 kHz with 1,024 point sample block transformed at the sampling rate 1024 kHz. Only a small amount of energy leakage remains on the neighboring points of the input frequency. The small remaining leakage is unavoidable as long as the DFT is used on the blocks of finite length size.

$$Y[k] = 0.5 - 0.5\cos(2\pi k / N - 1)\,, \tag{7}$$

where k: index, N: Block Size(=1024)

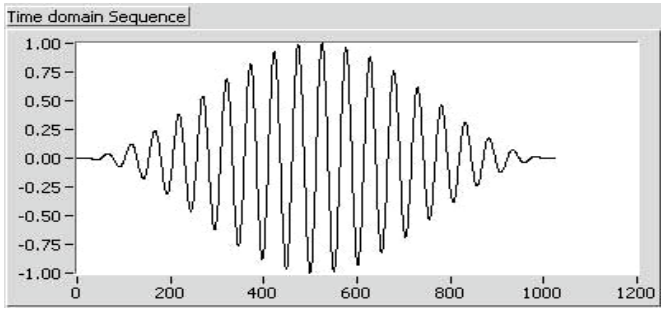

Figure 17. Hanning window function

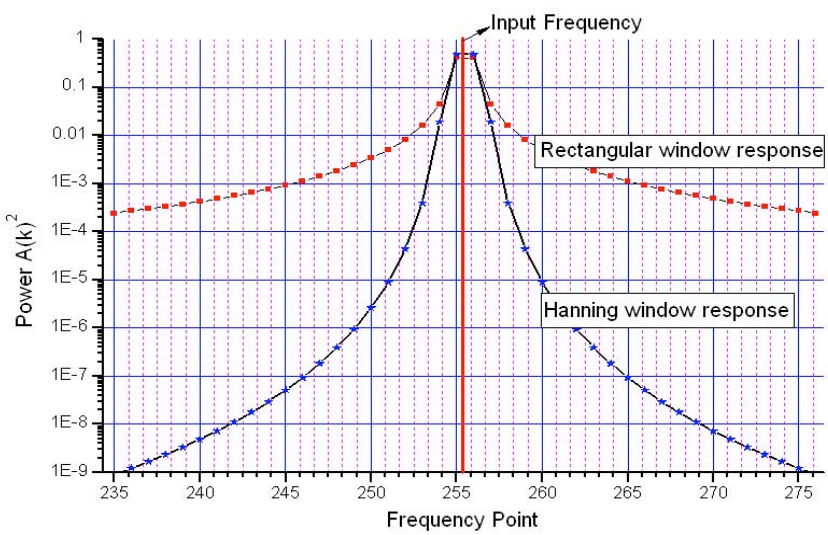

Figure 18. Energy leakage enhancement of Hanning window response

4.5. Discrete Fourier Transform

The data stored in the input array are transformed into the frequency domain by a DFT function. The output of DFT module expresses the amplitude of each frequency component for the sampled data, i.e., the DFT algorithm converts the 1024 time domain signal values into 1024 frequency domain signal values. Among those 1024 points, the second half of 512 points is the duplicate of the first 512 points. Therefore, the double of the first 512 points are used (a 'single sided DFT'). The measured signals only from Channel A and B are transformed into the frequency domain.

An FPGA is used to perform the high speed DFT function. The speed of DFT calculation is one of the most important factors for the development of a JNT.

4.6. Cross Power Spectral Density

A cross correlation function of two signals is used to remove the independent noise generated in each high-frequency preamplifier. The cross correlation function indicates

the degree of similarity of two signals. The cross correlation of two independent random signals exhibits very low numerical value at most of points. Most of the random noise signals generated by each amplifier channel are canceled when the output signals of Channel A and B are subjected to a correlation function. The common mode signals from the RTD resistor or from external sources produce a spike at the "zero" point. In addition, the external sine wave calibration signal shows up in the correlation function. Therefore, known exogenous frequencies should be removed prior to applying the cross correlation function in order to extract the pure Johnson noise from the resistance sensor. The calculation of correlation function of the two signals takes a long period. Furthermore, it is very difficult to find any particular external frequency signal and remove it on the time domain. The cross correlation function in the time domain corresponds to the cross-energy spectral density in the frequency domain. Therefore, it takes a shorter time and is convenient to use DFT and calculate CPSD than to calculate a correlation function in the time domain. For measuring the average of the Johnson noise, only the average of CPSD function is needed. The cross-energy (power) spectral density of channel A and channel B will be:

$$\text{CPSD of X and Y} = X(\omega)\bullet Y(-\omega) = X(\omega)\bullet Y^{*}(\omega)\,. \tag{8}$$

And the correlation function of two signal x(n) and y(n) is

$$R_{xy}(k) = \sum_{n} x(n)y(n-k) \quad = \sum x(n+k)y(n) \qquad l = 0, \pm 1, \pm 2\ . \tag{9}$$

4.6.1. Short-term Average

Because of the limited size of sample block, i.e. 1024 of samples, the DFT of one block of random noise cannot be flat in the frequency domain. Therefore, it is necessary to make a long term average of the CPSD to extract the ensemble average magnitude of each frequency point. However, because the sinusoidal calibration signal is continuously sweeping all through the bandwidth, the period of averaging must be shorter than the period that the calibration signal remains for between two subsequent frequency points on CPSD. If the averaging period is longer, the peak of the sweeping calibration signal distorts the CPSD. It is assumed that 10 times of averaging of CPSD or less will be suitable to ensure that the calibration signal stays between two resolution points.

For implementation in a FPGA chip, a moving average method is used as follows,

$$
\begin{aligned}
\bar{x}_{n-1} &= \frac{1}{N}\left(x_{n-1} + x_{n-2} + \cdots x_{n-N}\right), \\
\bar{x}_{n} &= \frac{1}{N}\left(x_{n} + x_{n-1} + \cdots x_{n-N+1}\right) \\
&= \frac{1}{N}x_n + \frac{1}{N}\left(x_{n-1} + \cdots x_{n-N+1} + x_{n-N}\right) - \frac{1}{N}x_{n-N} \\
&= \frac{1}{N}x_n + \bar{x}_{n-1} - \frac{1}{N}x_{n-N} \\
&\approx \frac{1}{N}x_n + \bar{x}_{n-1} - \frac{1}{N}\bar{x}_{n-1} \\
&= \frac{1}{N}x_n + \left(1 - 1/N\right)\bar{x}_{n-1}
\end{aligned}
\tag{10}
$$

4.6.2. Magnitude of CPSD

The CPSD is a complex number and thus has real and imaginary parts. JNT calculation needs magnitude information to identify the strength of each frequency component. The magnitude of the short-term averaged CPSD is calculated as:

$$
\left|CPSD\right| = \sqrt{X_{re}^{\ 2} + X_{re}^{\ 2}}\ , \tag{11}
$$

where X_{re} is the real part and X_{im} is the imaginary part of X(w)

4.6.3. Bandwidth Cut-Off

The DFT function creates 512 data point on CPSD per block. Frequency range covers from 0 Hz to the half of the sampling frequency. However, the JNT needs the accepted CPSD within the bandwidth, because the CPSD value beyond the bandwidth is near zero. Therefore, data beyond the bandwidth from the 512 CPSD array are discarded. The first index and the last index of the CPSD array are calculated as

$$
FirstIndex = ArraySize(512) \times {LowCutoffFreq}/{HalfOfSampleFreq} \tag{12}
$$

$$
LastIndex = ArraySize(512) \times {HiCutoffFreq}/{HalfOfSampleFreq} \tag{13}
$$

4.6.4. Gain Correction and EMI cancellation

A pilot signal is fed into the preamplifier input circuit and the amplitude and frequency of the signal is known and very stable by careful electronics design. The frequency of the calibration signal is swept through the entire bandwidth of the amplifier channels. The amplitude of this pilot signal is measured from the CPDS data to extract the amplification gain of the amplifier channel.

The gain of amplifier channel on the total Johnson noise path is calculated by detecting the output magnitude of the calibration signal on CPSD and dividing it by the input magnitude fed into the RTD.

Even though the random and independent noise in the preamplifiers is canceled with a CPSD function, the peaks of particular frequencies caused from any EMI source may exist in the spectrum range. Those peaks above the flat range of spectrum should be regarded an EMI source — not a part of Johnson noise —and removed from FFT output the CPSD or cut to fit to the envelope of the CPSD.

4.6.4.1 Threshold Value

The calibration signal presents as a tall peak on the CPSD distribution. It is much taller than CPSD values contributed by Johnson noise signal. Therefore, it is detected by threshold comparison. The threshold value is determined by the magnitude of the middle area of the Johnson noise CPSD. If the threshold value is chosen as 10 times higher than middle value of the CPSD, it avoids most of fluctuation error of the CPSD distribution. Furthermore, it is assumed that the EMI noise peaks are always smaller than calibration signal peaks.

The logic of threshold calculation is

- Pick up the median value of 11 points centered at the middle of CPSD
- Threshold Curve: $Y[k] = 10 \times median \times \{0.5\sin(\pi k / N) + 0.5\}$

4.6.4.2 Gain Curve Extraction

The high peak of the calibration signal on the CPSD is extracted to form the amplification gain curve. The highest peak on the CPSD is regarded as the calibration signal. Because some part of energy is spread into neighboring points of the calibration peak, several other values around the peak are summed to the peak to produce the peak value of the calibration signal. The logic is as follows:

- Initially,
    - If the maximum value among the CPSD is lower than the corresponding threshold (no detection of calibration peak), then initialize the gain curve with the threshold curve.
    - Else, (detection of calibration peak), the maximum value of the CPSD becomes the gain value of the point and the other gain values are formed via a curve-fitting with a sine curve.
- Next iteration,
    - If the value of the (base-removed) CPSD is bigger than the threshold value then 9 values (including itself) around the index are summed and update (replace) the previous gain curve array element value.
    - Else, the previous gain-array is maintained.

4.6.4.3 Gain Curve Smoothing

The Gain Curve driven from the calibration signal has fluctuation because of the stochastic nature of Johnson noise and other influences such as DFT resolution, block

size, baseline CPSD error, etc. Therefore, the JNT makes a long-term average on the Gain Curve and performs a smoothing function. However, long-term averaging causes a long response time to sudden gain changes. A multi-order smoothing algorithm is applied as follows:

$$Y(w)_{smooth} = \tfrac{1}{380}X(w-3) + \tfrac{16}{380}X(w-2) + \tfrac{77}{380}X(w-1) + \tfrac{192}{380}X(w) + \tfrac{77}{380}X(w+1) + \tfrac{16}{380}X(w+2) + \tfrac{1}{380}X(w+3) \quad (14)$$

4.6.4.4 CPSD Flattening

The characteristic frequency curve of the Johnson noise path is not flat through the bandwidth because of three band-pass filters: gain near the center frequency is the highest. Therefore, the CPSD values on lower gains are compensated by the deviation between the highest gain and individual gain value of each frequency point.

The analog amplifier channel gain (including cable effects) is corrected as follows:

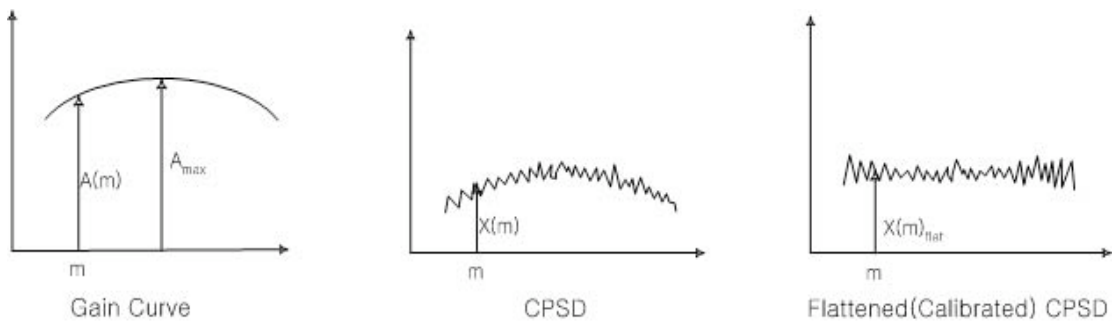

Figure 19. CPSD flattening

$$X(m)_{flat} = X(m) \bullet {A_{\max}}/{A_m}, when\ A_m > 0 \quad (15)$$

$$X(m)_{flat} = X_{\max}(m), when\ A_m \le 0 \quad (16)$$

- *X(m)* : Bandwidth-Cut-CPSD
- A_{max} : Average of 20 values around the point where the maximum value among the Smoothed Gain array(input-1) is located.
- A_m : The value (Gain value) of index *m* on the Smoothed Gain array(input-1)
- X_{max}: The greatest value among *X(m)*

4.6.4.5 Deglitch of EMI and Calibration Signal Peaks

Any EMI peak should to be removed from the CPSD distribution. By this function, the peak of the calibration signal is also removed. Theoretically, a sinusoidal signal presents as a big peak at one frequency point. In a real implementation, it has a certain width because of the frequency resolution limit, frequency misinterpretation in discrete DFT, ADC sampling, etc. In fact, the energy of one single frequency is spread through several frequency points around the nearest DFT point. Discrimination is performed by

differentiation of the magnitude of each CPSD value. The threshold is adjusted depending on the FFT block size (1024), cycles of short term averaging (10 times), and average of magnitude of Johnson noise. Assuming a 1024 sampling block and 10 averaging cycles, 7 times the standard deviation of CPSD is a useful threshold, which does not cut off any stochastic peak of Johnson noise.

The algorithm is

- Detect EMI peak and cancellation
    - Put the input flattened CPSD into a Temporary array
    - Calculate the Mean and Standard Deviation of the Temporary array
    - If the maximum value among the array is lower than the deglitching threshold (mean + 7-times of Std. Dev.), then pass the array and escape the loop. (No detection of EMI or Calibration peak)
    - If the maximum value among the array is bigger than the deglitching threshold (mean + 7-times of Std. Dev.), then 9 samples around the maximum value are deleted (DFT Leakage) and the array is rebuilt without the deleted 9 samples. (Detection of EMI or Calibration peak)
    - Do again from the beginning with the modified array until the escape condition is satisfied.

- Calculate the mean and standard deviation of the final modified array
    - Check the input flattened CPSD array
    - If any value of the array is larger than 2 times of Std. Dev plus the mean value of the modified array, then replace the value to the mean
    - Else no change
    - Calculate the new mean value as follows

$$\bar{x}_{new} = \frac{\sum_{0}^{N-1} x_{new}[m]}{N}, \quad x_{new}[m] \le 7\sigma + \bar{x}_{new} \tag{17}$$

4.6.4.6 De-flattening the Deglitched CPSD

In order to obtain a baseline CPSD to be used as a pure Johnson noise CPSD, it is necessary to restore the straitened-deglitched-CPSD into the original curve-shaped CPSD. This function is performed by the reversed operation of CPSD flattening algorithm. The de-flattened CPSD does not contain any EMI peak and calibration signal peak.

The function is expressed as following figures and equations.

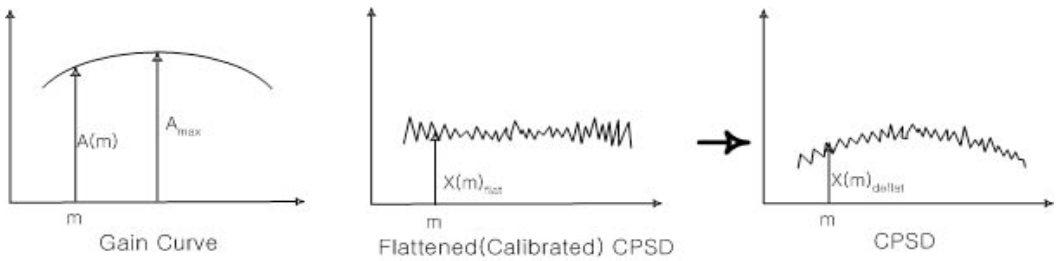

Figure 20. CPSD de-flattening.

$$X(m)_{deflat} = X(m)_{flat} \bullet {A_m}/{A_{\max}}, when\ A_m > 0 \quad (18)$$

$$X(m)_{deflat} = X(m)_{flat}, when\ A_m \le 0 \quad (19)$$

- $X(m)_{flat}$: Deglitched Flattened CPSD
- A_{max} : Average of 20 values around the point where the maximum value among the Smoothed Gain array(input-1) is located.
- A_m : The value (Gain value) of index m on the Smoothed Gain array (input-1)

4.6.4.7 Base line removal

The new input CPSD data for next iteration includes all of Johnson noise power and calibration signal power. Therefore, the magnitude of calibration signal is obtained by subtracting the de-flattened CPSD (CPSD of pure Johnson noise) from the new input CPSD.

4.7. Temperature Calculation and Display

4.7.1. Conversion of CPDS to JNT Value

From Equation(1), the absolute temperature value of RTD sensor is calculated as:

$T = \Sigma$ CPSD / ($4k_BR\ \Delta f\ A$), where, R is the measured resistance value of RTD, Δf is the bandwidth of the CPSD, k_B is Boltzmann's Constant, and A is the amplifier gain.

4.7.2. Update the Resistance-to-Temperature conversion table

The absolute temperature calculated by Johnson noise CPSD is used to compensate the resistance-temperature conversion table. A nominal 100Ω RTD is used as the sensor for JNT.

4.7.2.1 Table Form

The table consists of a one-dimensional array. The index indicates resistance and its content is the temperature value for the resistance.

X axis: 0 – 200 Ohms (one point per one Ohm)

Y axis: **T = (R-100)/0.385 [°C]** (from the equation R =100 + 0.385 T)

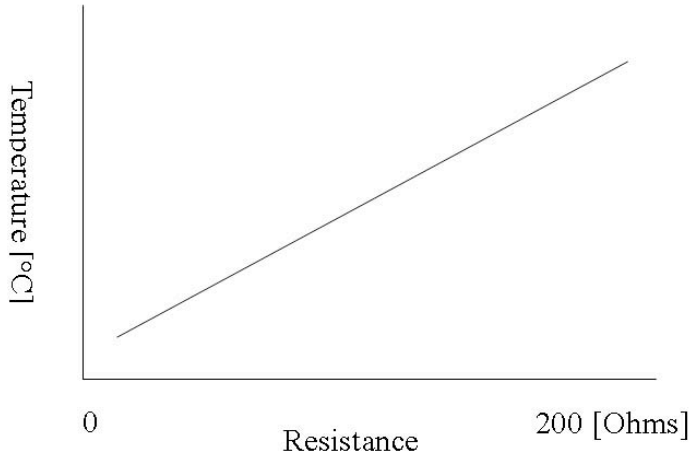

Figure 21. R-T Conversion table format.

So, the first value of array (index zero) becomes -259.7 corresponding zero Ohms and the second value (index 1) is - 257

4.7.2.2 Modification of R-T Table

When a new JNT value is created, the R-T table is modified based on the new value driven by Johnson noise. From the figure below and the relationship, the nearest index to the measured RTD resistance is modified by the following equation. For minor sensor resistance drifts, a linear correction is adequate. The eventual low-uncertainty temperature measurement of the Johnson noise applied at regular intervals, allows a linear interpolation to be useful.

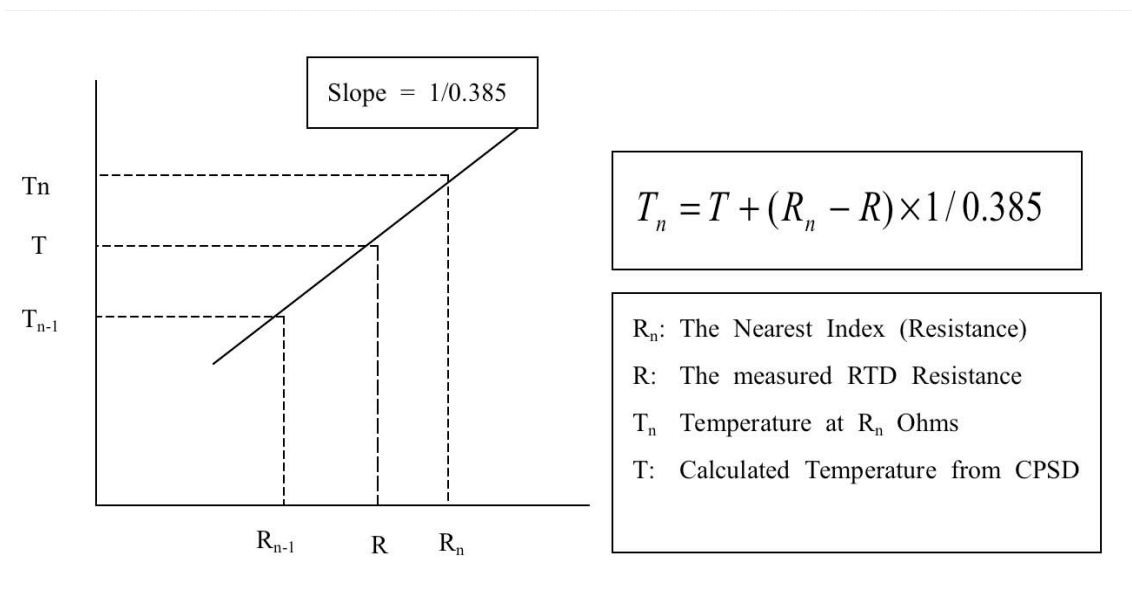

Figure 22. Principle of R-T conversion table modification.

The updating coefficient is very small to accommodate the stochastic uncertainty of JNT CPSD.

4.7.3. Temperature Display from the R-T Table

The temperature value is calculated from the modified R-T conversion table. The functionality is as followings.

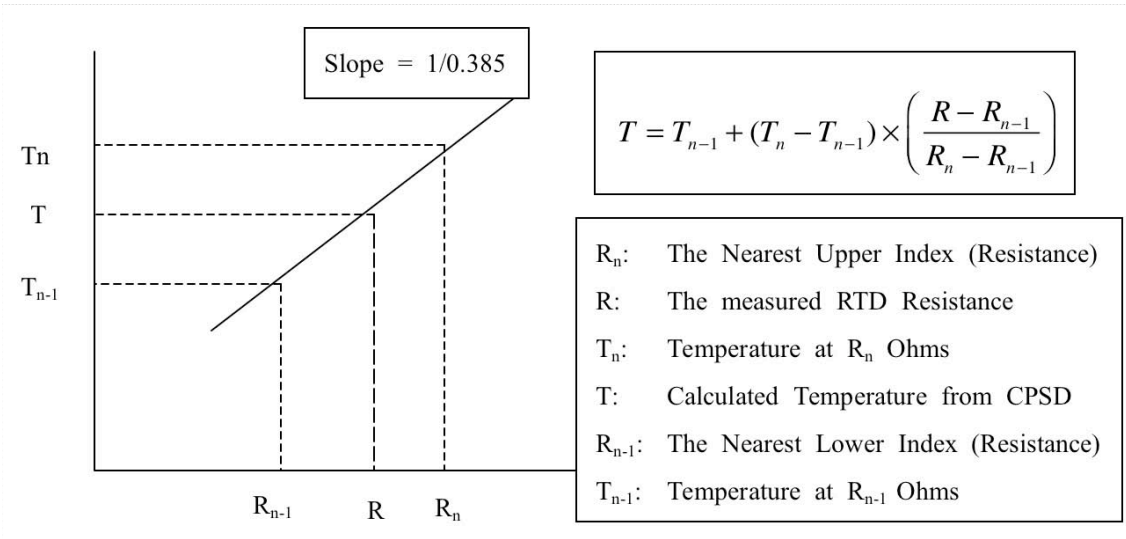

Figure 23. Interpolation of temperature value.

The temperature corresponding to a measured resistance R between two resolution points is estimated by interpolation method from the modified Resistance-Temperature table.

5. Equipment Development

The Johnson noise thermometer's head box consists of two circuit boards: one for the noise preamplifiers with line drivers and one for the RTD dc resistance measurement with voltage-to-frequency converter. These boards have been packaged in an aluminum enclosure along with a commercial RTD (enclosed in a one meter stainless steel sheath). Two such sheathed RTDs were purchased from Conex-Buffalo; one rated 100 Ω at 0°C and one at 200 Ω nominal resistances. Testing has been performed using the 100 Ω device. Two complete JNT systems were constructed. A user's guide to the ORNL JNT system is provided in Appendix C. Schematics are listed in Appendix D. A list of parts is provided in Appendix D.

Figure 24 shows the component side of the dc resistance measurement and noise-channel calibration circuit board. The circuit was implemented with both through-hole and surface-mount electronic components. This hybrid design was used to permit easy modification and testing of the circuits. Circuit boards for production would use surface-mount components exclusively, which would greatly reduce circuit board size and improve component reliability. However, careful design must be followed to prevent parasitic effects.

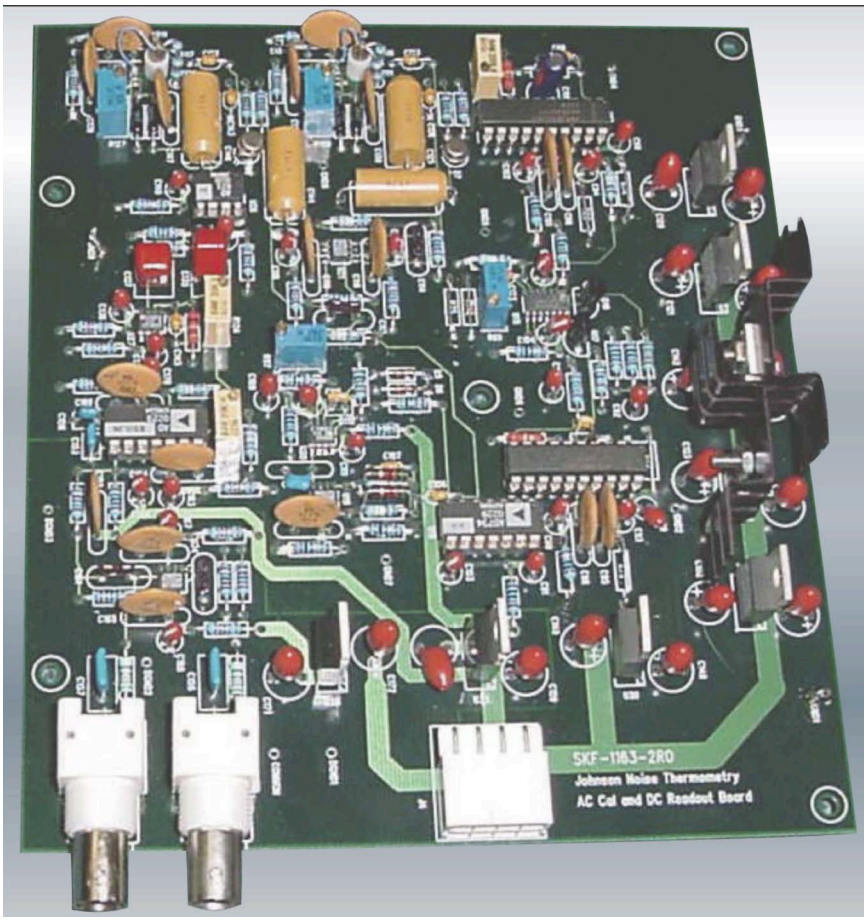

Figure 24. dc resistance measurement and noise channel calibration circuit board.

Figure 25 shows the component side of the dual channel, low noise preamplifier circuit board. This board was also constructed with both through-hole and surface-mount components. It likewise, would be manufactured using mostly surface-mount devices. Because gains of 80dB are present on the circuit board, a very careful layout must be observed to prevent parasitic oscillations and unexpected gain change effects.

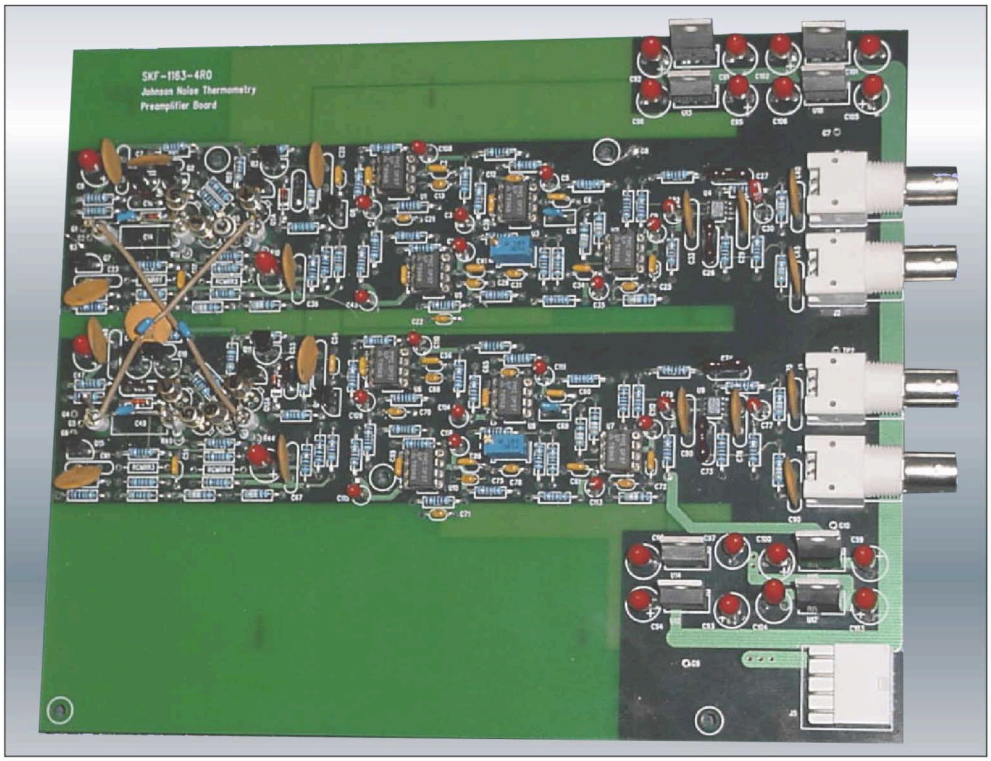

Figure 25. Dual channel, low noise preamplifier circuit board.

Figure 26 and Figure 27 show the two circuit boards mounted in the head box. A steel shield plate is placed between both circuit boards to prevent crosstalk. Grounding within the enclosure is critical. Experimentation of grounding configuration was necessary to minimize extraneous noise and other signals common to both preamplifier channels. Common signals do not cancel when cross-power spectral density function is applied. We were able to reduce the common unwanted noise signals by more than a factor of 20 by adjusting grounds and shields after the circuit boards were installed. The first fabricated head box is shown in Figure 28 below. Note that the RTD has not been attached in this photo. Also visible in this photo are corrections to the circuit board.

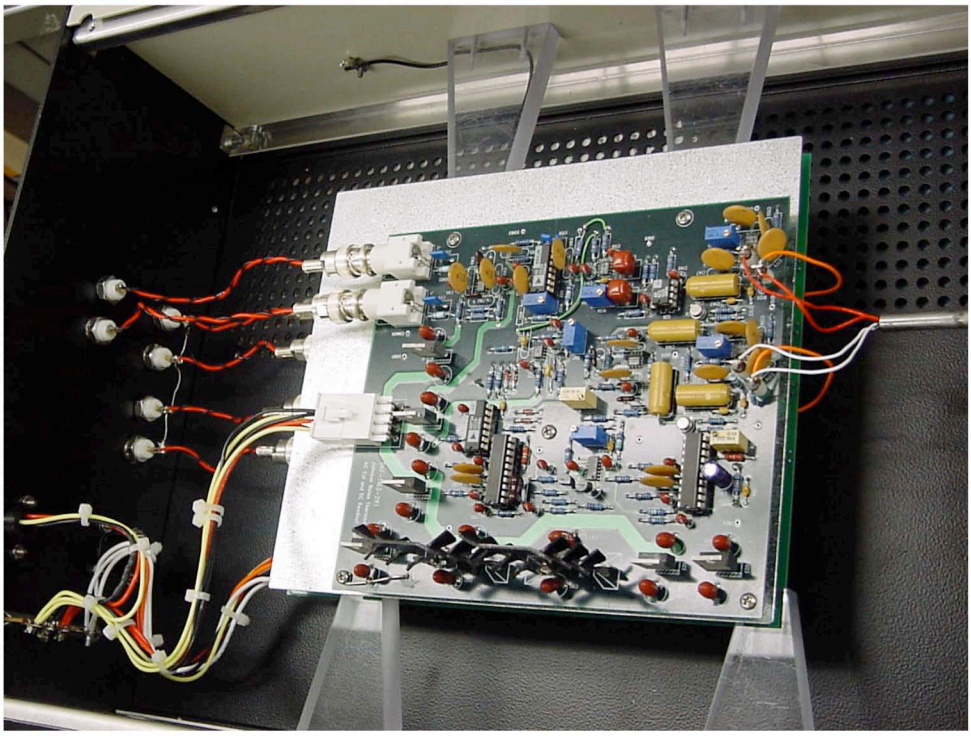

Figure 26. Cal Board (preamplifiers mounted on reverse side) mounted in enclosure. (Note metal shield between boards.)

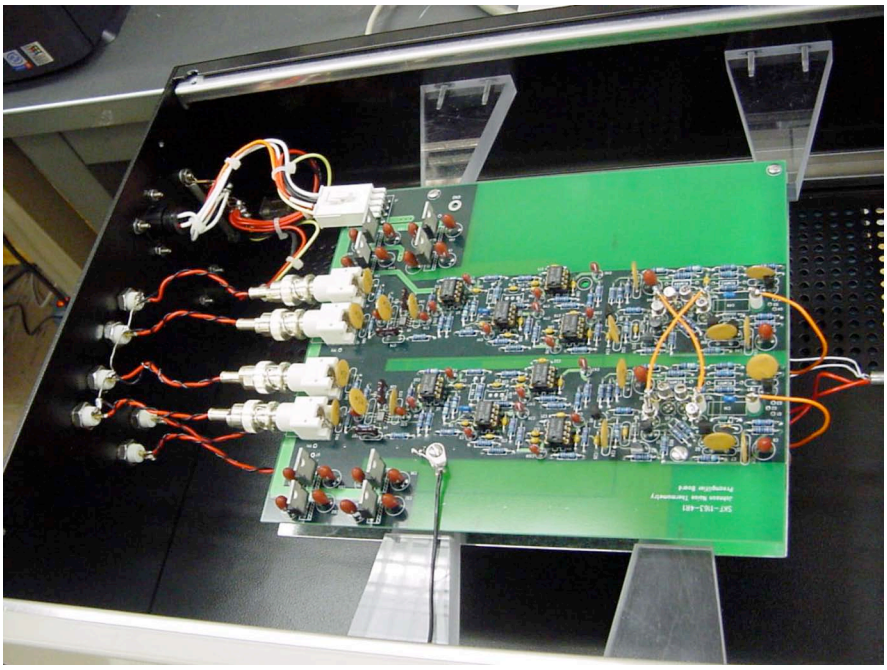

Figure 27. Preamplifier circuit board (Cal board on reverse side) mounted in enclosure.

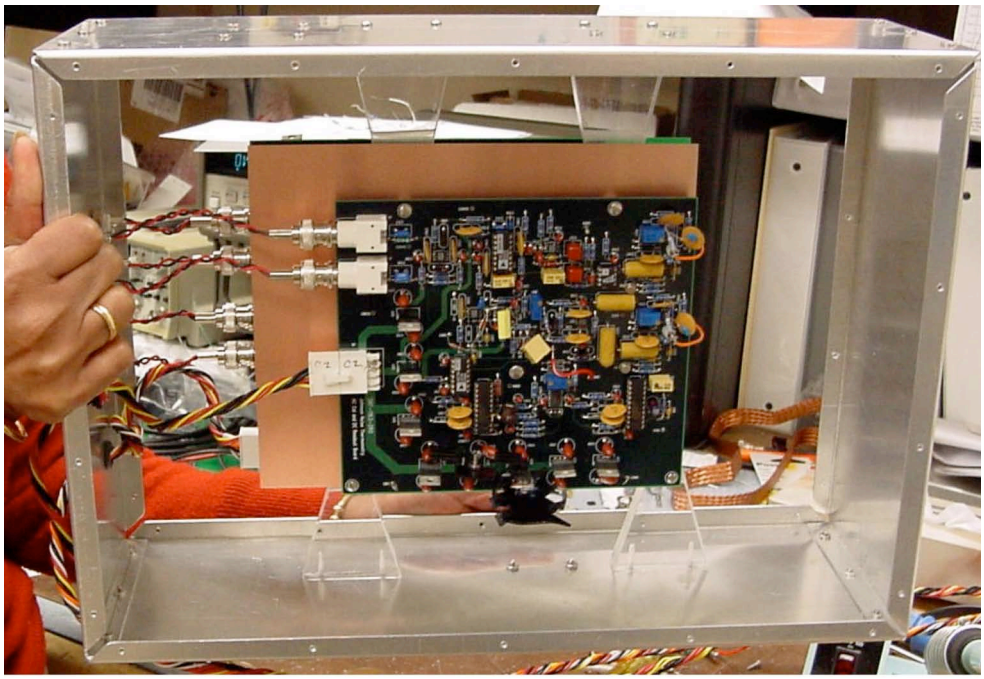

Figure 28. Head box showing preamplifier circuit board.

Figure 29 shows the receiver circuit board, which is mounted in a separate enclosure remotely located from the head box. The circuit board show is the first unit fabricated and has a small outboard circuit that was incorporated on the board in the second version.

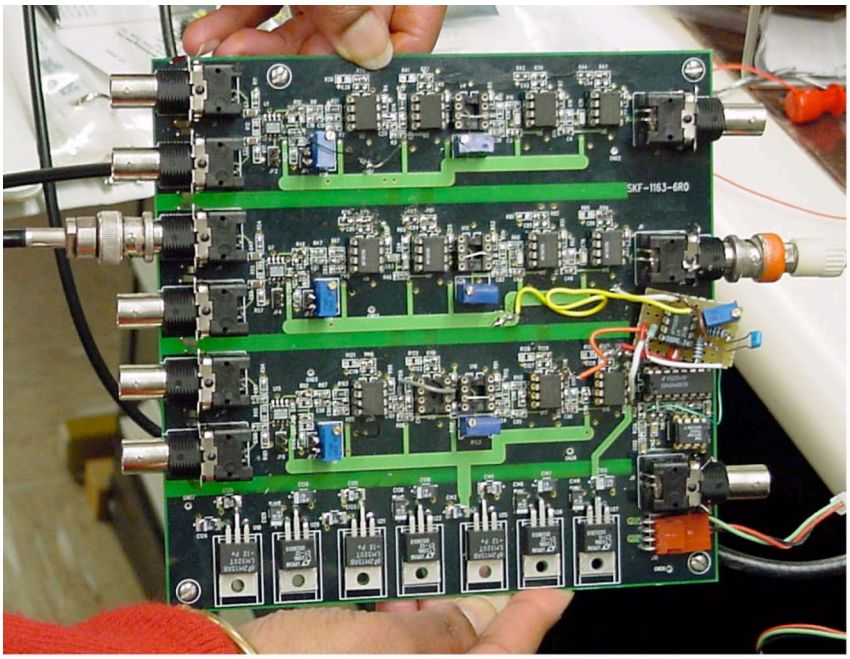

Figure 29. Receiver circuit board.

The JNT system enclosures are shown in Figure 30 and Figure 31. These enclosures were oversized to facilitate easy measurement and diagnostics. Production systems would be considerably smaller. Further, these enclosures are aluminum. The additional magnetic shielding of a steel enclosure is recommended for future devices.

Figure 30. Receiver enclosure (top) and power supply box (bottom).

Figure 31. JNT head enclosure (electrical connection side).

6. Implementation of Digital Signal Processing

6.1. Field Programmable Gate Array Implementation

Because the processing of DFTs and CPSDs requires many of arithmetic operations to complete the calculation, it becomes necessary to adopt a high-speed integrated circuit chip to perform the DFT and other time-consuming operation. An FPGA is an appropriate device to perform the fast calculation. The FPGA device handles the first part of the entire signal processing flow as Figure 32.

6.2. Digital Signal Processing Chip Implementation

Even though a FPGA device performs high-speed operations, it is not suitable to make precise floating-point mathematic calculations because of its integer-based hardware. Therefore, separate DSP chips are performing the algorithms for Gain Correction, EMI deglitching, JN temperature calculation, etc. Figure 32 illustrates the overall block diagram of digital signal processing structure.

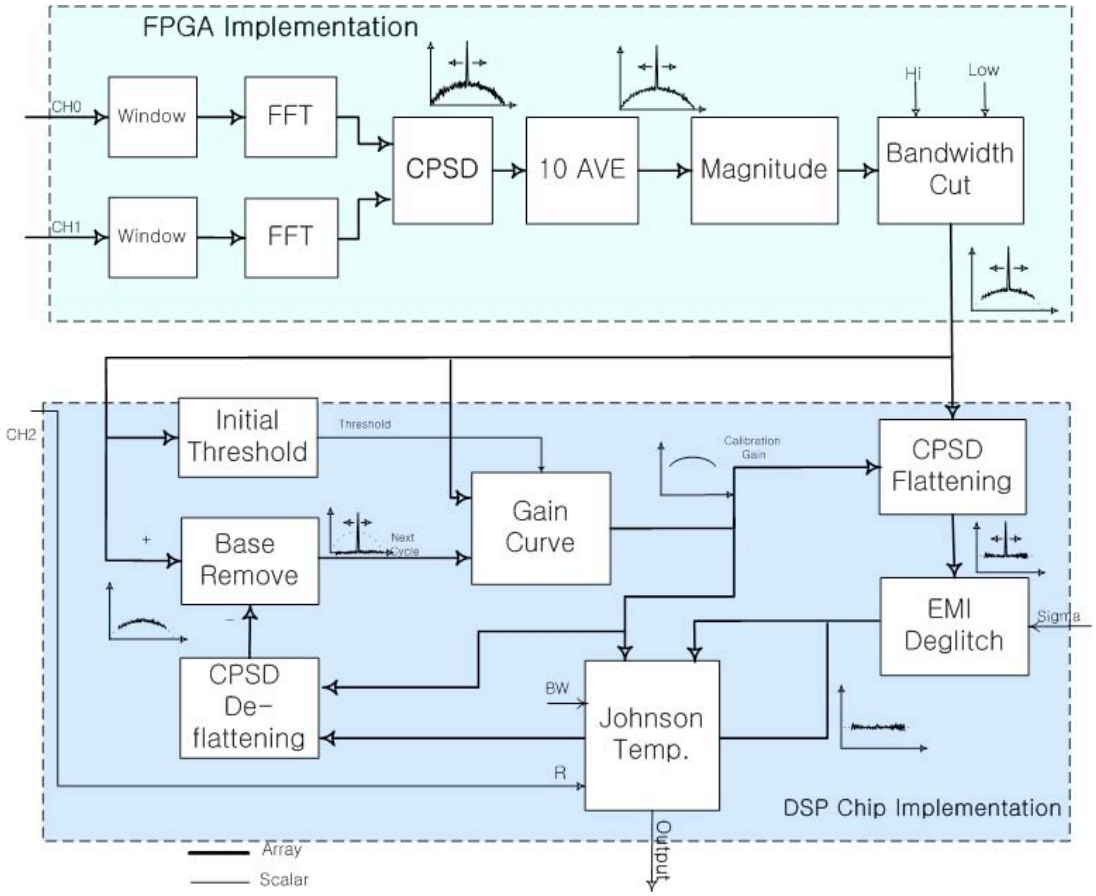

Figure 32. Block diagram of signal processing for Johnson noise thermometry.

Figure 33 illustrates the major components included in the DSP module and Figure 34 shows the enclosure of the system.

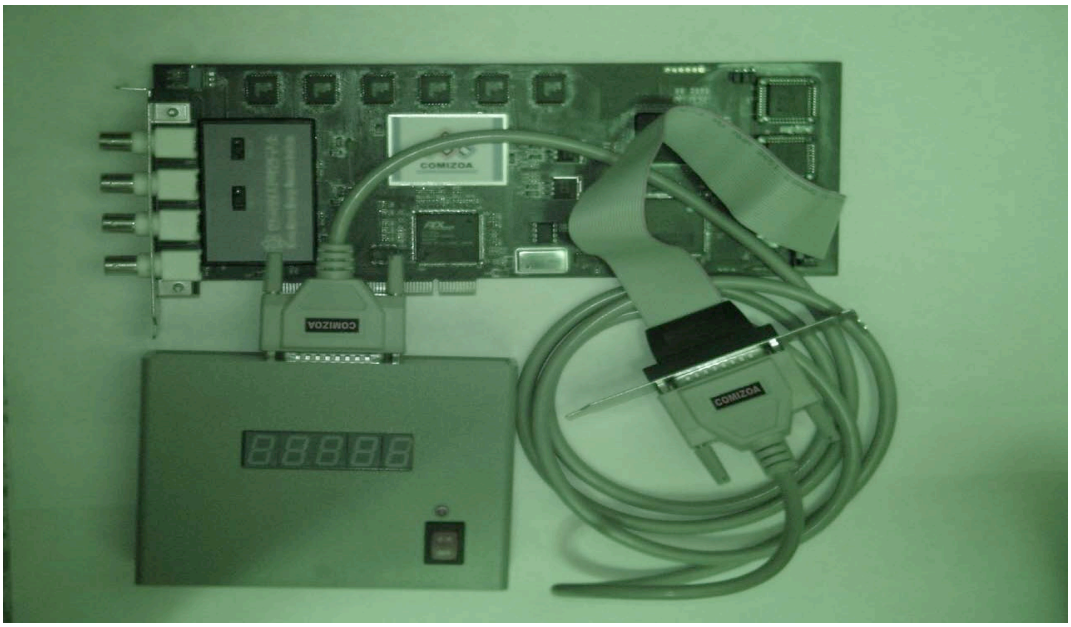

Figure 33. Major components of DSP module

Figure 34. Enclosure of JNT DSP system

7. Software Design for JNT Systems

A description of the overall approach to digital signal processing independent of the FPGA implementation is discussed in this section. The approach was taken by ORNL

researchers to develop a software-based system on a Pentium 4 class computer. This software system was used for preliminary development and evaluation of the JNT system analog hardware.

The JNT hardware generates three signals, two amplified-and-filtered noise voltage signals, and one temperature signal. These are acquired by a 12-bit ADC at a 4 MHz sampling rate in the computer system. The two noise voltages are partially correlated because they come from two amplifiers, each with independent amplifier noise, both of which also amplify the Johnson noise of the sensor, which is platinum RTD. The signals are acquired in blocks of 2^{14} (16384) points. Therefore, the acquisition of a single block takes about 4.1 ms. Multiple signal-processing algorithms process the data after each block is acquired. After the processing of one block is finished, the next block is acquired. A typical block of noise voltage is shown in Figure 35 with a closer view in Figure 36.

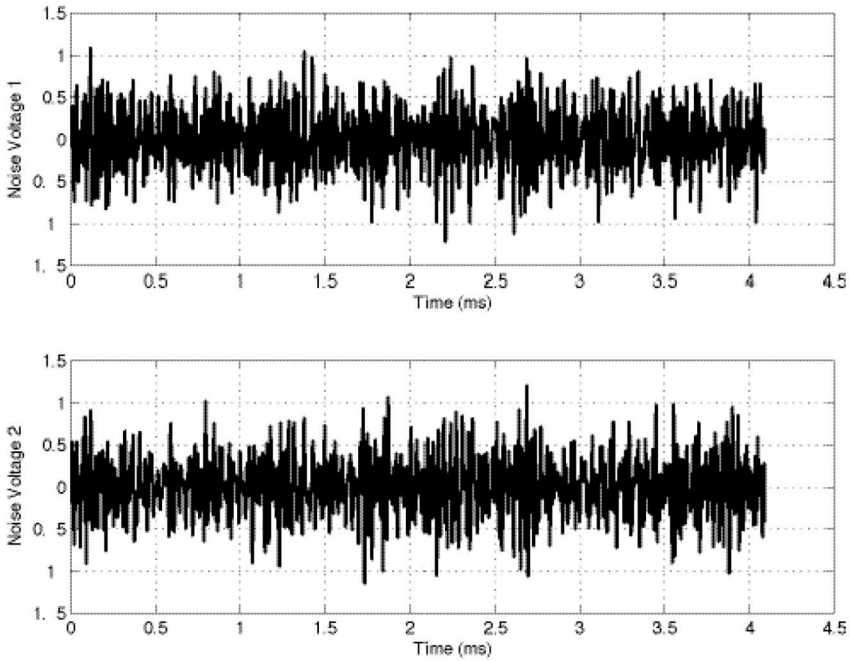

Figure 35. One block of typical noise-voltage data from the two noise-voltage channels.

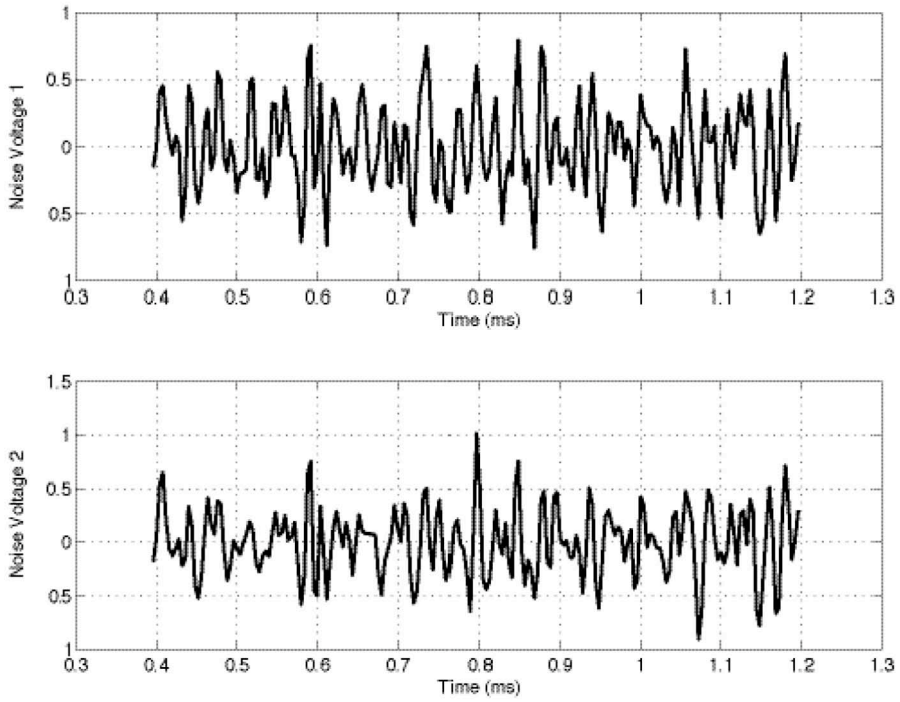

Figure 36. Signals from Figure 35 time-expanded to illustrate their partial correlation.

The first task of the software is to compute the CPSD of one block of data from each of the two noise-voltage signals. This is accomplished by taking the fast Fourier transform (FFT) of each noise-voltage signal and then multiplying one FFT by the complex conjugate of the other FFT. This produces a one-block CPSD estimate (Figure 37, upper half) that is averaged with the CPSDs of previous blocks. In addition to the CPSD, one would expect from the noise voltages that there are two sharp peaks (spikes) caused by the pilot tone (discussed later) and EMI.

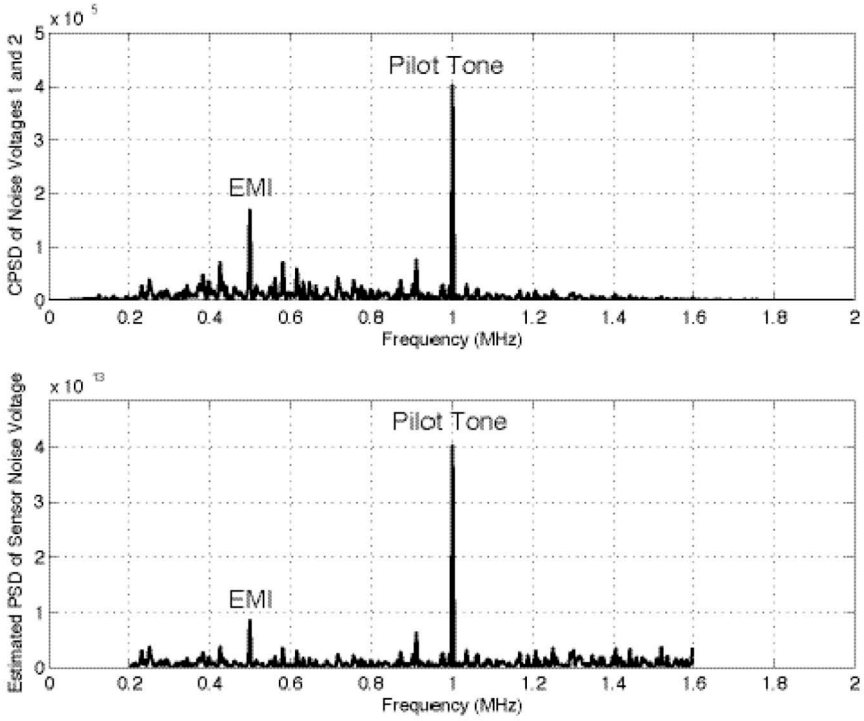

Figure 37. One-block estimates of the CPSD between the two noise-voltage signals and the PSD of the sensor voltage.

The averaging is a continuous process, in which the latest CPSD estimate is multiplied by some number, x, and the previous averaged CPSD is multiplied by $1 - x$ and these two products are added to form the new averaged CPSD. The value of x is chosen to determine the time constant of the averaging process. The time constant is $1/x$ blocks. Therefore, the smaller x is, the longer the averaging time is. Figure 38 (upper half) shows a 200-block average CPSD. The characteristic shape of the cross-power transfer function of the two amplifiers is evident but there are also two obvious spikes in the CPSD caused by EMI. The EMI spike from the one-block CPSD is still there but now another EMI spike — not obvious in the one-block CPSD — has appeared in this averaged CPSD. (The pilot-tone has been removed — more discussion below.)

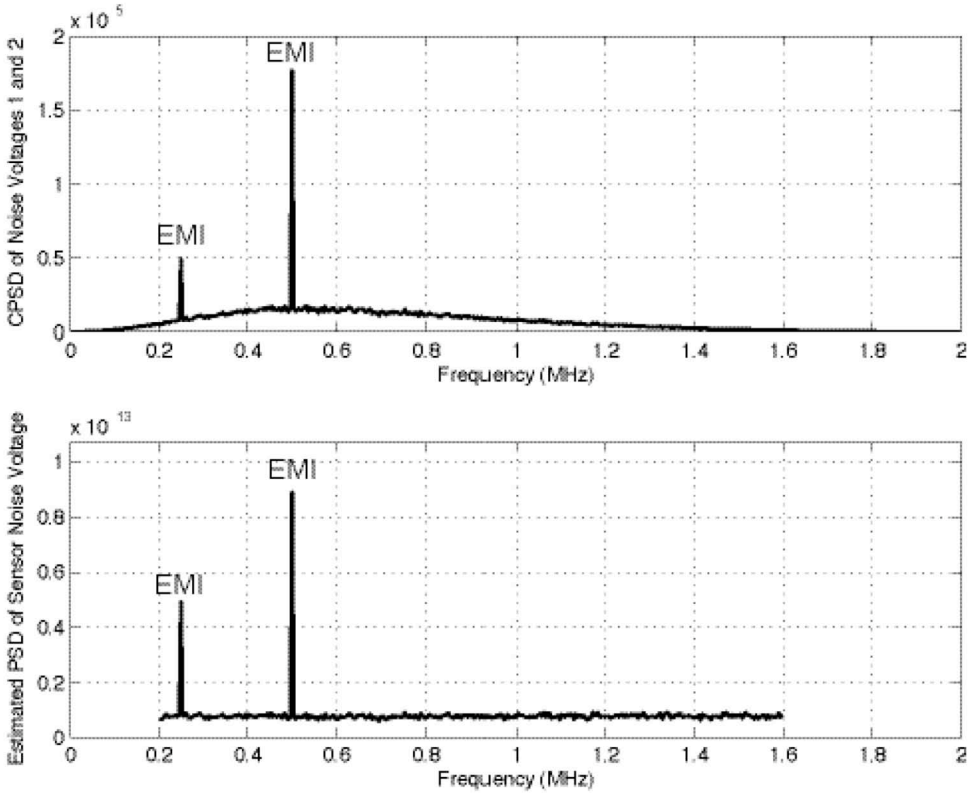

Figure 38. Averaged CPSD between the two noise voltage signals and estimated PSD of sensor noise voltage (200-block averages).

The next major task of the software is to recognize and eliminate any effects of narrow-band EMI in the noise-voltage signals. Before attempting to recognize EMI the CPSD is first divided by the latest estimate of the cross-power transfer function (CPTF) of the two voltage-amplifier-and-filter channels. (Cross-power transfer function is the ratio of the average CPSD of the two noise-voltage signals divided by the average PSD of the noise voltage at the sensor, as a function of frequency.) This yields an estimate of the spectral PSD of the noise voltage at the sensor, which is "white," meaning constant with frequency (Figure 37 and Figure 38, lower halves). Narrow-band EMI shows up in the CPSD and in the sensor voltage PSD as a tall narrow peak. There is also random variation of the PSD due to its stochastic nature. Therefore, an EMI peak must be recognized by being an "outlier" in the PSD.

To recognize EMI spikes, first the software computes the mean and standard deviation of the PSD. Then a threshold is set that is the mean plus some multiple of the PSD, typically about 3.5 standard deviations. For a Gaussian-distributed random variable, which these voltages are, the probability of the noise-voltage itself exceeding 3.5 standard deviations from the mean is below 0.1 percent. Each point in the PSD is compared with the threshold. If a point exceeds the threshold, all the points in the local neighborhood of that point are replaced by the mean of the PSD. (The local neighborhood is typically about 30 points on each side of the point that exceeds the threshold.) The mean that replaces these points is biased high by the presence of the EMI so the mean and standard deviation are recomputed based on the new PSD and a new

threshold is set. Then EMI spikes are removed again based on the new threshold. This process is iterated several times, typically 2 to 5 times. At the end of these iterations, the bias of the mean and standard deviation due to EMI are practically zero and the EMI spikes have been eliminated.

Note that the EMI spike is not completely localized to one frequency in the PSD. Because the noise-voltage signals are acquired in blocks of finite length, the effect of a single-frequency EMI signal actually shows up all across the spectrum although most of its power is in a very small frequency range centered at its actual frequency. The effect of spreading the power of the single-frequency EMI over the whole spectrum is called "leakage" and it is well known from digital signal analysis theory. To reduce the leakage effect, a block of data is first "windowed" by multiplying it by a window function that minimizes leakage in the spectrum. The window used is a Blackman window, which has very good spectral localization characteristics.

Longer CPSD averaging times produce smaller standard deviations of the PSD and make recognition and elimination of the EMI more accurate because during the averaging process the EMI peak "grows" out of the noise. This occurs because the EMI peak is always in the same place and always the same size while the noise is random. The PSD estimate of the noise at any frequency is independent of previous estimates at the same frequency. For example, a second, smaller EMI peak was not visible in the one-block sensor PSD but was obvious in the 200-block-averaged sensor PSD.

After the EMI peaks are removed, the software can estimate the temperature of the sensor. The relation between the sensor temperature, noise voltage, and resistance is shown in Equation (20).

$$\mathrm{G}(f) = 4kTR\,, \tag{20}$$

where $\mathrm{G}(f)$ is the PSD of the sensor noise voltage in volts-squared per hertz, k is Boltzmann's constant, 1.38×10^{-23} joules/Kelvin, T is the absolute temperature of the sensor in Kelvin, and R is the resistance of the sensor in ohms. (This formula is based on a single-sided PSD. For a double-sided PSD the relation would be $\mathrm{G}(f) = 2kTR$.) Computation of temperature requires knowledge of the sensor resistance, which is computed from a linear relation between the resistance-signal voltage and the resistance.

After an estimate of sensor temperature is made using Johnson noise, the resistance-temperature (R-T) pair is then used to update the sensor calibration. The sensor calibration is a functional relationship in which R is the independent variable and T is the dependent variable. This is typically a polynomial curve-fit to a set of R-T pairs from previous estimates of temperature using Johnson noise. An individual R-T pair will have significant error because it was based on a limited number of blocks of random noise data. However, the curve-fit to a large number of independent R-T pairs taken over a much longer period will have a much smaller statistical error. This error can be made so small as to be negligible compared to other errors in the system.

The description up to this point is the process of estimating temperature using Johnson noise and continuously calibrating the RTD, based on those estimates. There is another

important task that is being performed simultaneously, the continuous measurement of the CPTF of the two amplifier-filter, noise-voltage channels. This is currently done by injecting into the sensor a "pilot tone" current signal.

The pilot tone is a small frequency-modulated sinusoidal current whose frequency continuously varies up and down from some low frequency (less than 100 kHz) up to approximately half the sampling rate (about 2 MHz) and back down again. A full frequency up and down sweep typically takes 2 to 4 seconds. During the acquisition of one block of data, the pilot tone frequency moves a few kilohertz, typically less than 5 kHz. This is a frequency range that is much less than the filter bandwidths and can be reasonably considered a single frequency for purposes of CPTF calculation.

Before the CPSD is cleared of EMI, the pilot tone must be removed. The pilot tone amplitude must be set so that it is always the dominant peak on the sensor PSD. It is recognized by being the largest peak in the PSD and is removed from each block of PSD data before that block of data is further processed to remove the EMI and estimate sensor temperature. Knowledge of the pilot tone's amplitude as it is injected in the sensor allows the software to estimate the CPTF of the system at the mean frequency of the pilot tone in the latest block.

Since these single-frequency estimates of CPTF are based on one-block measurements of the pilot tone, they have large statistical error. However, the estimate of CPTF is based on a very large number (typically thousands) of these estimates. The set of noisy CPTF estimates is smoothed by a Gaussian smoother to produce a continuously-updated CPTF estimate. As was true in the temperature calibration, the statistical error in this estimate of CPTF can be made negligible.

8. System Implementation

8.1. RTD Placement

Reactor coolant system (RCS) temperature is measured for several purposes, including power control (control rod control), thermal power monitoring, and initiation of protective actions. Instrumentation for measuring coolant temperatures in power reactors contains narrow range and wide range temperature measuring devices, which are usually RTDs. The narrow and wide range RTDs are directly mounted in thermowells in the reactor hot and cold leg pipes. Narrow range temperature has to be measured within a predetermined response time from the coolant loop. To achieve rapid response, the temperature is sensed directly by a fast response type RTD in a thermowell. Usually three RTDs with thermowells are mounted in a hot leg pipe. They are spaced 120 degrees apart around the pipe's circumference to compensate for water flow stratification (see Figure 39). Each RTD is connected to an instrumentation circuit; the three temperature signals are averaged. Typical reactor coolant-temperature measurement has a tolerance of ±0.2°C.

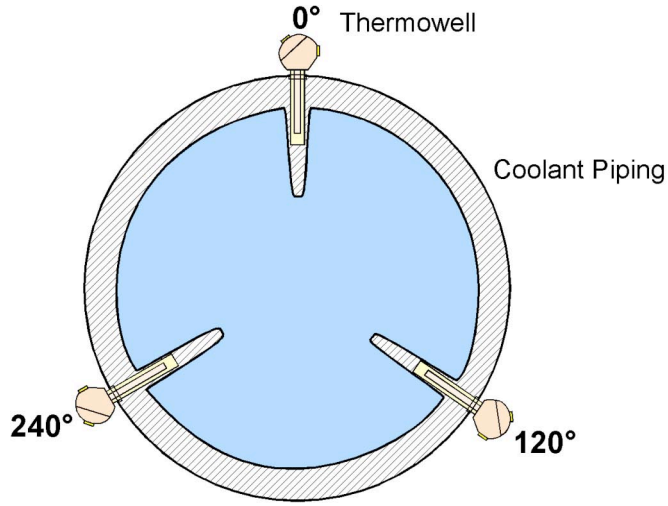

Figure 39. Reactor coolant piping temperature measurement made in three locations around pipe.

The reactor coolant-loop temperatures used by control systems and the reactor protection system are measured by narrow-range, fast-acting RTDs. These detectors are installed in thermowells and are part of the RCS pressure boundary. A dual element RTD is inserted into each thermowell. One element provides an electronic signal to a low-voltage amplifier and the amplified signals from three RTDs are averaged to generate a single signal (e.g., hot average temperature, $T_{h,av}$) from that loop. This temperature signal, along with the cold average temperature signal from the same loop, $T_{c,av}$, is used to generate ΔT and T_{av} for that loop. The cold-leg narrow range RTD is also a dual element, fast acting RTD that is inserted into a thermowell directly downstream of the reactor coolant pump. Because of the turbulent flow at this point in the piping, only one narrow range RTD is required to provide an accurate temperature indication. The second element in each RTD is considered an installed spare. It is wired directly to the reactor protection system (RPS) cabinets but not connected to any electronics. The second element is available for use in the event of a failure of the first element. The narrow range RTDs are calibrated to provide an output between 265°C and 343°C (510°F-650°F).

Hot- and cold-leg reactor coolant-loop temperatures are also measured by wide range (0–700°F, or –18 to 371°C) RTDs mounted in wells in the reactor coolant piping of each loop. These measurements are used for indication during heat-up and cooldown and during natural circulation operation. The cold-leg wide range RTDs are also used in the cold overpressure control system.

8.2. System Layout

A possible plant layout of the complete system is shown in Figure 40. The detector head and its power supply are mounted to the process piping as typical of a high-pressure penetration thermowell. The power supply is a purely analog supply and is mounted within a few meters of the head. Six coaxial cables connect the detector head to the receiver module. The line drivers in the detector head are capable of driving up to 300 meters of 50 ohm coaxial cables. The coaxial cables pass through the containment

boundary. The receiver and computer can be rack mounted. Within the computer are contained the ADC card, DSP software, and communications interface. Power conditioning should be applied to the line voltage supply. The distance is variable from the equipment rack to the control room display and operator interface since it depends on the communications protocol used.

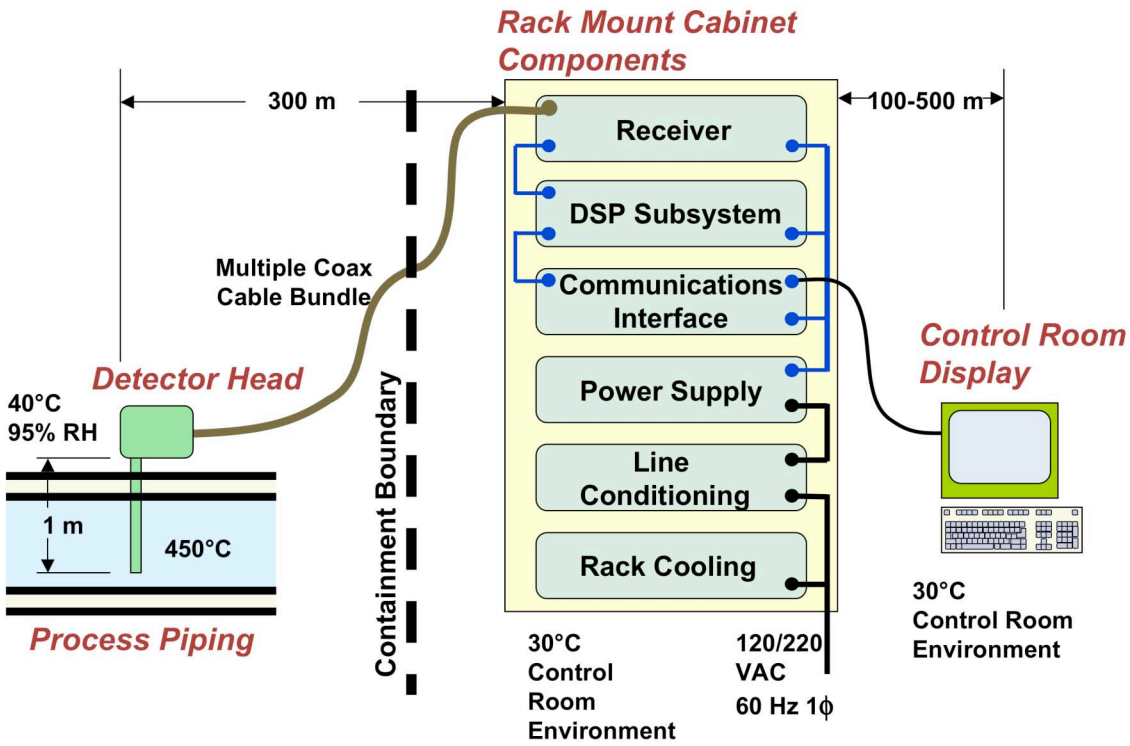

Figure 40. Possible system configuration at a nuclear power facility

An alternative approach to that shown in Figure 40, is to commit all the DSP functionality to a FPGA as discussed in Sections 4 and 6 and fabricate a self-contained system with ADC card and communications interface. The FPGA approach is preferable because of its rugged nature and there is no operating system to decrease reliability. Ultimately, the entire functionality of the rack-mounted equipment can be contained in a 1U (one standard height) rack module.

Future realizations of the detector head assembly can also be reduced in size and mass by using all surface-mount components (with only a few exceptions). This implementation will increase reliability and reduce cost.

9. System Results

9.1. Performance

Test runs of the system using calibrated metal-film resistors at room temperature in place of the RTD have been performed and the data is shown below. The system has been tested at room temperature with the chosen RTD and works equally well. These tests represent an end-to-end test using the entire system and testing algorithms.

Figure 41 is the voltage of the simultaneous dc readout plotted against resistance. The linearity is excellent. Figure 42 is a plot of the power spectral densities of each of the two noise channels versus resistance. Also included is the cross-power spectral density of the two channels. The difference between the PSDs and the CPSD represents the extraneous noise contributed by the preamplifiers, which appears to be about 4.5dB.

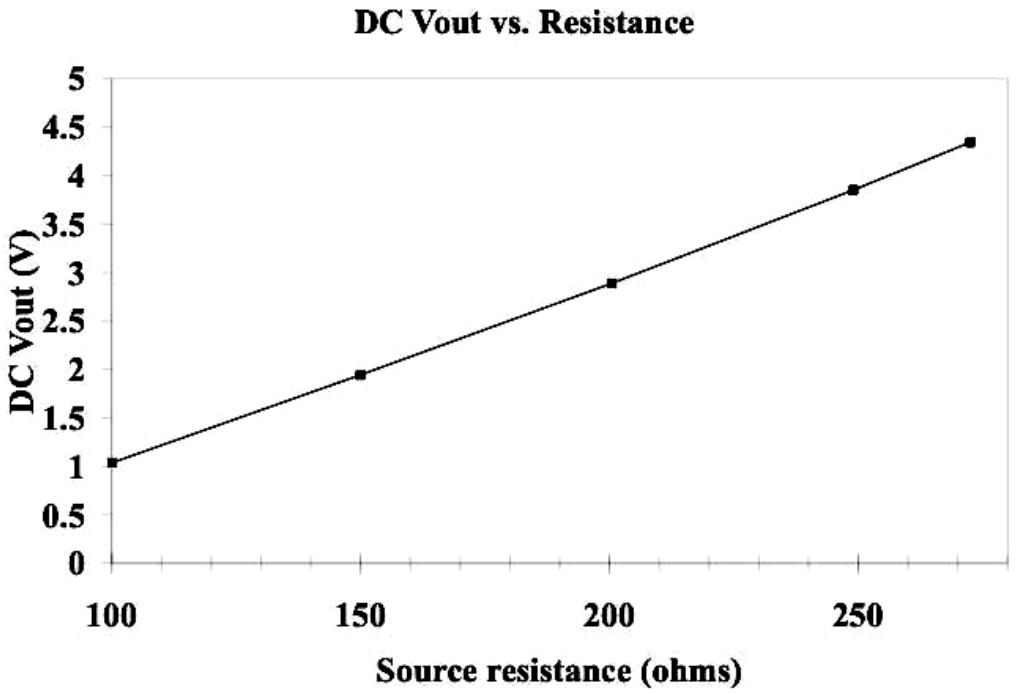

Figure 41. Tracking of the dc resistance measurement subsystem.

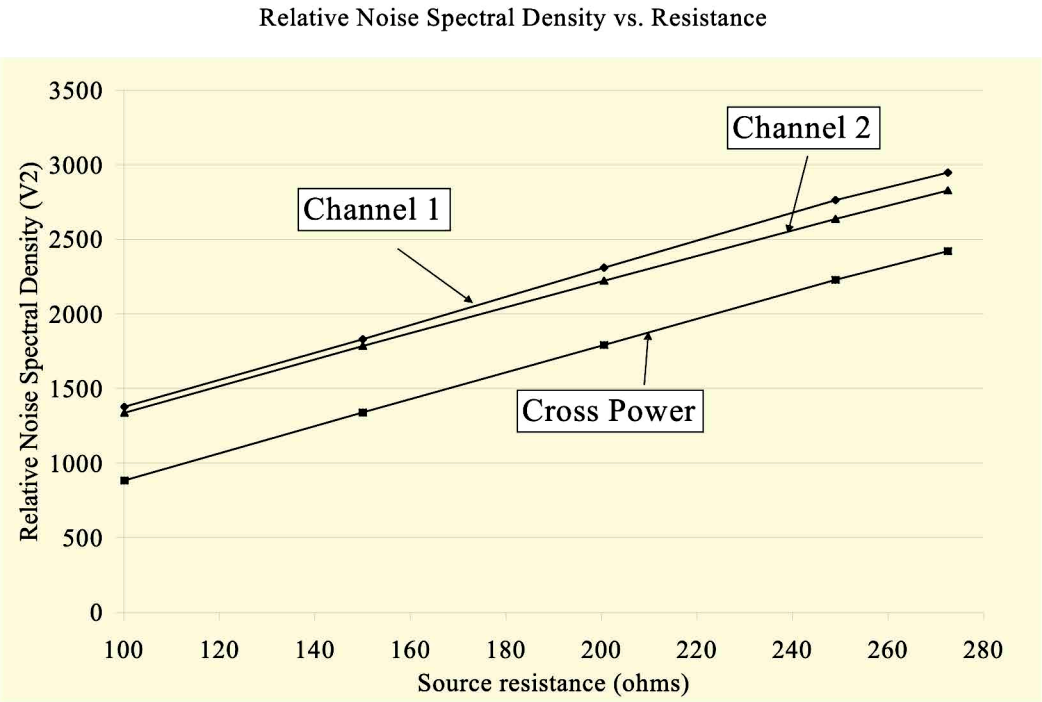

Figure 42. Linear response as predicted by theory is measured in practical circuit.

9.2. Technical Barriers and Issues

9.2.1. Discrepancy between Swept and Noise Spectrums

In the course of final examination and testing of the apparatus at ORNL prior to shipping to KAERI, an anomaly was discovered that potentially can affect the uncertainty of channel calibration. The front-end-electronics hardware uses a swept pilot tone to traverse the frequency spectrum employed by the Johnson noise signal. The swept-tone spectrum is used by software to create a transfer function for the noise channel independent of the Johnson noise emitted by the RTD and other electronic noise sources. Ultimately, the swept signal cross-power spectral density is utilized to normalize the actual noise spectrum. This procedure reduces uncertainty that arises from variations in amplifier gain and cable characteristics. We expected the swept-tone spectral shape and that from a known precision resistor at the system's input to be equal with only their amplitudes differing. The actual spectrums as measured are shown in Figure 43. It is clear that their spectral shapes are different.

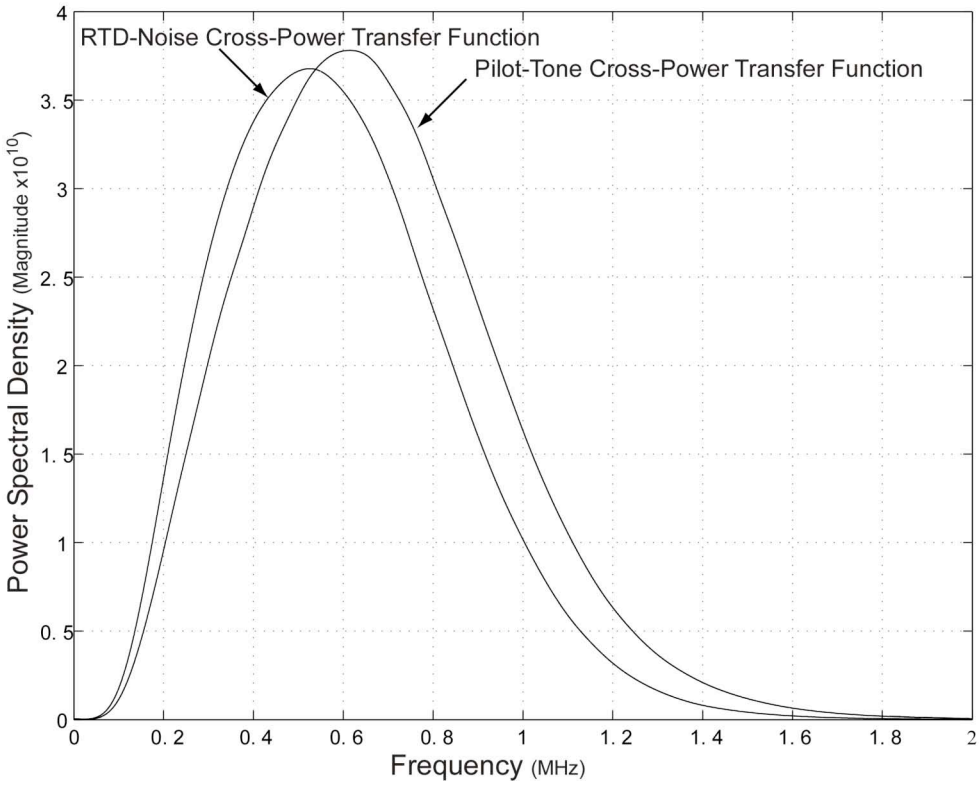

Figure 43. Differences in spectral response between pilot-tone and Johnson noise in the same channel.

We spent time investigating this spectral anomaly. A conclusion as to the cause has not been reached yet. However, several work-around solutions are possible: (1) a correction to the swept-tone spectrum can be applied to make it overlap with the resistance spectrum, (2) a single-frequency tone can be implemented, and (3) the time-averaged noise spectrum of the RTD can be used as a spectral shape correction (note however, that this does not yield an amplitude correction). The first work-around was tested in the laboratory and worked well. We verified that temperature variation of the head unit circuit boards did not affect the spectral anomaly and therefore did not cause a drift.

Our intention is to continue investigation into the cause of the anomalous spectral response. We anticipate that a proper solution as either a circuit modification or software function (or both) will be identified.

9.2.2. Effect of Electromagnetic Noise

The JNT portion of the system functions like a high-gain AM radio with a gain of 80dB. Such a system is very susceptible to EMI. The interference can come as random events with frequency components across the spectrum or as a narrowband carrier. Since the Johnson noise temperature is determined by the average value of the estimated sensor noise voltage PSD, noise can add offset and corrupt the temperature value.

The preamplifier circuits contain bandpass filters as do the receiver circuits. The system passband for the noise channels is from about 300 kHz to 1 MHz. Most industrial spike noise is below 150 kHz. Cable movement (capacitive and triboelectric) noise is usually

less than 20 kHz. The low frequency portion of the response has been placed to exclude these noise sources. Nevertheless, EMI will enter and contaminate the signals.

The solution contains two components: (1) apply the maximum physical shielding and (2) employ algorithmic methods to recognize and remove the noise. The enclosures are constructed of aluminum; however, there are cooling slots and the enclosure sides are attached with a minimum of screws. Steel, especially mu-metal, shielding would be better for AC magnetic field attenuation. The ORNL software (described in Section 7) was developed mostly for testing since KAERI developed FPGAs with integral DSP algorithms. We employed a two-part spike removal method. The first part removes extraneous noise bursts in the time domain while the second part removes continuous carriers in the frequency domain. No formal EMI testing was performed.

9.2.3. Environmental

Because of the very high gain and wide bandwidth amplifiers, physical changes to the enclosure, such as deforming it, results in slight internal-to-the-case capacitance shifts. These capacitance changes potentially could change calibration. We found that pressing on the detector head enclosure on the preamplifier side causes a very slight gain shift. This effect has been mitigated by implementing sturdy shielding on the preamplifier circuit board, which was not originally incorporated in these designs. Placement of the power supply too close to the head box causes a slight change in the Johnson noise spectral response. The interaction of magnetic fields from the transformers seems to be the cause. A ferromagnetic enclosure for the head-end electronics would prevent the problem.

9.2.4. Time Response

As anticipated, the dc measurement of the RTD yields a fast response. The time response limitation is not in the electronics but in the RTD and sheath. The JNT measurement is much slower and can require several minutes to achieve a 0.2 percent uncertainty. For temperature measurement in most plant systems, hourly calibration of the RTD temperature value is adequate. However, the time response of the JNT calculation is directly related to the channel bandwidth. It is possible to design future systems to a greater bandwidth by increasing the upper cut-off frequency. With an upper frequency of 2 MHz, a 40 percent decrease in response time can be achieved.

10. Conclusions and Recommendations

This I-NERI project has been successful in developing a prototypic Johnson noise-based temperature measurement system that uses a typical industrial RTD as its sensing element. These components work well; however, there are still improvements that can be made and issues to resolve as described in the previous section.

The components used for this prototype were not radiation hardened. Developing a radiation hardening system was beyond the scope of this project. A next step in the development of the JNT system is to apply components and techniques to raise the radiation tolerance level suitable for nuclear power plant environments. Specifically, a

radiation and thermally hardened version of the preamplifier electronics remains to be developed.

11. Appendix A — Principles of Temperature Measurement Using Johnson Noise Thermometry

11.1. Correlated Voltage JNT

If a sensor resistor is connected directly across the inputs of two high-input-impedance voltage amplifiers, the output of each of the two amplifiers will consist of the sum of two parts, a noise voltage caused by the sensor, and a noise voltage caused by that amplifier (and no contribution from the other amplifier). Thus, the outputs of the two amplifiers are partially correlated because they both amplify the sensor voltage noise and partially uncorrelated because each independently generates its own noise. The outputs of the two amplifiers can be written in the forms,

$$\mathrm{v}_{o1}(t) = A_1\left[\mathrm{v}_s(t) + \mathrm{v}_{a1}(t)\right] \ , \ \mathrm{v}_{o2}(t) = A_2\left[\mathrm{v}_s(t) + \mathrm{v}_{a2}(t)\right]$$

where A_1 and A_2 are the voltage gains of the two amplifiers, v_{a1} and v_{a2}, are the equivalent input noise voltages of the two amplifiers and v_s is the noise voltage of the sensor resistor. The product of the two amplifier output voltages is then

$$\mathrm{v}_{o1}(t)\,\mathrm{v}_{o2}(t) = A_1A_2\left[\mathrm{v}_s(t) + \mathrm{v}_{a1}(t)\right]\left[\mathrm{v}_s(t) + \mathrm{v}_{a2}(t)\right]$$

or

$$\mathrm{v}_{o1}(t)\,\mathrm{v}_{o2}(t) = A_1A_2\left[\mathrm{v}_s^2(t) + \mathrm{v}_s(t)\,\mathrm{v}_{a1}(t) + \mathrm{v}_s(t)\,\mathrm{v}_{a2}(t) + \mathrm{v}_{a1}(t)\,\mathrm{v}_{a2}(t)\right] \ .$$

Since the amplifier noise voltages are uncorrelated with zero mean, the expected value (in practical terms, the long-term time average) of their product will be zero. Also the sensor noise voltage and the amplifier noise voltages are uncorrelated with zero mean and the expected value of their product is zero. Therefore,

$$\mathrm{E}\left[\mathrm{v}_{o1}(t)\,\mathrm{v}_{o2}(t)\right] = A_1A_2\,\mathrm{E}\left[\mathrm{v}_s^2(t)\right]$$

where "E(·) " means "the expected value of". Since the temperature of the sensor is proportional to the mean-squared noise voltage (which is the same as the expected value of the square of the noise voltage), the temperature can be computed from the Nyquist equation,

$$\overline{\mathrm{v}_s^2(t)} = 4kTR\Delta f = \mathrm{E}\left[v_s^2(t)\right] = \frac{\mathrm{E}\left[\mathrm{v}_{o1}(t)\,\mathrm{v}_{o2}(t)\right]}{A_1A_2}$$

or

$$T = \frac{\mathrm{E}\left[\mathrm{v}_{o1}(t)\,\mathrm{v}_{o2}(t)\right]}{4\,A_1A_2kR\Delta f}$$

where T is the temperature of the sensor in Kelvin, k is Boltzmann's constant, $1.38 \times 10^{-23} \frac{\mathrm{J}}{\mathrm{K}}$, R is the resistance of the sensor in ohms, and Δf is the equivalent noise bandwidth of the measurement system.

The main advantage of the correlated voltage method is that the noise contributions of the two amplifiers do not have to be known to eliminate their effect. However, any exogenous noise signal that injects itself into both amplifiers will be correlated at the output of the amplifiers and will thus cause an error in the measured temperature. If the exogenous noise signal is narrowband (which is usually the case), digital signal processing can identify this type of interference and eliminate it. (More details in digital signal processing section below.)

A disadvantage of the correlated voltage method is that a separate measurement of the sensor resistance is needed. This measurement is however easy to make with high accuracy if it is done at dc using the 4-wire technique. It should be pointed out that the R in the Nyquist equation is, strictly speaking, not the dc resistance of the sensor but the real part of the sensor impedance in whatever frequency band the measurement is made. If the measurement of the sensor noise is made in a bandwidth that is centered at a high frequency, the real part of the sensor impedance in that bandwidth may not be the same as the dc resistance. (For typical platinum resistance thermometers, the difference between the dc resistance and the real part of the sensor impedance is negligible from dc to beyond 1 MHz.) At higher frequencies, care must be taken to ensure that the resistance measured is the same as the real part of the impedance in the frequency range used. Most of the discrepancy between dc and at frequency resistances arises from the skin effect.

11.2. Tuned Circuit JNT

Pepper and Brown[5] reported a technique of using a resistive sensor with a capacitor and inductor in series (a series *RLC* circuit) and taking the mean-squared noise voltage across the capacitor as an indication of temperature. The advantage of this technique is that, *for lossless capacitors and inductors*, the mean-squared noise voltage across the capacitor is simply

$$\overline{\mathrm{v}_C^2(t)} = \frac{kT}{C}$$

where k is Boltzmann's constant, T is the sensor temperature and C is the capacitance of the capacitor.

The major advantage of this technique is that, for lossless inductors and capacitors, the measured output voltage is independent of the sensor resistance and the inductance. The capacitance can be well known and stable. No measurement of sensor resistance is needed. Any drifts in inductance or sensor resistance over time are inconsequential. Another advantage is that if the circuit is underdamped (a Q of 10 or so is typical), most of the signal power lies in a relatively small bandwidth near the resonant frequency. Thus, the amplifier's

bandwidth can be made relatively small, thereby reducing its noise contribution and increasing the signal-to-noise ratio in comparison with a wider-band measurement.

A problem with the tuned circuit method is that, unfortunately, truly *lossless* inductors and capacitors do not exist. Very high quality capacitors can be obtained so that it is not a problem. However, lossless inductors are another matter. Any real inductor has winding resistance (which is usually frequency dependent) and, if it has a magnetic core to increase the inductance, that is another source of loss (which is typically even more frequency dependent). Thus, although the method seems very good in principle, it is constrained by the quality of the inductor. For circuits using real inductors with loss, the ideal relationship,

$$\overline{\mathrm{v}_C^2(t)} = \frac{kT}{C}$$

becomes an approximation instead of an exact relationship. The error can be corrected for by making a sensor resistance measurement but that defeats one of the major advantages of the method. Of course, one could simply replace the inductance by a short circuit. This does indeed remove the problem of inductor loss and the ideal relationship

$$\overline{\mathrm{v}_C^2(t)} = \frac{kT}{C}$$

again applies, but now the measurement bandwidth is typically much greater than with an underdamped series *RLC* circuit. This lowers the signal-to-noise ratio when the amplifier noise is considered. The bandwidth can be reduced by making *C* larger, but that decreases the mean-squared capacitor noise voltage at the same rate, resulting in no net gain. In any case, amplifier noise must be corrected for and this is a disadvantage compared with the correlated noise technique.

The idea of tuned circuits can be extended beyond the simple series RLC circuit. Circuits with multiple inductors and capacitors can tailor the center frequency and bandwidth of the measurement to strongly attenuate interference signals that may be present in an industrial environment due to EMI or microphonics in the sensor or amplifiers. If the inductors and capacitors are lossless, the mean-squared noise voltage across *every* capacitor is

$$\overline{\mathrm{v}_C^2(t)} = \frac{kT}{C}$$

and, by the way, the mean-squared noise current through every inductor is

$$\overline{\mathrm{i}_L^2(t)} = \frac{kT}{L} \ .$$

(This is only true if a capacitor does not have another capacitor directly in parallel with it. In that case, the capacitance, C, above should be the equivalent parallel combination of the two capacitors; the sum. Similarly, for inductors, this is only true if the inductor is not directly in series with another inductor. In that case the inductance, L, should be the series combination of the two inductances; the sum.) The analysis of tuned circuits also extends to magnetically-coupled circuits (transformer circuits). In the case of either an ideal or non-ideal (but lossless) transformer, the mean-squared noise voltage across every capacitor is still

$$\overline{\mathrm{v}_C^2(t)} = \frac{kT}{C} \ .$$

As a practical matter, no inductor or transformer is lossless, or even very close to lossless. When losses are present, the mean-squared capacitor noise voltage deviates from $\frac{kT}{C}$ and the amount of deviation depends on the ideal Q of the circuit. The higher the ideal Q the greater the error. Therefore, although high-Q circuits, which confine the signal power to a small frequency range, look attractive from a signal-to-noise ratio point of view they suffer more calibration error due to component losses than lower Q circuits. Another disadvantage of high-Q circuits is that their measurement bandwidth is small and more time is required to achieve a desired statistical uncertainty than in a broader band system. (More later in statistical uncertainty analysis.).

11.3. Digital Signal Processing

Digital signal processing (DSP) is becoming more and more pervasive in engineering and scientific measurement, communication, and control applications. There are two main reasons. First, once a measurement or message or control signal is reduced to numerical form in a digital system, it can be manipulated without any further corruption due to noise or non-linearity or drift problems that can plague analog systems. Second, many operations can be performed easily in programmed digital systems, which would be difficult or impossible in analog systems. Programmed digital systems (computer-based systems) are inherently more flexible then analog systems because the operations are prescribed in software and can be quickly and easily changed.

In the case of JNT, the main advantage of a DSP system is that the power spectral density (PSD) of the signal can be computed and analyzed directly, something that would be very difficult with analog techniques. This allows easy recognition and removal of narrowband interference signals. This can be done on either of the JNT system types, tuned circuit or correlated voltage.

A DSP system for JNT requires the following minimum components:

1. A computer, the faster CPU the better.

2. A high-speed, multichannel A/D board. This hardware actually samples the amplified noise signals. For very-high-speed processing a dedicated FFT processor is desirable.

3. A programming language that allows control of the A/D board and computation and display of results (like LabVIEW™ by National Instruments).

The maximum sampling frequency of the DSP system sets the maximum bandwidth of the measurement system. The bandwidth of the amplified noise signals from the analog processor must be less than half the sampling frequency. The DSP system may or may not be able to keep up with the samples coming in in real time. The samples are typically taken in "blocks" which are usually an integer power of two in length to maximize the efficiency of the FFT algorithm. Each block from each of the two amplifiers is fast-Fourier-transformed on the board and reported to the CPU or done in the CPU directly. The CPU computes the cross power spectral density (CPSD) between the two signals and keeps a running average of the CPSD. The LabVIEW program can recognize narrowband noise spikes in the CPSD and remove them. This can be done by comparing the measured CPSD with a stored CPSD taken in the laboratory without any interference signals present. The CPU divides the "de-spiked" CPSD by the cross-power gain of the two amplifiers to make the best estimate of the sensor voltage noise PSD. From the sensor, PSD an estimate of the temperature is computed.

11.4. Statistical Uncertainty Analysis

The measurement of temperature with the digital signal processing system is based on the fundamental expression for the single-sided power spectral density (PSD), $\mathrm{G}_R(f)$, of the open-circuit noise voltage of a resistor of resistance, R, ohms at an absolute temperature, T, Kelvin,

$$\mathrm{G}_R(f) = 4kTR.$$

That is, a resistor at a constant temperature has a "flat" or "white" noise spectrum that is independent of frequency (up to very high frequencies). If everything else is known, temperature can be computed. That is,

$$T = \frac{\mathrm{G}_R(f)}{4kR}.$$

The two actual measurements are then resistance and PSD. Resistance can be measured at dc by a four-wire technique with high accuracy. Measurement of the PSD of the resistor's open-circuit noise voltage is more involved and difficult.

At typical resistances and temperatures encountered in practice, the PSD of the open-circuit sensor noise voltage is about $10^{-17}\,\frac{\mathrm{V}^2}{\mathrm{Hz}}$. In a bandwidth of 1 MHz, the RMS noise voltage would be about 3 μV. This must be amplified before it can be acquired by a data acquisition system. The input signal to the data acquisition system should typically be in the range of a few volts rms. Therefore, the required voltage gain of the amplifier should be about 1 million. The amplifier itself is a noise source. Therefore, its output noise is a combination of the amplified resistor noise and the amplified amplifier equivalent-input-voltage noise. If the amplifier's expected noise contribution is known, and its transfer function is known, the PSD of the resistor's open-circuit noise voltage, and therefore its

temperature, can be computed. There is some uncertainty, since the amplifier's noise contribution in any given time interval is not the expected value, but rather a value within some uncertainty of the expected value, which depends on the time and bandwidth of the measurement.

An alternate strategy is to use two amplifiers, both amplifying the noise from the same resistor, and find the "cross" power of their outputs. The cross power is the product of the voltage outputs of the two amplifiers. Those parts of their noise outputs that come from the resistor are 100% correlated. Those parts of their noise outputs that come from their own noise are completely uncorrelated. The cross power is a random variable whose expected value is simply related to the PSD of the resistor's open-circuit noise voltage and the transfer functions of the amplifiers. This expected value can be approached arbitrary closely by averaging the cross power over time. As the measurement time increases, the contributions of the amplifiers' noise diminish toward zero, regardless of its expected value. Therefore, knowledge of the exact value of the amplifier's expected noise contribution is not necessary. (However, it should be noted that a lower noise level from the amplifier shortens the averaging time necessary for a given measurement uncertainty.)

Two problems with all low-level noise measurement techniques are electromagnetic interference (EMI) and microphonics. They tend to generate non-thermal noise that, in most practical situations, is usually "narrowband" in nature. That is, their power spectra tend to consist of narrow "spikes" at some fundamental frequency and integer multiples (harmonics) of that fundamental frequency. If the cross power is measured directly by multiplying and averaging the amplifier outputs, then any correlated EMI or microphonics will cause a positive error in the estimation of the resistor's temperature. This kind of interference can be quite effectively detected and eliminated by observing the cross power spectral density (CPSD) of the two amplifier outputs instead of simply computing their cross power. The CPSD is computed by first Fourier transforming the two voltage outputs and then multiplying one transform by the complex conjugate of the other. That is, the CPSD of the amplifier output voltages, $G_{12}(f)$, is given by

$$\mathrm{G}_{12}(f) = \mathrm{V}_{01}(f)\mathrm{V}_{02}^{*}(f)$$

where $\mathrm{V}_{01}(f)$ is the transform of one amplifier output and $\mathrm{V}_{02}(f)$ is the transform of the other. If the two outputs were identical (no amplifier noise and identical amplifier transfer functions) this CPSD would be identical to the PSD of the resistor's open-circuit noise voltage, except multiplied by the power gain of either of the amplifiers. The expected value of $G_{12}(f)$ is the same as the expected value of

$$\mathrm{G}_{oR}(f) = \mathrm{G}_{R}(f)\mathrm{H}_{1}(f)\mathrm{H}_{2}^{*}(f),$$

where $\mathrm{H}(f)$ is the transfer function of an amplifier, because over a very long time interval (approaching infinity) the amplifier noise contributions become negligible. Over a finite time interval there is always some residual error which is minimized by making the time interval (and/or bandwidth) greater.

11.4.1. Analysis of Measurement Uncertainty Using Noiseless Amplifiers

In this section is a derivation of the uncertainty of the measurement of temperature based solely on the statistical properties of the resistor noise and ignoring the effects of amplifier noise. Of course, the amplifiers have significant noise that cannot simply be neglected. However, this analysis will serve as a starting point for the more general analysis that includes the effects of amplifier noise.

Digital measurement of signal characteristics begins with sampling the signal. If the white noise of the resistor could be bandlimited and sampled at the Nyquist rate without noise its mean-squared value could be directly estimated from the samples and knowledge of the bandwidth. (Actually, the signal could be sampled below the Nyquist rate. All that is important in the current statistical analysis is that the samples be independent. However if the signal is sampled below the Nyquist rate the noise and narrowband interference will both be aliased and that complicates some of the later analysis involving the CPSD.) If N independent samples are taken, an unbiased estimate of the mean-squared resistor noise voltage is

$$\overline{\mathrm{v}_R^2} = \frac{1}{N}\sum_{n=0}^{N-1} \mathrm{v}_R^2[n]$$

where $\mathrm{v}_R[n]$ is the "nth" sample of the resistor's open-circuit noise voltage. (The divisor is N instead of N-1 in this case because the mean value is known apriori to be zero and therefore a degree of freedom is not lost in trying to estimate the mean from the set of N data.) This can be rewritten as

$$\overline{\mathrm{v}_R^2} = \frac{\mathrm{E}\left(\mathrm{v}_R^2\right)}{N}\sum_{n=0}^{N-1}\frac{\mathrm{v}_R^2[n]}{\mathrm{E}\left(\mathrm{v}_R^2\right)} = \frac{\mathrm{E}\left(\mathrm{v}_R^2\right)}{N}\chi^2(N)$$

where $\chi^2(N)$ is the "chi-squared" random variable defined by

$$\chi^2(N) = \sum_{i=1}^{N}\left(\frac{x_i - \mu}{\sigma}\right)^2$$

where the x's are Gaussian distributed and independent with a mean of μ and a standard deviation of σ. Therefore $\frac{N\overline{\mathrm{v}_R^2}}{\mathrm{E}\left(\mathrm{v}_R^2\right)}$ is chi-squared. The mean and variance of $\chi^2(N)$ are

$$\mathrm{E}\left[\chi^2(N)\right] = N \quad \text{and} \quad \mathrm{Var}\left[\chi^2(N)\right] = 2N$$

Therefore

$$\mathrm{E}\left[\frac{N\overline{\mathrm{v}_R^2}}{\mathrm{E}\left(\mathrm{v}_R^2\right)}\right]=N \quad \text{and} \quad \mathrm{Var}\left[\frac{N\overline{\mathrm{v}_R^2}}{\mathrm{E}\left(\mathrm{v}_R^2\right)}\right]=2N$$

It is immediately evident from the left-hand equation that $\mathrm{E}\left(\overline{\mathrm{v}_R^2}\right)=\mathrm{E}\left(\mathrm{v}_R^2\right)$. That is, the estimate of the mean-squared voltage is unbiased. Using the property of random variables that

$$\mathrm{Var}(ax)=a^2\,\mathrm{Var}(x)$$

$$\mathrm{Var}\left(\overline{\mathrm{v}_R^2}\right)=2\frac{\left[\mathrm{E}\left(\mathrm{v}_R^2\right)\right]^2}{N}$$

The variance, $\mathrm{Var}\left(\overline{\mathrm{v}_R^2}\right)$, of the estimate, $\overline{\mathrm{v}_R^2}$, of the mean-squared noise voltage can be used to estimate the standard deviation of the estimate of the mean-squared voltage, $\sigma_{\overline{\mathrm{v}_R^2}}$. (The previous statement will probably require two or three readings to get the meaning exactly!) The standard deviation of the estimate of the mean-squared voltage is

$$\sigma_{\overline{\mathrm{v}_R^2}}=\sqrt{\mathrm{Var}\left(\overline{\mathrm{v}_R^2}\right)}=\sqrt{2\frac{\left[\mathrm{E}\left(\mathrm{v}_R^2\right)\right]^2}{N}}=\sqrt{\frac{2}{N}}\,\mathrm{E}\left(\mathrm{v}_R^2\right)$$

and, dividing both sides by the estimate of the mean-squared voltage,

$$\frac{\sigma_{\overline{\mathrm{v}_R^2}}}{\overline{\mathrm{v}_R^2}}=\frac{\sqrt{\frac{2}{N}}\,\mathrm{E}\left(\mathrm{v}_R^2\right)}{\overline{\mathrm{v}_R^2}}\cong\frac{\sqrt{\frac{2}{N}}\,\overline{\mathrm{v}_R^2}}{\overline{\mathrm{v}_R^2}}=\sqrt{\frac{2}{N}}$$

(The approximation is good for large values of *N*.) This final result simply says that (for large *N*) the fractional standard deviation of the estimate of the mean-squared, open-circuit noise voltage is simply $\sqrt{\frac{2}{N}}$ where *N* is the number of independent samples from which the mean-squared, open-circuit noise voltage is estimated. Therefore, to achieve 0.1 percent uncertainty with a bandwidth of 100 kHz requires at least 10 seconds of measurement time or averaging of samples.

11.4.2. Analysis of Measurement Uncertainty Using Real Amplifiers with Noise

Now we will include the effects of amplifier noise on the measurement uncertainty. Instead of considering the simple model of sampling the resistor noise directly we must now consider sampling the output voltages of the amplifiers which are affected by the resistor noise voltage and the amplifier noise voltages. Let the two amplifier output voltages be

$$\mathrm{v}_{o1}(t) = A_1\left[\mathrm{v}_s(t) + \mathrm{v}_{a1}(t)\right] \ , \ \mathrm{v}_{o2}(t) = A_2\left[\mathrm{v}_s(t) + \mathrm{v}_{a2}(t)\right] \ .$$

(We are assuming here that the amplifier gains are both known and independent of frequency.) In the absence of narrowband interference, we would simply sample these voltages and use the average of their product to estimate temperature. The average of their product is

$$\overline{\mathrm{v}_{o1}\,\mathrm{v}_{o2}} = \frac{1}{N}\sum_{n=0}^{N-1}\mathrm{v}_{o1}[n]\,\mathrm{v}_{o2}[n]$$

or

$$\overline{\mathrm{v}_{o1}\,\mathrm{v}_{o2}} = \frac{1}{N}\sum_{n=0}^{N-1}A_1A_2\left(\mathrm{v}_s[n] + \mathrm{v}_{a1}[n]\right)\left(\mathrm{v}_s[n] + \mathrm{v}_{a2}[n]\right)$$

or

$$\overline{\mathrm{v}_{o1}\,\mathrm{v}_{o2}} = \frac{A_1A_2}{N}\sum_{n=0}^{N-1}\left(\mathrm{v}_s[n]\,\mathrm{v}_s[n] + \mathrm{v}_s[n]\,\mathrm{v}_{a1}[n] + \mathrm{v}_s[n]\,\mathrm{v}_{a2}[n] + \mathrm{v}_{a1}[n]\,\mathrm{v}_{a2}[n]\right)$$

The expected value of this product is

$$\mathrm{E}\left(\overline{\mathrm{v}_{o1}\,\mathrm{v}_{o2}}\right) = \frac{A_1A_2}{N}\sum_{n=0}^{N-1}\left(\begin{array}{l}\mathrm{E}\left(\mathrm{v}_s[n]\,\mathrm{v}_s[n]\right) + \underbrace{\mathrm{E}\left(\mathrm{v}_s[n]\,\mathrm{v}_{a1}[n]\right)}_{=0} \\ +\underbrace{\mathrm{E}\left(\mathrm{v}_s[n]\,\mathrm{v}_{a2}[n]\right)}_{=0} + \underbrace{\mathrm{E}\left(\mathrm{v}_{a1}[n]\,\mathrm{v}_{a2}[n]\right)}_{=0}\end{array}\right)$$

or

$$\mathrm{E}\left(\overline{\mathrm{v}_{o1}\,\mathrm{v}_{o2}}\right) = \frac{A_1A_2}{N}\sum_{n=0}^{N-1}\mathrm{E}\left(\mathrm{v}_s^2[n]\right) = A_1A_2\,\mathrm{E}\left(\mathrm{v}_s^2\right) \ .$$

The variance of $\overline{\mathrm{v}_{o1}\,\mathrm{v}_{o2}}$ is the expected value of its square minus the square of its expected value,

$$\mathrm{Var}\left(\overline{\mathrm{v}_{o1}\,\mathrm{v}_{o2}}\right) = \mathrm{E}\left(\overline{\mathrm{v}_{o1}\,\mathrm{v}_{o2}}^{\,2}\right) - \left[\mathrm{E}\left(\overline{\mathrm{v}_{o1}\,\mathrm{v}_{o2}}\right)\right]^2 \ .$$

The expected value of its square is

$$\mathrm{E}\left(\overline{\mathrm{v}_{o1}\,\mathrm{v}_{o2}}^{\,2}\right) = \mathrm{E}\left\{\left(\frac{A_1A_2}{N}\right)^2\sum_{n=0}^{N-1}\left(\begin{array}{l}\mathrm{v}_s[n]\,\mathrm{v}_s[n] + \mathrm{v}_s[n]\,\mathrm{v}_{a1}[n] \\ +\mathrm{v}_s[n]\,\mathrm{v}_{a2}[n] + \mathrm{v}_{a1}[n]\,\mathrm{v}_{a2}[n]\end{array}\right)\sum_{m=0}^{N-1}\left(\begin{array}{l}\mathrm{v}_s[m]\,\mathrm{v}_s[m] + \mathrm{v}_s[m]\,\mathrm{v}_{a1}[m] \\ +\mathrm{v}_s[m]\,\mathrm{v}_{a2}[m] + \mathrm{v}_{a1}[m]\,\mathrm{v}_{a2}[m]\end{array}\right)\right\}$$

$$\mathrm{E}\left(\overline{\mathrm{v}_{o1}\,\mathrm{v}_{o2}}^{\,2}\right) = \left(\frac{A_1A_2}{N}\right)^2\mathrm{E}\left\{\sum_{n=0}^{N-1}\sum_{m=0}^{N-1}\left(\begin{array}{l}\mathrm{v}_s[n]\,\mathrm{v}_s[n] + \mathrm{v}_s[n]\,\mathrm{v}_{a1}[n] \\ +\mathrm{v}_s[n]\,\mathrm{v}_{a2}[n] + \mathrm{v}_{a1}[n]\,\mathrm{v}_{a2}[n]\end{array}\right)\left(\begin{array}{l}\mathrm{v}_s[m]\,\mathrm{v}_s[m] + \mathrm{v}_s[m]\,\mathrm{v}_{a1}[m] \\ +\mathrm{v}_s[m]\,\mathrm{v}_{a2}[m] + \mathrm{v}_{a1}[m]\,\mathrm{v}_{a2}[m]\end{array}\right)\right\}$$

$$\mathrm{E}\left(\overline{\mathrm{v}_{o1}\,\mathrm{v}_{o2}}^{\,2}\right)=\left(\frac{A_1A_2}{N}\right)^2\sum_{n=0}^{N-1}\sum_{m=0}^{N-1}\mathrm{E}\left(\begin{array}{l}\mathrm{v}_s[n]\mathrm{v}_s[n]\mathrm{v}_s[m]\mathrm{v}_s[m]+\mathrm{v}_s[n]\mathrm{v}_{a1}[n]\mathrm{v}_s[m]\mathrm{v}_s[m]\\+\mathrm{v}_s[n]\mathrm{v}_{a2}[n]\mathrm{v}_s[m]\mathrm{v}_s[m]+\mathrm{v}_{a1}[n]\mathrm{v}_{a2}[n]\mathrm{v}_s[m]\mathrm{v}_s[m]\\+\mathrm{v}_s[n]\mathrm{v}_s[n]\mathrm{v}_s[m]\mathrm{v}_{a1}[m]+\mathrm{v}_s[n]\mathrm{v}_{a1}[n]\mathrm{v}_s[m]\mathrm{v}_{a1}[m]\\+\mathrm{v}_s[n]\mathrm{v}_{a2}[n]\mathrm{v}_s[m]\mathrm{v}_{a1}[m]+\mathrm{v}_{a1}[n]\mathrm{v}_{a2}[n]\mathrm{v}_s[m]\mathrm{v}_{a1}[m]\\+\mathrm{v}_s[n]\mathrm{v}_s[n]\mathrm{v}_s[m]\mathrm{v}_{a2}[m]+\mathrm{v}_s[n]\mathrm{v}_{a1}[n]\mathrm{v}_s[m]\mathrm{v}_{a2}[m]\\+\mathrm{v}_s[n]\mathrm{v}_{a2}[n]\mathrm{v}_s[m]\mathrm{v}_{a2}[m]+\mathrm{v}_{a1}[n]\mathrm{v}_{a2}[n]\mathrm{v}_s[m]\mathrm{v}_{a2}[m]\\+\mathrm{v}_s[n]\mathrm{v}_s[n]\mathrm{v}_{a1}[m]\mathrm{v}_{a2}[m]+\mathrm{v}_s[n]\mathrm{v}_{a1}[n]\mathrm{v}_{a1}[m]\mathrm{v}_{a2}[m]\\+\mathrm{v}_s[n]\mathrm{v}_{a2}[n]\mathrm{v}_{a1}[m]\mathrm{v}_{a2}[m]+\mathrm{v}_{a1}[n]\mathrm{v}_{a2}[n]\mathrm{v}_{a1}[m]\mathrm{v}_{a2}[m]\end{array}\right)$$

Most of these 4-factor products have expected values of zero because of the independence of the resistor and amplifier noise voltages. When those are deleted the expression becomes

$$\mathrm{E}\left(\overline{\mathrm{v}_{o1}\,\mathrm{v}_{o2}}^{\,2}\right)=\left(\frac{A_1A_2}{N}\right)^2\sum_{n=0}^{N-1}\sum_{m=0}^{N-1}\mathrm{E}\left(\begin{array}{l}\mathrm{v}_s^2[n]\mathrm{v}_s^2[m]+\mathrm{v}_s[n]\mathrm{v}_s[m]\mathrm{v}_{a1}[n]\mathrm{v}_{a1}[m]\\+\mathrm{v}_s[n]\mathrm{v}_s[m]\mathrm{v}_{a2}[n]\mathrm{v}_{a2}[m]+\mathrm{v}_{a1}[n]\mathrm{v}_{a1}[m]\mathrm{v}_{a2}[n]\mathrm{v}_{a2}[m]\end{array}\right)$$

$$\mathrm{E}\left(\overline{\mathrm{v}_{o1}\,\mathrm{v}_{o2}}^{\,2}\right)=\left(\frac{A_1A_2}{N}\right)^2\left\{\begin{array}{l}N\,\mathrm{E}\left(\mathrm{v}_s^4\right)+\left(N^2-N\right)\left[\mathrm{E}\left(\mathrm{v}_s^2\right)\right]^2\\+N\,\mathrm{E}\left(\mathrm{v}_s^2\right)\mathrm{E}\left(\mathrm{v}_{a1}^2\right)+N\,\mathrm{E}\left(\mathrm{v}_s^2\right)\mathrm{E}\left(\mathrm{v}_{a2}^2\right)+N\,\mathrm{E}\left(\mathrm{v}_{a1}^2\right)\mathrm{E}\left(\mathrm{v}_{a2}^2\right)\end{array}\right\}$$

$$\mathrm{Var}\left(\overline{\mathrm{v}_{o1}\,\mathrm{v}_{o2}}\right)=\left(\frac{A_1A_2}{N}\right)^2\left\{\begin{array}{l}N\,\mathrm{E}\left(\mathrm{v}_s^4\right)+\left(N^2-N\right)\left[\mathrm{E}\left(\mathrm{v}_s^2\right)\right]^2\\+N\,\mathrm{E}\left(\mathrm{v}_s^2\right)\mathrm{E}\left(\mathrm{v}_{a1}^2\right)+N\,\mathrm{E}\left(\mathrm{v}_s^2\right)\mathrm{E}\left(\mathrm{v}_{a2}^2\right)+N\,\mathrm{E}\left(\mathrm{v}_{a1}^2\right)\mathrm{E}\left(\mathrm{v}_{a2}^2\right)\end{array}\right\}-\left\{A_1A_2\,\mathrm{E}\left(\mathrm{v}_s^2\right)\right\}^2$$

$$\mathrm{Var}\left(\overline{\mathrm{v}_{o1}\,\mathrm{v}_{o2}}\right)=\left(\frac{A_1A_2}{N}\right)^2\left\{\begin{array}{l}N\,\mathrm{E}\left(\mathrm{v}_s^4\right)+\left(N^2-N\right)\left[\mathrm{E}\left(\mathrm{v}_s^2\right)\right]^2-N^2\,\mathrm{E}\left(\mathrm{v}_s^2\right)\\+N\,\mathrm{E}\left(\mathrm{v}_s^2\right)\mathrm{E}\left(\mathrm{v}_{a1}^2\right)+N\,\mathrm{E}\left(\mathrm{v}_s^2\right)\mathrm{E}\left(\mathrm{v}_{a2}^2\right)+N\,\mathrm{E}\left(\mathrm{v}_{a1}^2\right)\mathrm{E}\left(\mathrm{v}_{a2}^2\right)\end{array}\right\}$$

Using the fact that, for any random variable, X, which is Gaussian distributed (and these noise processes are Gaussian distributed) the nth central moment is given by

$$\mathrm{E}\left\{\left[X-\mathrm{E}(X)\right]^n\right\}=\begin{cases}0 & ,\ n\ \text{odd}\\ 1\cdot 3\cdot 5\ldots(n-1)\sigma_X^n & ,\ n\ \text{even}\end{cases}$$

we get

$$\mathrm{Var}\left(\overline{\mathrm{v}_{o1}\,\mathrm{v}_{o2}}\right)=\frac{\left(A_1A_2\right)^2}{N}\left\{3\left[\sigma_{\mathrm{v}_s}^2\right]^2-\left[\sigma_{\mathrm{v}_s}^2\right]^2+\sigma_{\mathrm{v}_s}^2\sigma_{\mathrm{v}_{a1}}^2+\sigma_{\mathrm{v}_s}^2\sigma_{\mathrm{v}_{a2}}^2+\sigma_{\mathrm{v}_{a1}}^2\sigma_{\mathrm{v}_{a2}}^2\right\}$$

or

$$\mathrm{Var}\left(\overline{\mathrm{v}_{o1}\,\mathrm{v}_{o2}}\right)=\frac{\left(A_1A_2\right)^2}{N}\left\{2\left[\sigma_{\mathrm{v}_s}^2\right]^2+\sigma_{\mathrm{v}_s}^2\left(\sigma_{\mathrm{v}_{a1}}^2+\sigma_{\mathrm{v}_{a2}}^2\right)+\sigma_{\mathrm{v}_{a1}}^2\sigma_{\mathrm{v}_{a2}}^2\right\}$$

The standard deviation is the positive square root of the variance and the fractional standard deviation is the standard deviation divided by the expected value or

$$\frac{\sigma_{\overline{\mathrm{v}_{o1}\mathrm{v}_{o2}}}}{\mathrm{E}\left(\overline{\mathrm{v}_{o1}\mathrm{v}_{o2}}\right)} = \frac{\sqrt{\frac{\left(A_1A_2\right)^2}{N}\left\{2\left[\sigma^2_{\mathrm{v}_s}\right]^2 + \sigma^2_{\mathrm{v}_s}\left(\sigma^2_{\mathrm{v}_{a1}} + \sigma^2_{\mathrm{v}_{a2}}\right) + \sigma^2_{\mathrm{v}_{a1}}\sigma^2_{\mathrm{v}_{a2}}\right\}}}{A_1A_2\underbrace{\mathrm{E}\left(\mathrm{v}_s^2\right)}_{=\sigma^2_{\mathrm{v}_s}}}$$

or

$$\frac{\sigma_{\overline{\mathrm{v}_{o1}\mathrm{v}_{o2}}}}{\mathrm{E}\left(\overline{\mathrm{v}_{o1}\mathrm{v}_{o2}}\right)} = \sqrt{\frac{2}{N}}\sqrt{1+\frac{1}{2}\left(\frac{\sigma^2_{\mathrm{v}_{a1}} + \sigma^2_{\mathrm{v}_{a2}}}{\sigma^2_{\mathrm{v}_s}} + \frac{\sigma^2_{\mathrm{v}_{a1}}\sigma^2_{\mathrm{v}_{a2}}}{\left(\sigma^2_{\mathrm{v}_s}\right)^2}\right)} \quad .$$

By knowing the relative magnitudes of the resistor and amplifier noise PSD's one can estimate the fractional error in the measurement of the resistor's mean-squared noise voltage. Notice that, in the last expression, if the amplifier noise is set to zero, the fractional standard deviation reduces to

$$\frac{\sigma_{\overline{\mathrm{v}_{o1}\mathrm{v}_{o2}}}}{\mathrm{E}\left(\overline{\mathrm{v}_{o1}\mathrm{v}_{o2}}\right)} = \sqrt{\frac{2}{N}} \quad .$$

as in the previous analysis.

In the case in which the system limits the bandwidth ideally (with an ideal lowpass filter), and sampling is done at exactly the Nyquist rate, the relation between the number of samples, *N,* bandwidth, Δf , and measurement time, Δt, is

$$\Delta t \Delta f = \frac{N}{2} \quad .$$

Therefore, the fractional measurement uncertainty is

$$\frac{\sigma_{\overline{\mathrm{v}_{o1}\mathrm{v}_{o2}}}}{\mathrm{E}\left(\overline{\mathrm{v}_{o1}\mathrm{v}_{o2}}\right)} = \sqrt{\frac{1}{\Delta t \Delta f}}\sqrt{1+\frac{1}{2}\left(\frac{\sigma^2_{\mathrm{v}_{a1}} + \sigma^2_{\mathrm{v}_{a2}}}{\sigma^2_{\mathrm{v}_s}} + \frac{\sigma^2_{\mathrm{v}_{a1}}\sigma^2_{\mathrm{v}_{a2}}}{\left(\sigma^2_{\mathrm{v}_s}\right)^2}\right)}$$

leading to the general principle that the fractional measurement uncertainty is proportional to the reciprocal of the square root of the product of bandwidth and time.

12. Appendix B — RTD to Front-End Electronics Cable Calculations

A simple model of the interconnecting cable and its associated capacitance is developed to estimate the allowable distance of the electronics from the sensor. This analysis ignores almost all of the actual electronic implementation issues such as amplifier stability with long cables, microphonics, etc. that will need to be addressed in an actual system. These calculations only represent the limits in bandwidth to be expected with some first-order assumptions.

The noise power due to any passive network is known to be

$$\overline{v^2} = 4kT\,\mathrm{Re}\{Z(f)\}df \ ,$$

where *Z(f)* is the impedance as a function of frequency of the passive network and *df* is the frequency over which the measurement is to be made. The network between the input JNT amplifier and the RTD can be configured as a four-wire network as shown in Figure 44. Assume that the network connecting the RTD and preamplifier consists of the resistive RTD and the cable capacitance; the system can be modeled as shown in Figure 45, where the cable capacitances are reduced to the simple lumped-element, conductor-to-shield capacitances that are proportional to cable length.

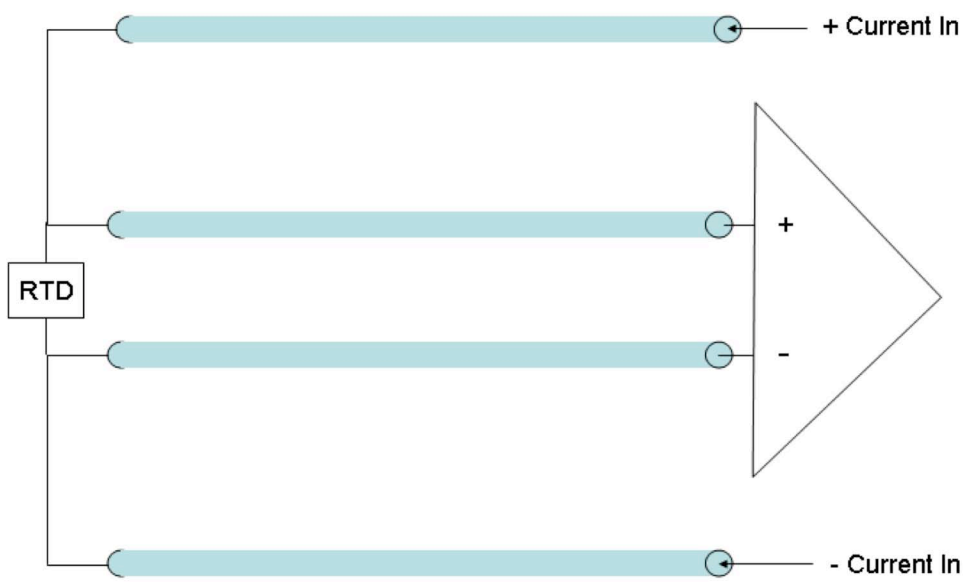

Figure 44. Four-wire RTD configuration on which model is based

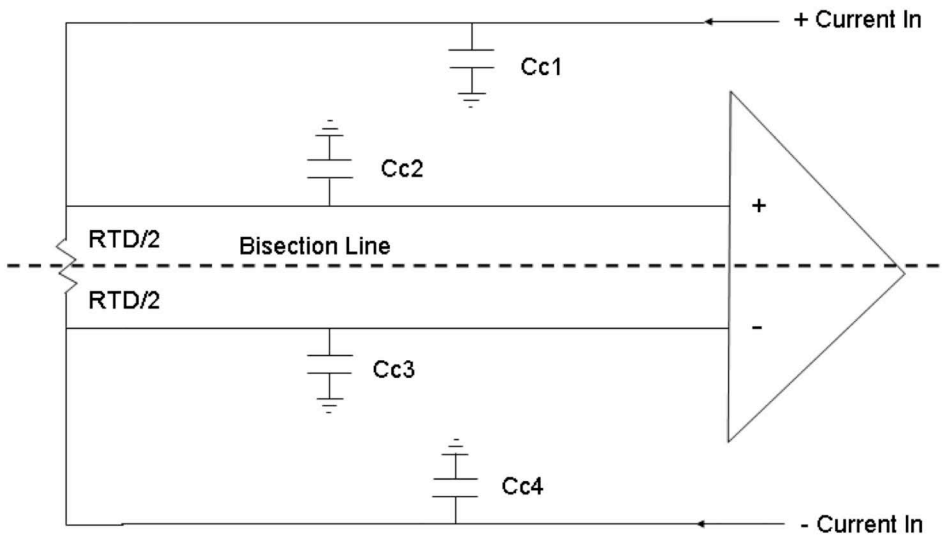

Figure 45. Simple RC model showing use of Bisection theorem

Applying the bisection theorem to simplify the symmetrical network results in the impedance equation between the amplifier input and ground of

$$Z(f) = \frac{RTD/2}{1 + j2\pi f(RTD/2)(Cc1 + Cc2 + Cin)},$$

where RTD/2 is half the value of the RTD (bisected), and Cin is the input capacitance of one side of the differential FET amplifier input. The real part of the impedance above can be found to be

$$\mathrm{Re}\{Z(f)\} = \frac{RTD/2}{1 + (2\pi f)^2 (RTD/2)^2 (Cc1 + Cc2 + Cin)^2}$$

The assumption is made that the impedance may degrade no more than 0.1 percent at the highest frequency of interest for the measurement. This results in less than a 0.1 percent variation of noise power over the measurement bandwidth. This requirement is given as

$$(2\pi f)^2 (RTD/2)^2 (Cc1 + Cc2 + Cin)^2 \leq 0.001$$

A further assumption is that the connecting cable exhibits a capacitance of 30 pF/ft or 98.4 pF/m (a nominal value exhibited by many types of cable), we can graph the maximum available bandwidth versus cable length for a 100-ohm RTD that exhibits loss of less than 0.1 percent of the noise power. Figure 46 assumes a 50 pF input capacitance of the JFET preamplifiers.

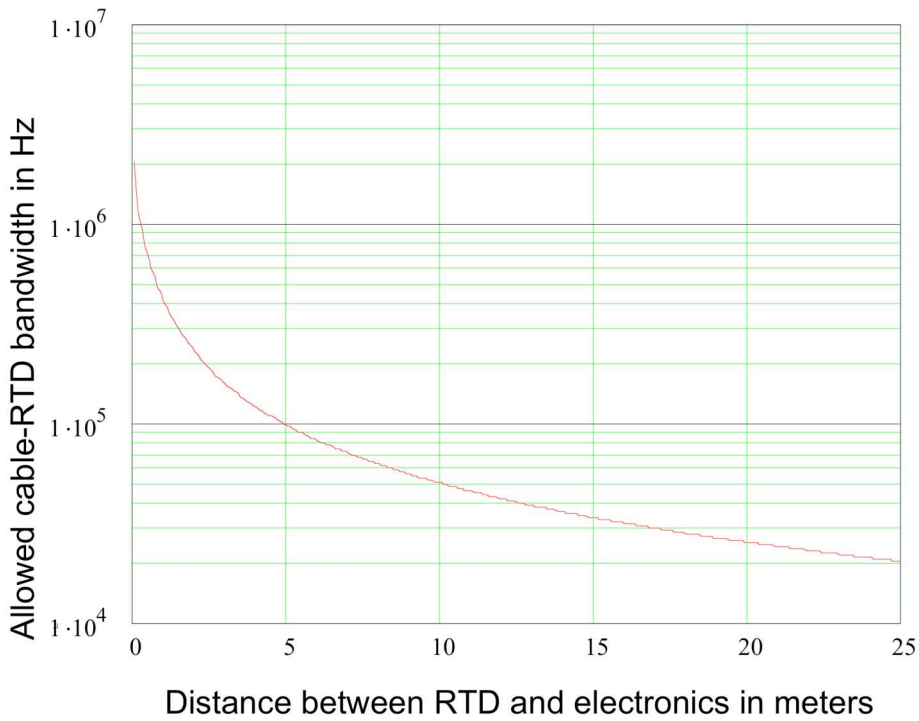

Figure 46. Estimated cable losses due to separation distance

According to the graph, if the electronics are located 25 m from the RTD, the JNT system would only operate with a bandwidth of about 20 kHz. In reality, the bandwidth will likely be higher without significant degradation since we chose the bandwidth limits based on 0.1 percent reduction in the noise power. A narrow bandwidth of 20 kHz does not necessarily pose a problem from a theoretical measurement standpoint but could present practical problems in a real implementation. Low-frequency vibrations in the environment can appear in the audio range because of microphonic interference. The bandwidth, assumptions made in this derivation, and other implementation issues need to be carefully considered in the conceptual design of the system.

13. Appendix C — User's Guide to ORNL Johnson Noise Thermometry System

Rev. B
6/14/2004

Contents

Specifications ……x
Introduction ……x
The Receiver Box ……x
The Transmitter Box ……x
System Connections ……..x

Specifications

Name	*Description*
JNT TX Power Box: (1)	2 separate dc supplies (+/-15, +/-12). Universal ac input. Jumpers set for 120V ac.
JNT Transmitter Box: (1)	Input for thermocouple sensor. Three differential outputs: 2 for noise channels and 1 for dc temperature value.
JNT Receiver Box: (1)	Three differential inputs to receive 2 noise channels and 1 dc temperature channel. Three Single ended outputs of amplified and filtered noise and temp values.
Connectors: (6+6+3)	BNC connectors for all signal outputs of transmitter box and inputs and outputs of receiver box.
Power cords: (2+ 2)	United States standard 3-conductor ac cords for JNT TX Power Box and JNT Receiver Box. AMP # 206060-1 four contact (3 used) plug w/pins to connect dc power from JNT TX Power Box to JNT Transmitter Box.

NOTE: All power supplies are Power-One model HBB15-1.5-A. Input fuse on the JNT Receiver Box is 1A fast blow. Input fuse on the JNT TX Power Box is a 1.25A slow-blow (Bussman MDL 1.25).

Introduction

The hardware for doing this experiment is intended to measure the temperature based on the principles of Johnson Noise thermometry. The transmitter box has two circuit boards. The first board has 2 high gain preamp channels that senses and filters the Johnson noise of an attached RTD sensor. The second board supplies a calibration signal for the Johnson noise preamplifier board and processes the dc value of the sensor resistance. The transmitter box is powered by two dc power supplies provided by an external, remote power supply box.

The receiver box has 3 channels – 2 for receiving the noise values transmitted and 1 for receiving the dc temp values. The single-ended outputs from the receiver are connected to a PCI9812 ADC board mounted in a computer with which the values are processed using software. The ADC board and programs are not supplied.

Allow ten minutes after applying power for circuits in the head and receiver boxes to thermally equilibrate.

The Receiver Box

The following diagram shows the Receiver box input and output connectors as well as the adjustment potentiometers and their intended function.

Potentiometer Adjustments in the JNT Receiver Box

1. R26 - adjusts the gain of Noise Ch1 input stage from x1 to x10
2. R66 - adjusts the gain of Noise Ch2 input stage from x1 to x10
3. R108 - adjusts the gain of Temperature input stage from x1 to x10
4. R158 - adjusts the discriminator level for the 4046 PLL chip
5. R152 - For adjusting the dc offset of the Temperature output filter stage

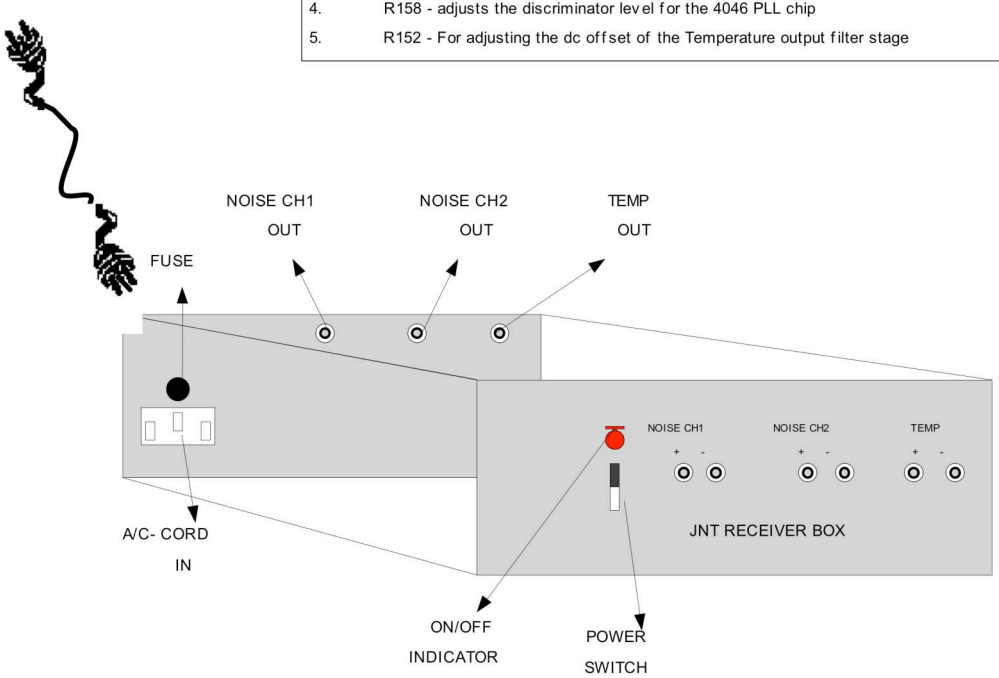

The Transmitter Box

The following diagram shows the transmitter box input and output connectors as well as the adjustment potentiometers and their intended functions. **NOTE: Only the AC Calibration Board has any user adjustments.**

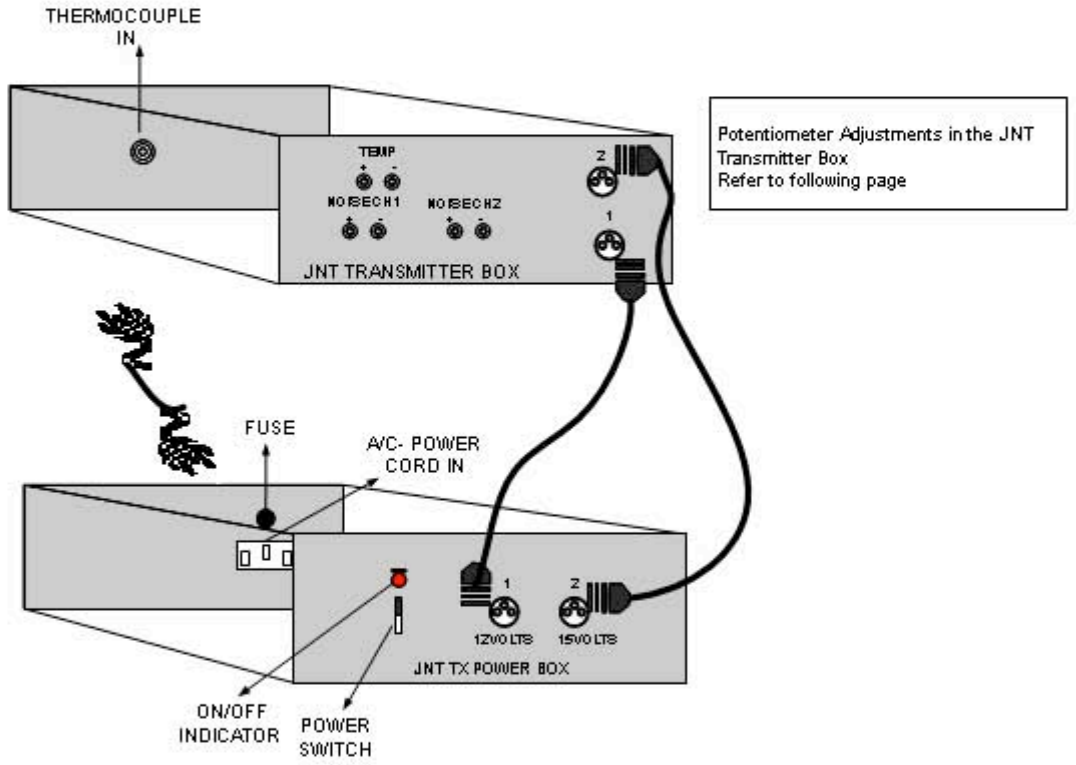

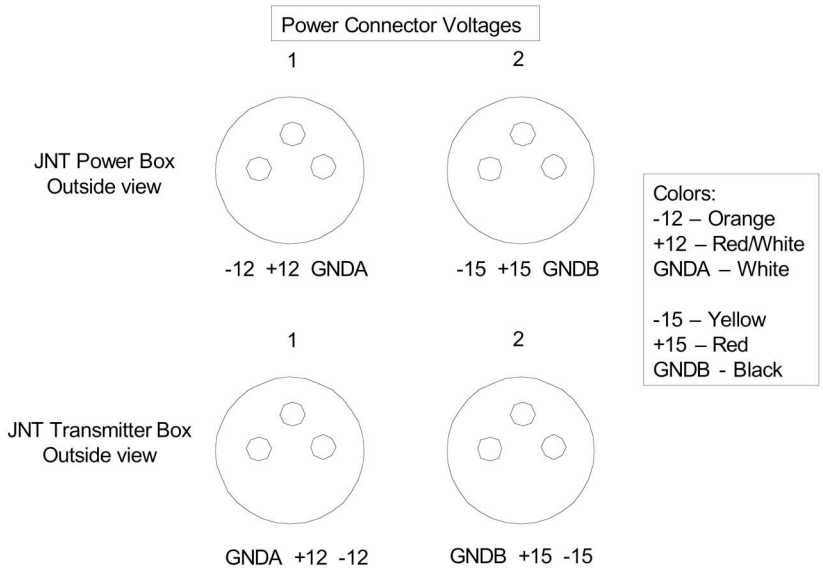

OPERATION AND ADJUSTMENTS ON THE AC CALIBRATION BOARD

Slow Sawtooth Waveform generator

U17 and U15 constitute a sawtooth waveform generator that provides the drive for the frequency modulation of the AC calibration signal. U17 is a waveform generator that generates a sawtooth with a frequency of 1Hz or less. The output of U17 is between -1V and +1V. This is offset positively by U15 and R69 to 0V to +2V. That voltage signal is then converted into a current at the collector of Q18. The value of the current linearly sweeps between 7µA and 700µA.

50kHz-2MHz Waveform Generator

U16 is configured as a sine generator that is frequency modulated by the collector current of Q18 as described above. The waveform supplied by U16 is a sine wave that sweeps linearly between 50kHz and 2MHz. Please note these frequencies are approximate and not critical as they only need to cover the majority of the bandpass of the preamplifier.

Automatic Gain Control for Output

This automatic gain control (AGC) takes the output from U16 and sets it at a fixed 1VPP at pin 12 of U18. This value can be adjusted by R97.

U21 Differential Driver

U21 supplies the actual drive of the swept signal to the RTD and is adjusted by R148. The value of signal required is dependent on the software being used. The value is set to 0V as shipped from ORNL.

dc Resistance Bias Circuit

This circuitry supplies a 100µA constant current to the RTD. The resultant voltage across the RTD is then an indicator of its value.

dc Resistance Measurement Circuit

This is a differential-to-single-ended conversion, gain, and filtering section that takes the voltage across the RTD, amplifies and filters it for measurement. R109 and R127 are offset adjustments for the input JFET amplifiers. They can be adjusted so that the respective outputs at pin 6 of U24 and U29 are at 0V when the inputs to R151 and R152 are grounded. This should not need to be adjusted as it was set at ORNL.

U32 and U34 Voltage to Frequency Converter

U32 is a Voltage-Frequency Converter (VFC). R134 should be set such that for an RTD value of 100Ω, the output of U34 is a frequency of ~17kHz and for an RTD value of 275Ω , the output is ~90kHz. R137 is not used.

System Connections

NOTE: <u>All six signal cables</u> between the transmitter and receiver boxes MUST be connected during data acquisition. Oscillation and/or excess noise will result if they are not.

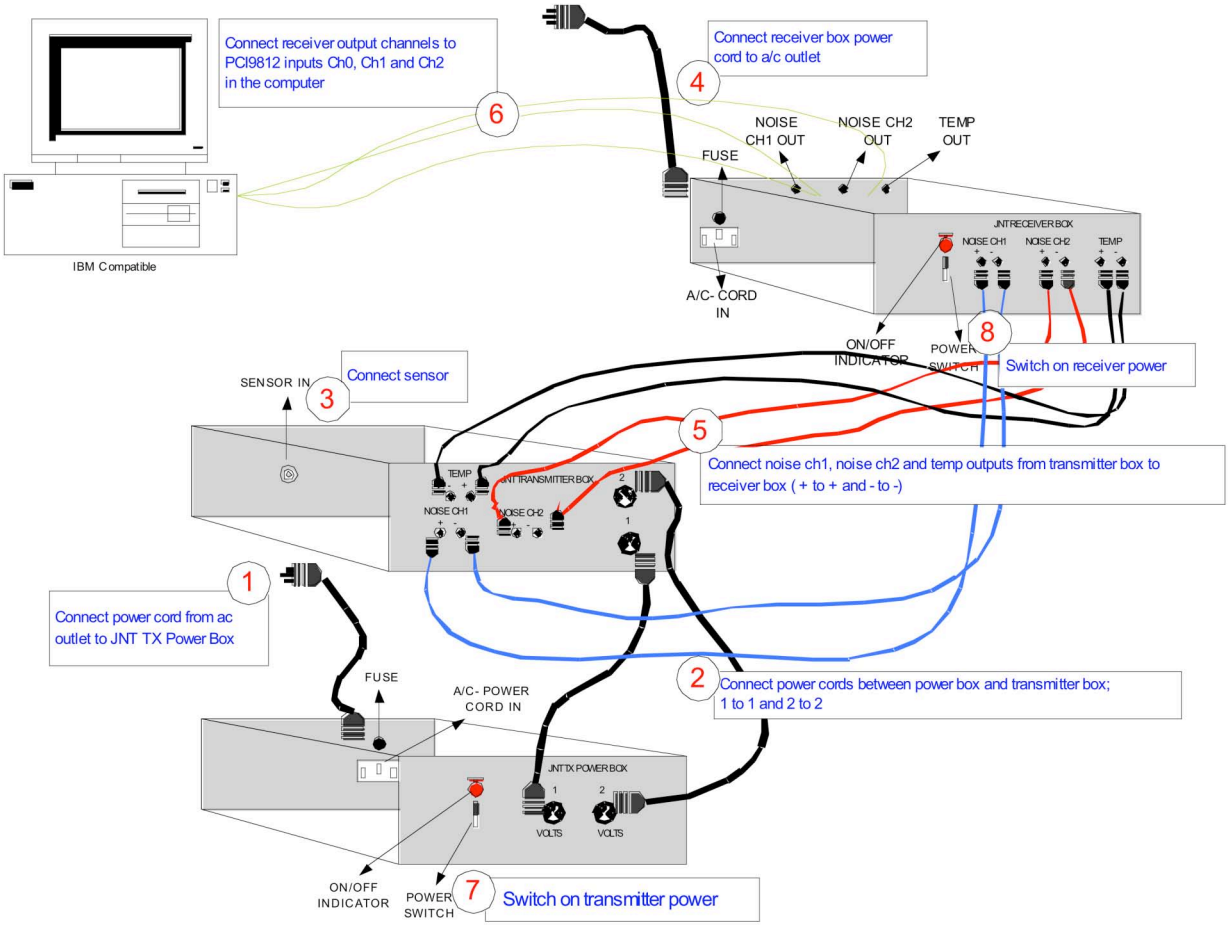

NOTE: <u>All six signal cables</u> between the transmitter and receiver boxes MUST be connected during data acquisition. Oscillation and/or excess noise will result if they are not.

14. Appendix D — Schematic Diagrams

Diagram Number	Date	Diagram Title
SKF-1163-1R1	4/03	ORNL Johnson Noise Thermometry AC Calibration and dc Readout Circuit Board
SKF-1163-4	4/03	ORNL Johnson Noise Thermometry Preamp Circuit Board
SKF-1163-5	4/03	Johnson Noise Thermometry Differential Receiver Circuit Board

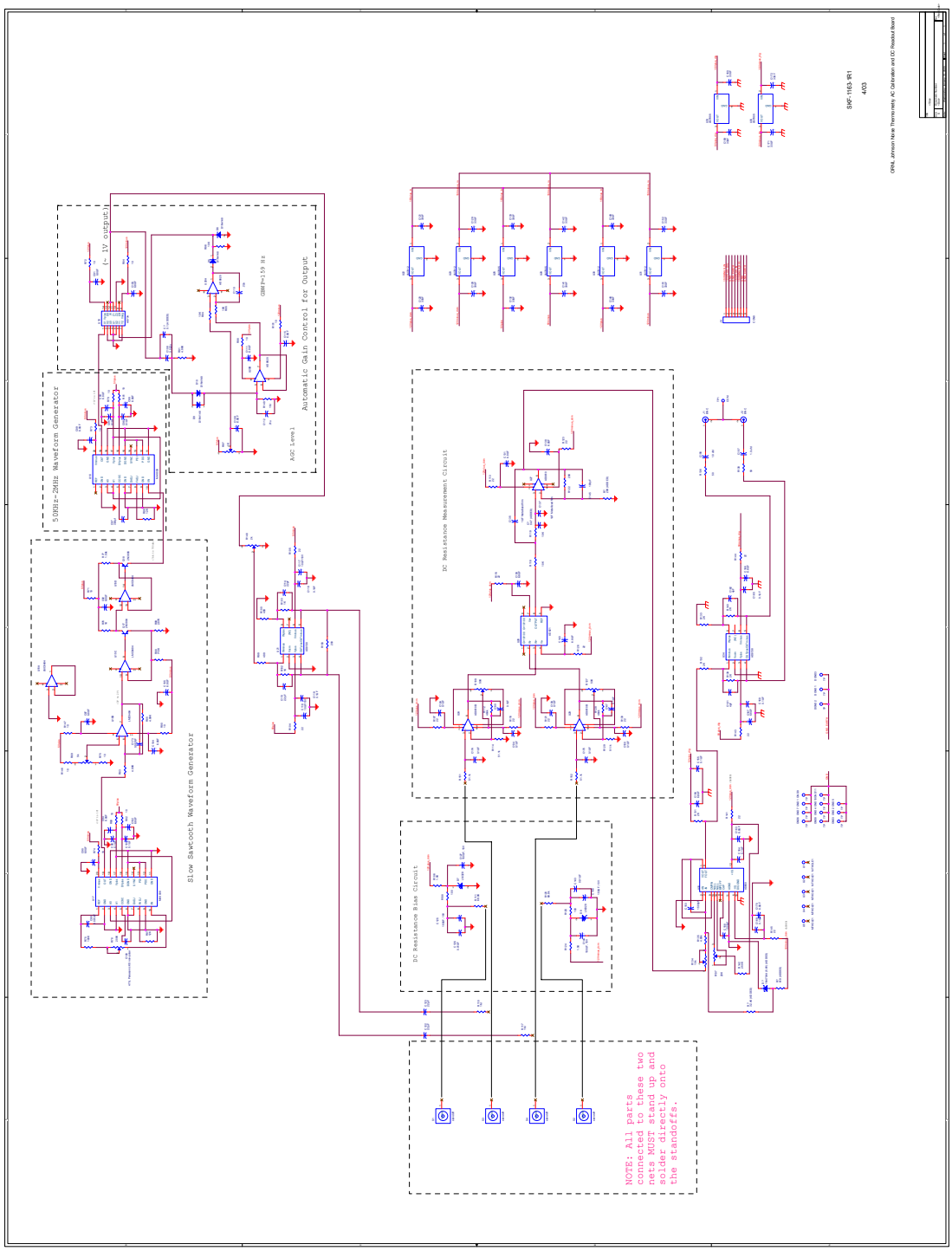

Figure 47. ORNL Johnson Noise Thermometry AC Calibration and dc Readout Circuit Board

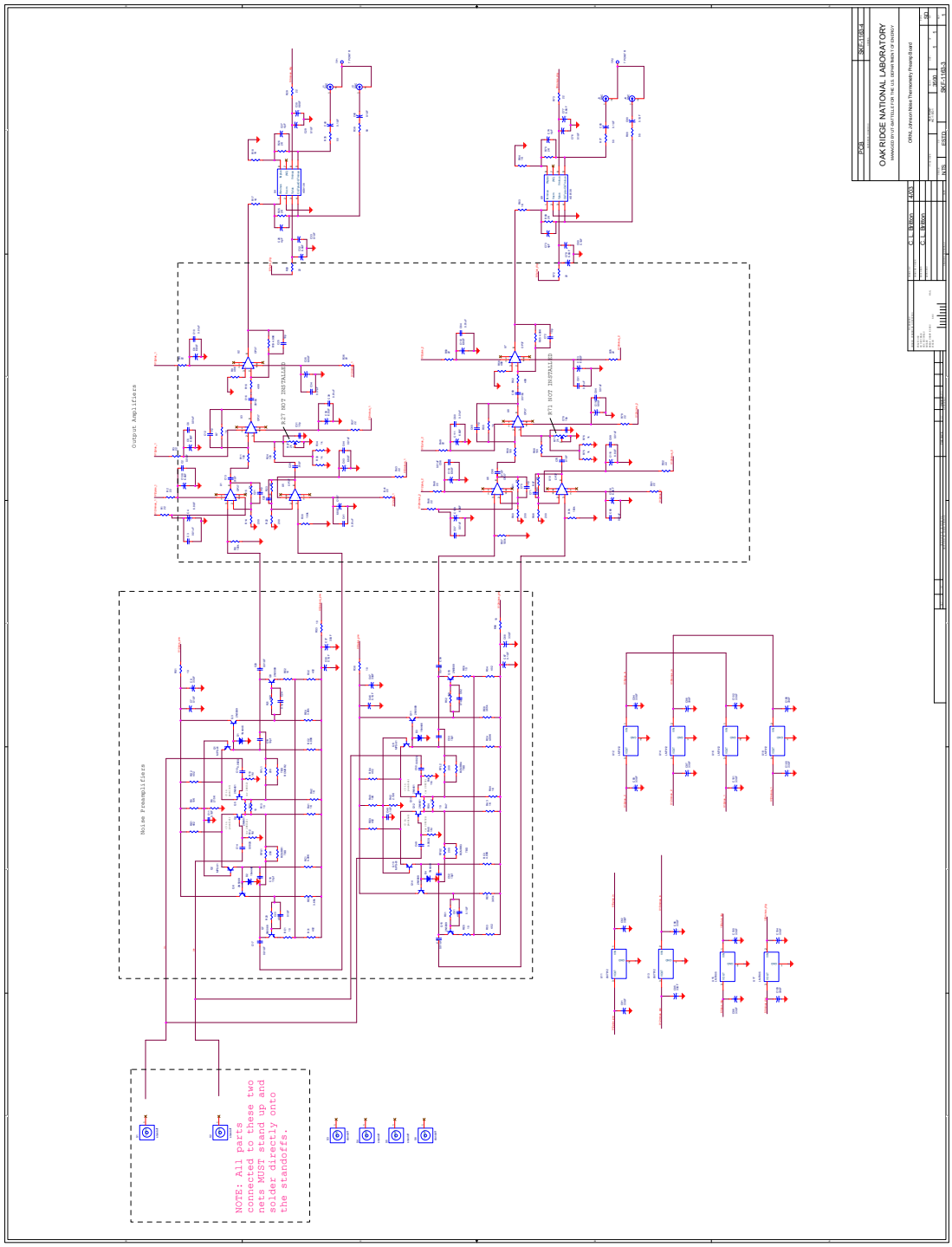

Figure 48. ORNL Johnson Noise Thermometry Preamp Circuit Board

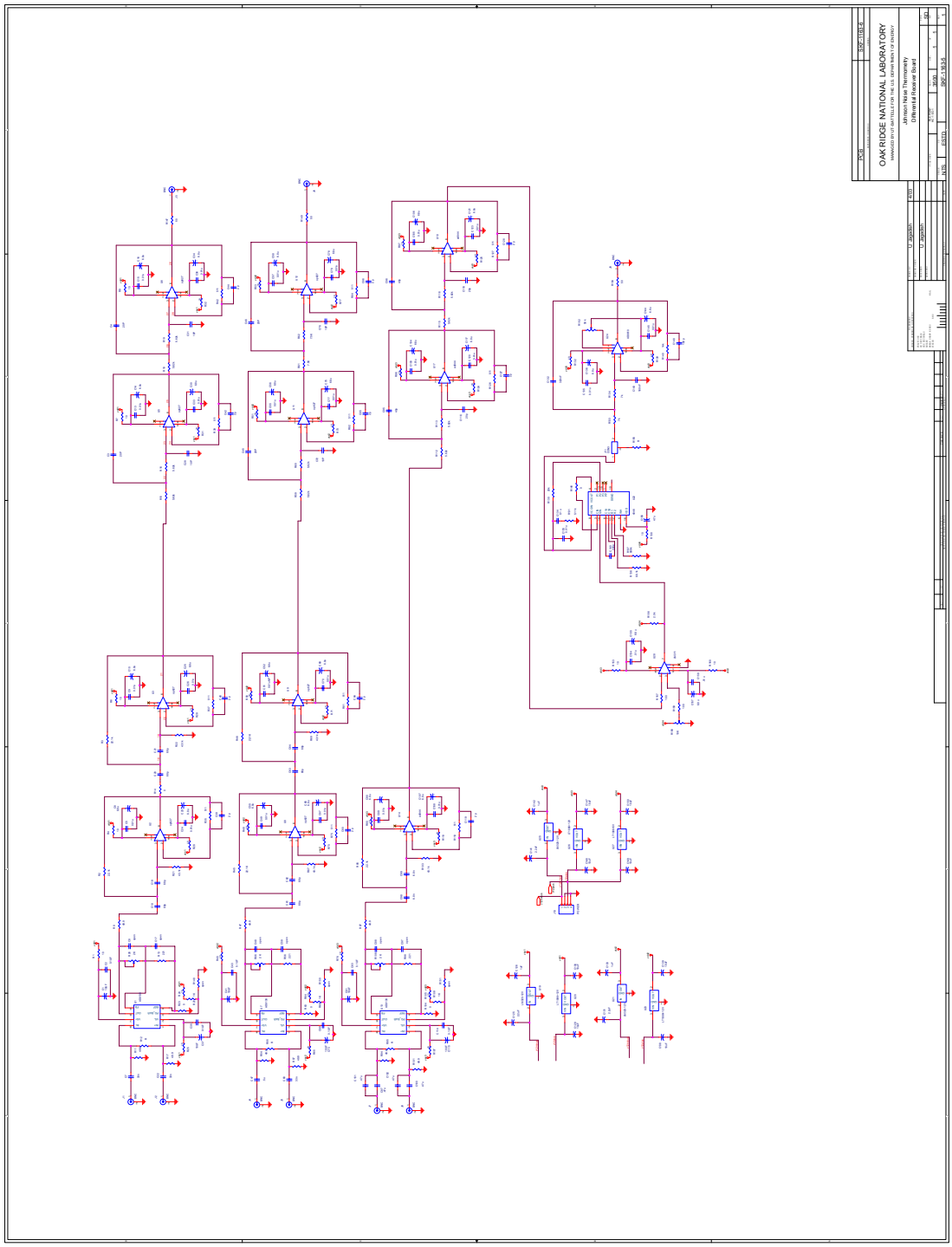

Figure 49. Johnson Noise Thermometry Differential Receiver Circuit Board

15. Appendix E — ORNL JNT Parts List

Bill of Materials
May 10, 2004

ORNL JNT AC Calibration and DC Readout Board

Item	Quantity	Reference	Part
1	26	C87,C89,C90,C91,C92,C93, C94,C99,C102,C103,C104, C105,C109,C111,C115,C117, C118,C131,C136,C138,C140, C154,C163,C166,C167,C170	6.8UF
2	2	C173,C88	0.001UF
3	19	C95,C96,C98,C101,C116, C119,C124,C130,C134,C139, C147,C150,C155,C164,C165, C168,C169,C174,C175	0.1UF
4	1	C97	300pf
5	1	C100	47U, Panasonic KS non-polar
6	1	C106	0.022u
7	1	C110	.22u
8	1	C112	.01u
9	4	C113,C114,C161,C162	4pF
10	16	C120,C121,C128,C129,C132, C133,C141,C142,C148,C149, C151,C152,C159,C160,C171, C172	33UF
11	2	C123,C122	22pF
12	4	C125,C127,C144,C146	150UF, 15V
13	2	C126,C143	0.01UF
14	2	C137,C135	1UF Metallized film
15	1	C145	100pF
16	1	C153	1500pf
17	2	C156,C157	1.0 ufd
18	1	C158	1000pf
19	14	GND1,DGND1,GND2,DGND2, GND3,DGND3,GND4,GND5, GND6,GND7,GND8,GND9, GND10,GND11	TP
20	4	D5,D6,D9,D10	D1N4148
21	2	D8,D7	LM329

ORNL JNT AC Calibration and DC Readout Board

Item	Quantity	Reference	Part
22	2	J1,J2	BNC
23	1	J4	CON8
24	1	Q17	2N3904
25	1	Q18	2N3906
26	1	R69	5k
27	1	R70	100K
28	15	R71,R72,R73,R74,R75,R79, R80,R81,R82,R84,R90,R98, R101,R146,R147	10
29	4	R76,R97,R102,R103	1K
30	1	R77	1.58k
31	1	R78	200K
32	4	R83,R85,R91,R135	4.99k
33	2	R86,R87	12K
34	1	R88	715K
35	1	R89	2.87K
36	6	R94,R95,R96,R118,R119, R134	10K
37	2	R99,R100	499
38	14	R104,R105,R107,R113,R115, R116,R121,R123,R126,R130, R141,R143,R144,R145	22
39	2	R106,R124	1.5K
40	2	R108,R125	100
41	2	R109,R127	50K
42	3	R110,R117,R149	1M
43	2	R111,R120	69.8k
44	2	R112,R128	464k
45	4	R114,R129,R151,R152	51.1k
46	2	R122,R137	20K
47	6	R131,R132,R133,R139,R140, R148	2K
48	2	R136,R138	50
49	1	R142	250K
50	1	R150	200
51	4	S1,S2,S3,S4	standoff
52	1	TP1	COM
53	5	U1,U2,U3,U4,U5	MTHOLE1
54	1	U15	LMC6484
55	2	U16,U17	MAX038
56	1	U18	AD734
57	1	U20	AD8620
58	2	U21,U34	AD8138
59	2	U22,U30	LM7812

ORNL JNT AC Calibration and DC Readout Board

Item	Quantity	Reference	Part
60	2	U31,U23	LM7912
61	2	U24,U29	AD8610B
62	2	U25,U33	LM7805
63	1	U26	AD621
64	1	U27	AD8610
65	2	U28,U35	LM7905
66	1	U32	AD650

ORNL JNT Differential Receiver Board

Item	Quantity	Reference	Part
1	14	C1,C37,C41,C73,C81,C115, C129,C130,C138,C139,C146, C147,C149,C150	10UF
2	6	C2,C35,C43,C69,C83,C114	0.1UF
3	6	C3,C4,C45,C46,C116,C118	20p
4	22	C5,C9,C13,C15,C24,C26, C33,C36,C49,C55,C57,C67, C70,C77,C79,C89,C103, C105,C108,C120,C123,C145	0.01u
5	22	C6,C10,C14,C16,C23,C25, C30,C34,C50,C52,C56,C58, C65,C68,C75,C78,C90,C104, C106,C107,C117,C121	6.8u
6	3	C7,C22,C60	33n
7	9	C8,C17,C48,C59,C88,C97, R148,R150,R151	open
8	8	C18,C19,C20,C21,C61,C62, C63,C64	68p
9	4	C28,C31,C72,C76	10P
10	11	C39,C40,C42,C44,C80,C84, C85,C86,C119,C127,C128	2 p
11	1	C47	.5u
12	1	C51	0.01uNP
13	2	C87,C100	.47u
14	2	C95,C96	40p
15	2	C98,C99	6.8 n
16	3	C125,C131,C141	2.2uF
17	3	C126,C133,C142	1uF
18	1	C132	320nF
19	1	C134	0.1 u
20	2	C135,C153	0.01 u
21	4	C136,C144,C155,C157	6.8 u
22	1	C140	220p
23	1	C143	160nF
24	1	C148	100 p
25	2	C152,C151	.47 u
26	2	C158,C154	.01 u
27	1	C156	4.7u
28	9	J1,J2,J3,J4,J5,J6,J7,J8, J9	BNC
29	1	J10	POWER
30	1	J11	CON3
31	36	R1,R4,R6,R7,R9,R24,R25,	10

ORNL JNT Differential Receiver Board

Item	Quantity	Reference	Part
		R28,R29,R31,R32,R40,R48, R50,R51,R53,R64,R65,R70, R71,R73,R77,R78,R90,R96, R97,R105,R107,R110,R124, R125,R132,R138,R139,R153, R160	
32	5	R2,R3,R45,R46,R85	22.1k
33	9	R8,R11,R17,R47,R54,R57, R87,R94,R101	49.9
34	4	R12,R55,R95,R155	R
35	3	R13,R56,R98	221
36	5	R14,R23,R63,R104,R146	0
37	10	R15,R16,R18,R19,R59,R60, R112,R113,R115,R116	5.62k
38	5	R21,R22,R67,R69,R103	43.1k
39	3	R26,R66,R108	2 K
40	3	R27,R68,R109	1K
41	11	R35,R37,R39,R42,R75,R81, R82,R84,R118,R126,R127	511
42	2	R62,R61	7.5K
43	1	R130	20k
44	2	R131,R135	5.11K
45	2	R134,R133	7k
46	1	R136	68.1k
47	1	R137	909k
48	1	R140	14k
49	3	R147,R149,R154	50
50	1	R152	50 k
51	1	R156	2.0 k
52	2	R157,R159	100
53	1	R158	10K
54	3	U1,U7,U13	AD8130
55	8	U2,U3,U5,U6,U8,U9,U11, U12	op627
56	3	U14,U17,U18	ad844
57	3	U19,U21,U25	LM320-12V
58	3	U20,U23,U26	LT1086+12V
59	1	U22	4046
60	1	U24	AD8610
61	1	U27	LT1086+5V
62	1	U28	LM311

ORNL JNT Dual Preamplifier Circuit Board

Item	Quantity	Reference	Part
1	20	C2,C3,C6,C10,C17,C20,C34, C39,C41,C44,C51,C54,C56, C57,C60,C64,C81,C84,C86, C89	0.01uF
2	20	C4,C5,C9,C30,C32,C35,C38, C43,C77,C79,C107,C108, C109,C110,C111,C112,C113, C114,C115,C116	6.8UF
3	18	C7,C11,C23,C24,C29,C33, C36,C40,C45,C46,C48,C61, C62,C67,C76,C80,C85,C90	0.1UF
4	20	C8,C37,C47,C68,C91,C92, C93,C94,C95,C96,C97,C98, C99,C100,C101,C102,C103, C104,C105,C106	33UF
5	10	C12,C21,C22,C25,C31,C65, C70,C71,C72,C78	10p
6	4	C13,C28,C66,C75	.01UF
7	4	C14,C15,C49,C50	0.082U
8	2	C16,C69	.0018u
9	4	C18,C19,C52,C53	10pf
10	4	C26,C27,C73,C74	4pF
11	4	D1,D2,D3,D4	1N4446
12	4	J1,J2,J3,J4	BNC
13	4	Q1,Q2,Q9,Q10	MPS-81
14	8	Q3,Q6,Q7,Q8,Q11,Q14,Q15, Q16	2N5089
15	4	Q4,Q5,Q12,Q13	2N6451
16	14	RA1,RA2,RA3,RA4,R7,R17, R18,R33,R34,R55,R63,R64, R75,R76	1K
17	4	RCMRR1,RCMRR2,RCMRR3, RCMRR4	TBD
18	6	RC1,RC2,RC3,RC4,R19,R65	4.99K
19	8	RD1,RD2,RD3,RD4,R31,R32, R53,R54	402
20	12	RS1,RE1,RS2,RE2,RS3,RS4, RE5,RE6,R13,R38,R47,R56	10
21	4	RE3,RE4,RE7,RE8	3.65k
22	8	RFU1,RFL1,RFU2,RFL2,R14, R22,R60,R66	200
23	20	R1,R2,R3,R4,R28,R29,R36, R37,R41,R43,R46,R48,R49,	22

ORNL JNT Dual Preamplifier Circuit Board

Item	Quantity	Reference	Part
		R50,R72,R73,R78,R79,R81, R82	
24	2	R40,R5	10K
25	2	R6,R42	2.15K
26	4	R8,R30,R57,R74	100k
27	8	R9,R16,R20,R21,R51,R52, R58,R62	499
28	4	R10,R12,R44,R45	1M
29	4	R11,R24,R59,R68	100
30	10	R15,R23,R25,R26,R27,R61, R67,R69,R70,R71	2k
31	4	R35,R39,R77,R80	50
32	6	S1,S2,S3,S4,S5,S6	standoff
33	2	TP1,TP2	T POINT R
34	8	U1,U2,U3,U5,U6,U7,U8,U10	OP37
35	2	U4,U9	AD8138
36	3	U11,U12,U16	LM7812
37	3	U13,U14,U18	LM7912
38	1	U15	LM7805
39	1	U17	LM7905